Characterization of Mineral-Based Colloidal Microbubble and Its Subsequent Application in Separation of Fine Mineral Particles

THESIS

Submitted in Partial Fulfilment of the Requirements for the Degree of

Doctor of Philosophy
In
Engineering
By

KUMARI RUBY

Roll No. 156107025

Under the supervision of

Prof. Subrata Kumar Majumder

DEPARTMENT OF CHEMICAL ENGINEERING

INDIAN INSTITUTE OF TECHNOLOGY GUWAHATI

GUWAHATI-781039, INDIA

July 2022

INDIAN INSTITUTE OF TECHNOLOGY GUWAHATI

GUWAHATI-781039, ASSAM, INDIA

DEPARTMENT OF CHEMICAL ENGINEERING

CERTIFICATE

This is to certify that the thesis entitled "***Characterization of Mineral-Based Colloidal Microbubble and Its Subsequent Application in Separation of Fine Mineral Particles***" submitted by Mrs. Kumari Ruby in fulfilment of the requirement of the **Degree of Doctor of Philosophy in Engineering** is a record of bonafide research work carried out by her, in the Department of Chemical Engineering, Indian Institute of Technology Guwahati, under my guidance and supervision. The work documented in this thesis has not been submitted to any other University or Institute for the award of any degree or diploma. In my opinion, the thesis has reached the standard fulfilling the requirements of the Ph.D. degree as prescribed in the regulations of this institute.

Prof. Subrata Kumar Majumder

Professor

Department of Chemical Engineering

Indian Institute of Technology Guwahati

Guwahati-781039, India

ACKNOWLEDGEMENTS

I would like to express my gratitude to all those who helped me in different ways in completing this research work, directly or indirectly. First and foremost, I would like to express my deep-felt gratitude to my supervisor, **Prof. Subrata Kumar Majumder** for providing me continuous inspiration and guidance throughout the entire course of work. In addition, his philosophical guidance has built up a momentum inside me. His uncompromising approach to complete the experimental part, data analysis, writing manuscripts as well as thesis within the stipulated time period helped me a lot in completing my research work. The numerous brain storming sessions during the project meetings for his understanding, support and caring during the times when I was really down and depressed due to personal problems. I also thank almighty for making me to feel fortunate to work under his great stewardship.

I wish to acknowledge **Prof. Anugrah Singh**, former HOD and **Prof. Kaustubha Mohanty**, present HOD, Department of Chemical Engineering, for extending all the necessary facilities for carrying-out my research work. I am also grateful to all the professors in the department for their sincere cooperation.

I must also thank my doctoral committee members **Prof. Mihir Kr. Purkait, Dr. R Anandalakshmi** of the Department of Chemical Engineering and **Prof. T. V. Bharat** of the Department of Civil Engineering, for their valuable suggestions and contribution towards my research work.

Last but not the least, I wish to thank all the non-teaching staff of our department for the help received from them.

I would like to thank my co-researchers Dr. Bharat Kumar, Dr. Fahad M. K, Dr. Ritesh Prakash, Dr. Somen Modal, Mrs. Surbhi Patel, Mr. Bongliba T. Sangtam, Mr. Dhiren Boro, Mr. Amlan Jyoti Das and Mr. Gaurav Singh for their enormous help and support during research work. I would also like to express my gratitude to the former doctorate student, Dr. Rajeev Parmar for his suggestion during the research work. I am thankful to all my departmental friends, seniors, and juniors for their support and good wishes. I would also like to thank my family to have patiently support me in the completion of my Ph. D. and stood by me throughout my life.

Date: 11/07/22

Kumari Ruby

Place: IIT Guwahati

Mrs. Kumari Ruby

CURRICULUM VITAE

Name **KUMARI RUBY**

Date of birth **30-08-1989**

Education Qualifications:

Degree	University/Institute	Year of Passing
Bachelor of Engineering in Chemical Engineering	SLIET, Longowal Punjab	2012
Master of Technology in Mineral Processing	IIT-ISM, Dhanbad, Jhakhand	2015
Research Scholar in Chemical Engineering	Indian Institute of Technology Guwahati	Since 2015

Awards Scholarships and Recognitions:

MHRD Govt. of India Scholarship for Ph. D. from July 2015 to July 2019.

MHRD Govt. of India Scholarship for M. Tech. from July 2013 to May 2015.

Qualified Gate-2012 and secured all India rank 2084 in Chemical Engineering

RESEARCH PUBLICATIONS

A. Research Papers in Journal:

- Ruby, K., Majumder, S. K., (2018). Studies on stability and properties of micro and nano-particle-laden ionic microbubbles. Powder Technol., 335, 77–90.
- Ruby, K., Majumder, S. K., (2019). Effect of Salt on Stability of Microbubbles in the Presence of Micro-Nanoparticles: Substantial Adsorption in the Separation of Particles by Flotation. Ind. Eng. Chem. Res., 58, 18881-18895.

B. Research Papers in conferences:

- Ruby, K., Boro, D., and Majumder, S. K., 2017. Stability, Volume fraction and fine particles recovery potentials of ionic microbubbles. International seminar on mineral processing technology.
- Ruby, K., Das, A. J., and Majumder, S. K., 2018. Microbubble-aided nanoparticle entrainment efficiency in a floatation column. International seminar on mineral processing technology.
- Ruby, K., Majumder, S. K., 2018. Studies on micro and nanoparticle laden ionic microbubbles for water treatment and its purification. International conference on water: From pollution to purification (ICW-2018).
- Ruby, K., Majumder, S. K., 2018. Stability of colloidal microbubble in presence of fine particle with different surfactants. Research Conclave 2018.

ABSTRACT

Ionic Microbubbles are miniature gas bubbles of less than 100 µm in diameter, which are surrounded by charged ions. Fine bubbles are used in many environmental and industrial processes for solid-liquid separations. They have been used for treatment techniques, removal of pulp fiber, separation of fine particles, protein recovery, deinking wastewater, etc. The important characteristics of microbubbles are their large specific area and small buoyancy; therefore, effective dissolution of gas-phase and high adsorption rate is expected (Lee et al., 2005). Microbubbles are the type of bubbles, which consists of gas inside their core, they are separated from each other, so they cannot agglomerate, having a size range of micrometers, usually 1-100 micrometers (Kataria, 2012). Microbubbles have been used in biological fluids, such as blood, for ultrasound in therapeutic and contrast imaging (Kataria, 2012) and drug and gene delivery (Sirsi and Borden, 2009). Collapsing MBs can be an alternative green chemical-free technology for the biofouling reduction of the membrane (Agarwal et al., 2013). But no significant works are available in the literature on fine mineral particle separation by microbubbles. There is a lack of research to explore the characteristics of microbubbles in the presence and absence of micro-nano particles and their efficiency in removing them. This work aimed to examine the stability of microbubbles generated with surface-active agents with and without particles. The drainage kinetic study was done for the microbubbles generated in the presence of particles with and without salt. The effects of some primary parameters on entrainment of particles of ZnO, Al_2O_3, etc., in a flotation column, using microbubbles.

Based on the present status of research, this work was undertaken with the following objectives:

- Study the stability of ionic microbubbles in the presence of a different concentration of surfactant, different types of surfactant, temperature, and pH. Development of correlations to interpret the stability with the change in surfactant concentration and temperature.

- Study the bubble size and its holdup, affecting the stability of the particle-laden microbubbles. Development of a model to interpret the stability of the ionic microbubble based on drainage kinetics.
- Study the CMC of the surfactant in the presence and absence of salts (Sodium chloride, lithium chloride, and cesium chloride). Determination of the lifetime of a microbubble in various liquid media based on the assemblage at air-water and liquid-solid interfaces containing surfactants and micro or nanoparticles.
- Study the influence of changes in parameters such as gas flow rate and concentration of pulp on the entrainment of particles by microbubble. Development of the mathematical model incorporating the impact of changes in variables on the entrainment and extended to different mixtures of particles consisting of desired and gangue minerals.
- Study the recovery efficiency of micro-nano particles by ionic microbubble in batch plant prototype. Development of phenomenological kinetic model based on collision, attachment, and detachment mechanisms of fine particles, for the recovery of the micro-nano particles.

In the present study, experiments have been conducted to study the stability of microbubbles and its application in fine particle separation. The first attempt was made to understand the stability characteristics of microbubbles at different variables. The physical properties of microbubbles have been characterized by a range of surfactants concentration, surfactant types, additives present like salt or nanoparticles, and a range of temperature and pH. Knowledge of the stability would enable us to use these ionic microbubbles more efficiently for their distinct applications. The stability of microbubbles was estimated by measuring the drained volume of liquid with respect to time as per the drainage curve method. Once the microbubbles are prepared, it is transferred to a 50 ml measuring cylinder, which is kept in a constant temperature water bath. The stability measurement is done immediately by the video of the drainage of the liquid through the microbubbles. The video is further used to analyze the volume of drained liquid with time and plotted to estimate the half-life of microbubbles. The ratio of half-life to the total time of liquid drainage is referred to as the degree of stability. The experimental results revealed that the stability of microbubbles could be significantly affected by the change in the concentration of surfactant, temperature, and pH. The half-life of SDS microbubbles increased from 84 s to 259 s as the SDS concentration increased from 100 ppm to 2500 ppm. The half-life of microbubbles formulated with

500 ppm SDS at 313 K, 333 K, and 353 K was found to be 102 s, 104 s, and 118 s, respectively. The stability of the microbubbles generated by SDS decreases from 180 s to 158 s for pH changing from 6 to 8; however, at lower pH < 6, the stability decreases further. The same trend of influence of pH on stability has been reported for anionic surfactant SDS by Lye and Stuckey (1998).

An insight is given on the studies on the effect of preparation parameters on the stability of microbubbles, the number of microbubbles formed, and the holdup of microbubbles. In the present work, the phase isolation method is used to estimate gas-phase fraction. Microbubbles solution is filled in the transparent glass cylinder and the camera is used to record the change in the height of the clean liquid with time. After a certain time, the bubbles at the top start disappearing as they are in contact with the atmosphere directly. The size of microbubbles is determined based on the rise velocity of the microbubbles as a function of gas holdup in the ionic microbubble dispersion and by using the photographic method. Within the low range of viscosity, the microbubble size depends on gas-liquid interfacial tension. The bubble size decreased from 56.41 to 47.55 μm when 500 ppm SDS was added to the water, while the addition of 1000 ppm Saponin decreased the size to 43.29 μm. The microbubble size distribution in SDS solution follows the log-logistic distribution for all pH. When nanoparticles were added to microbubbles formulated at 500 ppm SDS with varying concentrations of 0.02 to 0.10 (w/w %), the stability increased from 135 s to 170 s.

Next, an attempt has been made to study the hydrodynamic parameters such as bubble size distribution and the rise velocity of microbubbles in various liquids. The results reveal that the microbubble size distribution becomes narrow with decreasing surface tension. Microbubble systems are dynamic and change continuously, which results in bubble breakage, coalescence, and disproportionation [i.e., transfer of core air from smaller bubbles (higher pressure) to the larger bubbles (lower pressure)]. This limits its stability and the other features of microbubbles. Its other features depend on the bubble size and its holdup. Microbubble rise velocity reduces as the surfactant concentration increases in liquid. The stability of microbubbles is analyzed by the drainage mechanism. The liquid drainage of the microbubble dispersions occurs in three distinct phases. Initially, the drainage rate increases due to the uniform water distribution in the ionic gas microbubbles throughout the tube just after its preparation. The distribution of the microbubbles changes with time. The increase in the liquid drainage increases the size of the microbubbles until

the drainage rate reaches its maximum value. Higher concentrations result in decreasing drained liquid.

Next, an attempt has been made to study the stability of microbubbles based on the assemblage at air-water and liquid-solid interfaces with prominence on the systems containing surface-active agents and micro- or nanoparticles. Adsorption of surfactant at the solid-liquid interface is substantial in the separation of particles by flotation. The surfactant molecules get adsorbed at the solid-liquid and liquid-liquid interfaces and attach to the microbubbles, moving along with the microbubbles for effective separation. The present study showed that various parameters affect the stability of microbubbles. The presence of nanoparticles, size of particles, the concentration of particles, temperature, and pH affect the stability of particles. It was also found that the presence of particles modifies the stability of ionic microbubbles in three different ways: (i) adsorption loss (get adsorbed on the surface of particles) caused by reduction of surfactant concentration, (ii) increase in the viscoelastic property of the microbubbles, and (iii) increase in the viscoelastic property of the liquid films. Sodium chloride, lithium chloride, and caesium chloride salts in the presence of anionic surface-active agent SDS are efficacious in decreasing air-water interfacial tension. For systems involving salt-water interfaces, the addition of salt effectively lowers the surface tension by reduction of the CMC of the surface-active agent. Present observation shows that the maximum reduction in the CMC with the addition of salt was obtained in the order: CsCl > LiCl > NaCl. The insertion of negatively charged hydrophilic copper oxide nanoparticles (size < 50 nm TEM) increases the efficacy of an ionic surface-active agent of SDS molecules. This efficacy is due to the repulsive Coulomb interactions at the interfaces, which arise the adsorption at the interfaces. The stability of microbubbles increased with an increase in the concentration of salt in the case of CsCl while it decreased for NaCl, and a mixed effect was found with LiCl.

Contents

CERTIFICATE ii

ACKNOWLEDGEMENTS iii

CURRICULUM VITAE v

RESEARCH PUBLICATIONS vi

ABSTRACT vii

Chapter 1 1

1. Introduction 1

1.1. Background to the study 1

1.1.1. Separation of the fine particles by micro-flotation 1

1.1.2. Colloidal gas microbubbles 4

1.1.3. Components of colloidal gas microbubbles 4

1.1.4. Generation techniques of colloidal gas microbubble 5

1.1.4.1. Method based on flowing liquid 6

1.1.5. Characteristics of colloidal gas microbubbles 9

1.1.6. Physics of particle attachment and detachment on colloidal gas microbubble 12

1.1.7. Rate of recovery by microbubble flotation based on conventional flotation 16

1.2. Importance of the research area 17

1.2.1. Applications of microbubbles in the field of water and wastewater treatment 17

Chapter 2 24

2. Literature Review and Formulation of Research 24

2.1. Literature survey 24

2.1.1. Rheological behavior of the microbubble in particle-laden solution 24

2.1.2. Holdup, the size distribution of microbubbles in particle-laden solution 27

2.1.3. Stability and zeta potential of microbubble 29

2.1.4. Entrainment characteristics of microbubble 34

2.1.5. Separation kinetics of fine particle by microbubble flotation 37

2.2. Formulation research 39

2.2.1. Scope of the research 39

2.2.2. Objective of the work 40

2.2.3. Significance of the formulated work 41

2.2.4. Novelty importance of the proposed project in the context of the current status 43

Chapter 3 44

3. Holdup Characteristics and Mean Size of Ionic Microbubbles 44

3.1. Introduction 44
3.2. Theoretical background 46
3.2.1. Ionic microbubble holdup 46
3.2.2. Rise velocity of ionic microbubbles 47
3.3. Experimental Procedure 48
3.3.1. Estimation of ionic microbubble gas holdup 48
3.3.2. Estimation of ionic microbubble size from its rise velocity 49
3.3.3. Determination of ionic microbubble size by photographic method 50
3.3.4. Properties of the system 52
3.4. Results and Discussion 54
3.4.1. Holdup of the ionic microbubbles at different variables 54
3.4.2. Size of the ionic microbubbles at different variables 57
3.4.3. Effect of Salt on the Size of Microbubbles 62
3.4.4. Salt Effect on the Holdup of Microbubbles 66
3.5. Conclusions 67
CHAPTER 4 68
4. Interfacial Adsorption Phenomena of Microbubble 68
4.1. Introduction 68
4.2. Theoretical background 71
4.2.1. Adsorption of surfactants at the bubble-liquid interface. 71
4.2.2. Adsorption of the surfactant in the presence of salt 72
4.2.3. Adsorption behavior in the presence of particles 73
4.3. Experimental procedure 76
4.3.1. Determination of CMC 76
4.4. Results and Discussion 77
4.4.1. Effect of salts on adsorption 77
4.4.2. Effect of salt on critical micelle concentration 79
4.4.3. Effect of different salts on the film thickness around the interface 81
4.4.4. Effect of salt and particles on adsorption 81
4.5. Conclusions 84
CHAPTER 5 86
5. Stability of Ionic Microbubbles and Its Kinetics 86
5.1. Introduction 86
5.2. Experimental 89

5.2.1. Generation of ionic microbubbles 89
5.2.2. Stability measurement of ionic microbubbles 89
5.2.3. Properties of the system 91
5.3. Results and Discussion 92
5.3.1. Drainage kinetics 92
5.3.2. Half-life of ionic microbubble at different pH 97
5.3.3. Mechanism of liquid drainage through ionic microbubbles 100
5.4. Model kinetics of ionic microbubbles 102
5.5. Conclusions 107
CHAPTER 6 108
6. Effect of Salt on Stability of Ionic Microbubbles 108
6.1. Introduction 108
6.2. Experimental 109
6.3. Results and Discussion 110
6.3.1. Effect of different salts on microbubble stability when the particles are absent 110
6.3.2. Effect of different salts on microbubble stability when the particles are present 115
6.3.3. Effect of salt on drainage characteristic 119
6.3.4. Effect of salt and particles on the stability and liquid drainage 121
6.4. Conclusions 123
Chapter 7 124
7. Overall Conclusion and Future Recommendation 124
7.1. Overall conclusions 124
7.2. Future recommendation 127

Nomenclature

References

List of Figures

Chapter 1

Figure 1.1. Classification of the adsorptive bubble separation techniques (Karger and Devivo 1968). 3

Figure 1.2. Schematic diagram of the structure of charged microbubbles proposed by Sebba (1987). 5

Figure 1.3. Rotary liquid flow type micro bubble generator (Terasaka et al. 2011). 6

Figure 1.4. Venturi-type microbubble generator (Fujiwara et al. 2003). 7

Figure 1.5. Ejector-type microbubble generator (Terasaka et al. 2011). 7

Figure 1.6. Multi fluid mixture device type microbubble generator (Sadatomi et al. 2012). 8

Figure 1.7. Hydrodynamic 1, diffusiophoretic 2, and surface force 3, zones of interaction between a bubble and a particle (Derjaguin and Dukhin, 1993). 14

Figure 1.8. Sub-processes of particle collection by an air bubble as it rises through the pulp: (i) collision, (ii) attachment, and (iii) stabilization of particle-bubble aggregates with respect to external stresses. 16

Chapter 3

Figure 3.1. Experimental photographs of drainage process at room temperature with 500 ppm of SDS. 50

Figure 3.2. Schematic diagram of the photographic method to determine the bubble size. 51

Figure 3.3. Typical snapshot of ionic microbubble after editing it by image processing software and its distribution. 52

Figure 3.4. Variations of the holdup of microbubbles, (a) with temperature and (b) with glycerol concentration. 55

Figure 3.5. Effect of SDS surfactant concentration on bubble size at stirring speed of 20000 rpm for 15 s in the absence of particles at temperature 298 K and pH = 6.29. 58

Figure 3.6. Variations of bubble size with temperature at different doses of surfactant. 59

Figure 3.7. Variations of bubble size with the concentration of glycerol at different doses of surfactant. 59

Figure 3.8. Variations of bubble size with the concentration of nanoclays. 60

Figure 3.9. Variation of microbubble size (Sauter mean bubble diameter) with pH. 61

Figure 3.10. Bubble size distribution Optical microscopy images of microbubble generated with SDS only, (b) histogram of the bubble size distribution for SDS, (c) Optical microscopy images of microbubble generated with SDS and NaCl. 64

Figure 3.11. Variations of bubble size with (a) increasing concentration of SDS only, the addition of salt NaCl (10 mol m^{-3}) at same concentrations of SDS and with addition CuO (0.79 w/w %) nanoparticle at the same concentration of SDS and salt and (b) Effect of different size of the particle on the bubble diameter of microbubbles. 65

Figure 3.12. (a) Effect of different salt on the size of microbubbles at 10 mol m^{-3} concentration of salt with varying concentration of SDS and (b) Effect of varying concentrations of different salt on the size of microbubbles at 0.5 mol m^{-3} concentration. 66

Figure 3.13. Variations of the holdup of microbubbles. (a) with different salt at different concentrations of surfactant and constant concentration of salt & particles, and (b) at different concentrations of particles with a constant amount of salt. 67

Chapter 4

Figure 4.1. Variation of surface tension with varying concentrations of SDS at 0, 50, and 100 mol m^{-3} concentration of salts (a) in the presence of NaCl, (b) in the presence of LiCl, (c) in the presence of CaCl, and (d) in the presence of different salts with 10 mol m^{-3} of its concentration. 79

Figure 4.2. Variation of CMC with a salt concentration in an aqueous solution of SDS.....80

Chapter 5

Figure 5.1. Pictorial representation of the subsequent steps in the drainage process. (a) (i) Maximum dispersion volume of microbubbles immediately poured into the cylinder just after stirring at t = 0, start of drainage process; (ii) progress of drainage at time (iii) clear liquid after drainage, and (b) Typical outline to estimate the half-life of ionic microbubbles. 90

Figure 5.2. Effect of different concentrations of surfactant (with anionic surfactant (SDS) without particles) on drainage at room temperature. 92

Figure 5.3. Effect of different concentrations of surfactant on drainage at room temperature with cationic surfactant (CTAB) without particles. 93

Figure 5.4. Effect of nanoclay addition on stability of charged microbubble with an anionic surfactant SDS (500 ppm) at room temperature. 94

Figure 5.5. Effect of nanoclay addition on stability of charged microbubble with the Saponin (non-ionic surfactant, 1000 ppm) at room temperature. 94

Figure 5.6. Effect of temperature on the stability of charged microbubbles with an anionic surfactant SDS (500 ppm).....96

Figure 5.7. Effect of temperature on the stability of charged microbubbles without particles and with non-ionic surfactant Saponin (1000 ppm).....96

Figure 5.8. Effect of pH on drainage profile (a) with anionic solution (500 ppm SDS) in the absence of particles and (b) with aluminum oxide particles at a concentration of 1.96 (w/w %) with anionic surfactant at (SDS) room temperature. 97

Figure 5.9. Effect of pH on the half-life of colloidal microbubbles, (a) microbubbles without particles in the presence of SDS (500 ppm) and (b) microbubbles with Al_2O_3 particles in the presence of SDS (500 ppm) at room temperature. 98

Figure 5.10. Effect of pH on the zeta potential of CuO particles in the surfactant (SDS 500 ppm) solution. 99

Figure 5.11. Variations of drainage rate of microbubbles in the absence of particles at 298 K temperature at 500 ppm SDS.....101

Figure 5.12. Effect of temperature on drainage rate for microbubbles with cationic surfactant CTAB in the presence of CuO particles.....102

Figure 5.13. Comparison of experimental liquid drainage data and model data at 500 ppm of SDS in the presence of 3.85 w/w % of Al_2O_3 particles at room temperature.....104

Chapter 6

Figure 6.1. Experimental representation of microbubble drainage at 293 K, with SDS (1 mol m^{-3}), CuO (0.79 w/w %), and salt NaCl (10 mol m^{-3}). 110

Figure 6.2. Effect of varying concentrations of salt NaCl on the stability of charged microbubble prepared with different concentrations of anionic surfactant SDS (a) at 0.5 mol m^{-3}, (b) at 1 mol m^{-3}, and (c) at 3 mol m^{-3}. 113

Figure 6.3. Effect of salt on the half-life of colloidal microbubbles in the presence of varying concentrations of SDS (a) microbubbles without particles and (b) microbubbles with ZnO particles at room temperature.....116

Figure 6.4. Effect of varying concentration of particles (ZnO) on the stability of charged microbubble prepared with anionic surfactant SDS of 0.5 mol m^{-3}, (a) in the presence of 10 mol m^{-3} NaCl, (b) in the presence of 50 mol m^{-3} NaCl, and (c) in the presence of 10 mol m^{-3} NaCl. 117

Figure 6.5. Effect of varying concentration of particles (ZnO) on the stability of charged microbubble prepared with anionic surfactant SDS of 1.0 mol m^{-3}, (a) in the presence of 10 mol m^{-3} NaCl, (b) in the presence of 50 mol m^{-3} NaCl, and (c) in the presence of 100 mol m^{-3} NaCl. 118

Figure 6.6. Effective surface tension as a function of SDS concentration. The SDS aqueous solutions with 0 mol m^{-3} salt (presented in squares), 50 mol m^{-3} CsCl salt (presented in circles), and 50 mol m^{-3} CsCl along with 0.79 w/w% (50 mol m^{-3}) CuO nanoparticles (presented in triangles). 118

Figure 6.7. The rate constant k_d versus varying concentrations of salt (a) at the different types of salts without particles and (b) at the different types of salts with particles.....121

Figure 6.8. Drainage rate variation as a function of time through microbubbles in the presence of salt (NaCl) and particles CuO (0.79 w/w %) at 4 mol m^{-3} concentrations of SDS.....123

List of Tables

Chapter 1

Table 1.1. Utilization of ionic microbubbles (a new technique) in various areas. 19

Chapter 2

Table 2.1. Zeta potential of bubbles at the air/water interface-a summary and a brief description of selected studies. 34

Chapter 3

Table 3.1. Properties of surfactants. 53
Table 3.2. Physical properties of glycerol. 53
Table 3.3. Properties of the micro and nano particles. 53
Table 3.4. Properties of different salts. 54
Table 3.5. Holdup and half-life of microbubble at different parameters with ionic surfactant (SDS 500 ppm). 56
Table 3.6. Experimental values of parameters of Eq. (3.12) at pH = 6.29. 63
Table 3.7. Microbubble size and surface tension in the presence of salt (NaCl). 63

Chapter 4

Table 4.1. Parameters of Adsorption of SDS at the Air-Water Interface. 82
Table 4.2. Best fit parameter values to the Langmuir model. 83

Chapter 5

Table 5.1. Parity of experimental and model parameters. 105
Table 5.2. Coefficients of Equation (5.5). 106

Chapter 6

Table 6.1. Half-life, gas holdup, and maximum dissolution time data of microbubbles with ionic surfactant (SDS). 111

Table 6.2. Half-life, gas holdup, and maximum dissolution time data of microbubbles with ionic surfactant (SDS) in the presence of particles.....114

Chapter 1

1. Introduction

1.1. Background to the study

1.1.1. Separation of the fine particles by micro-flotation

Worldwide attempts are being made to develop new technologies by replacing conventional methods. Technologies are getting enhanced, changing day by day. Research is going to a higher level, leading to a smaller, cleaner, deeper, and more energy-efficient by exploring every field. In chemical engineering, separation processes play an important role to achieve any mass transfer phenomenon that converts a mixture of substances into two or more distinct product mixtures (which may be referred to as *fractions*), at least one of which is enriched in one or more of the mixture's constituents. Separation processes have been developed by early civilizations, which include (1) extraction of metals from ores, perfumes from flowers, and dyes from plants; (2) evaporation of seawater to obtain salt; (3) refining of rock asphalt; (4) distilling of liquors. Modern chemical engineering is concerned with understanding and developing systematic procedures for the design and optimal operation of chemical, petrochemical, pharmaceutical, food, mineral processing, cosmetics, and many other process systems, ranging from the nano and micro systems used for product analysis, tests or production to industrial-scale continuous and batch processes, all within the concept of the chemical supply chain (Grossmann, 2004).

Separation processes are mainly based on differences in chemical properties or physical properties such as size, shape, mass, density, or chemical affinity between the constituents of a mixture. They are often classified according to the particular differences used to achieve separation.

For example, distillation is based on differences in volatility; liquid extraction is based on differences in solubility and adsorptive bubble separation on differences in surface activity. The adsubble techniques or adsorptive bubble separation have been accepted by common consent (Karger and Devivo, 1968). The various individual adsubble techniques are shown in Figure 1.1. Adsorptive bubble separation processes involve mainly two processes: foam separation-requires the generation of foam or froth to carry off material, and non-foaming adsorptive bubble separation.

Further foam separation is subdivided into foam fractionation, the foaming off of the dissolved material from a solution to get adsorbed at the bubble surfaces, and the froth flotation (Gaudin, 1957); this process removes particulate material by frothing (foaming). Under froth flotation, many subdivisions come, which include ore flotation, macro-flotation, micro-flotation, precipitate flotation, ion flotation, molecular flotation, and adsorbing colloid flotation. Solvent sublation (Sebba, 1962) and bubble fractionation (Dorman and Lemlich, 1965) are two nonforming adsorptive bubble separation subdivisions.

Froth flotation is one of the most important processes used to separate mineral particles. Its use and application are frequently amplified to treat greater tonnages and cover new areas. This process is used in mineral processing (such as sulphides of lead, zinc, and copper), paper recycling, and waste-water treatment industries. Flotation is a physicochemical separation process involving a complex theory of three phases (solids, water, and froth) with various sub-processes and interactions (Wills and Napier-Munn, 2005).

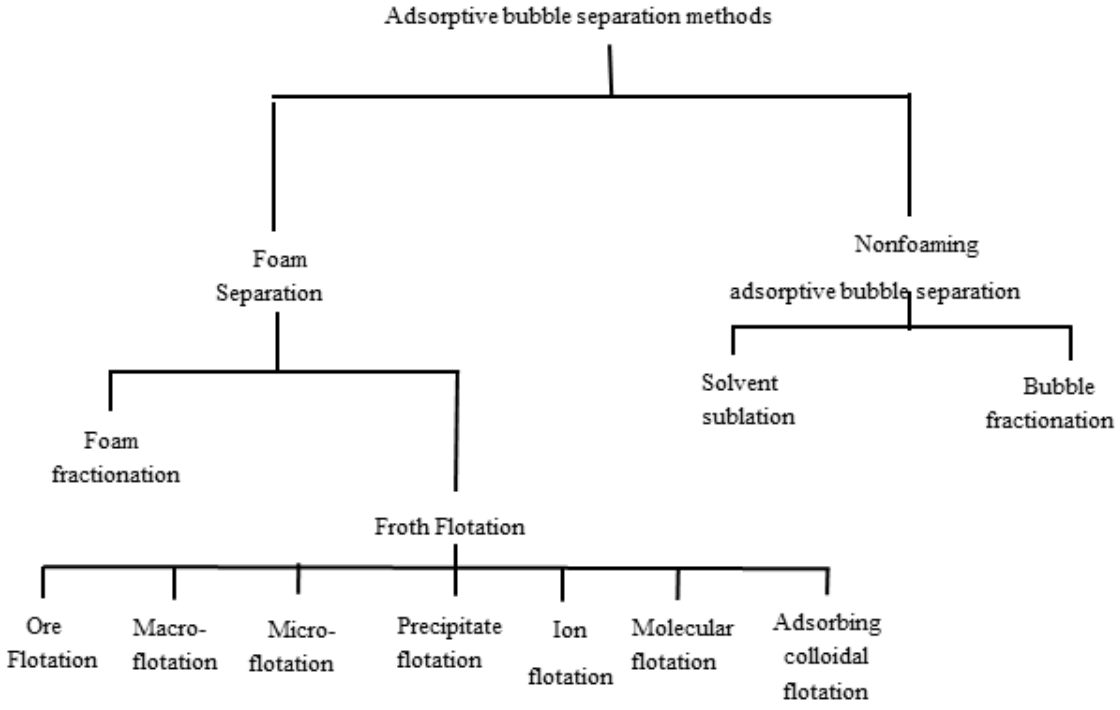

Figure 1.1. Classification of the adsorptive bubble separation techniques (Karger and Devivo 1968).

Flotation mainly works on three mechanisms (1) selective attachment to air bubbles, i.e., true flotation, (2) entrainment of particles through the froth, and (3) physical entrapment. Entrainment is the froth phase mechanism that plays a vital role in the recovery of particles to the concentrate. Recovery depends on selective separation and bubble-particle interaction by electrostatic and hydrophobic forces (Yoon, 2000). The poor recovery of fines by flotation holds responsibility for the low probability of bubble-particle collision, which decreases with decreasing particle size (Yoon, 2000). The properties of microbubbles can significantly enhance the flotation of fine particles, as it affects the mechanism of attachment of particles to the bubble surfaces.

The probability of collision is inversely proportional to bubble size, which suggests improved fine particle recovery by flotation using small bubbles. Thus, focus has been given to methods of generating small bubbles, including dissolved air flotation (Yalcin and Byers, 2006). In recent studies, it has been reported that smaller bubbles give rise to the larger interfacial area, which initiates several processes for intensification (Tsuge, 2014).

1.1.2. Colloidal gas microbubbles

Colloidal gas microbubbles, first described by (Sebba, 1987), are microbubbles composed of a surfactant film and a third surfactant layer (Figure 1.2). They are also called microfoams and consist of closely packed spherical microbubbles having a size range of micrometers, usually 1–100 micrometers. The dimensions of colloidal gas microbubbles are not truly in the colloidal range but have colloidal properties (Kurup and Naik, 2010).

1.1.3. Components of colloidal gas microbubbles

Sebba (1987) claimed that colloidal gas microbubbles are gas bubbles surrounded by three surfactant layers, as shown in Figure 1.2. He proposed that colloidal gas microbubbles consist of a gaseous inner core surrounded by a thin aqueous surfactant film or shell composed of two surfactant layers and, in addition, a third surfactant layer that stabilizes this structure. Microbubbles have three components, namely gas phase component, shell material, and aqueous or liquid phase.

Gas-phase component: The gas phase constitutes a single gas or combination of gases. The combination of gases is generally used for two reasons: first, to create differentials in partial pressure, and second, to generate gas osmotic pressures which stabilize the bubbles. One gas is a primary gas modifier, and the second gas is known as a gas osmotic agent. Air and nitrogen are examples of primary modifier gas. Sulfur hexafluoride is an example of an osmotic gas agent.

***Shell material*:** The gas phase is enclosed by shell material. The diffusion of gas out of microbubbles and the mechanical properties of microbubbles depend on the shell material. If the elasticity of shell material is more, the acoustic energy it can withstand before bursting or breakup is high, which increases the residence time of the bubbles.

***Aqueous or liquid phase*:** The external liquid surrounding the shell in which the bubble resides can be the same as shell material, or it can be a surfactant or foaming agent depending upon the operations.

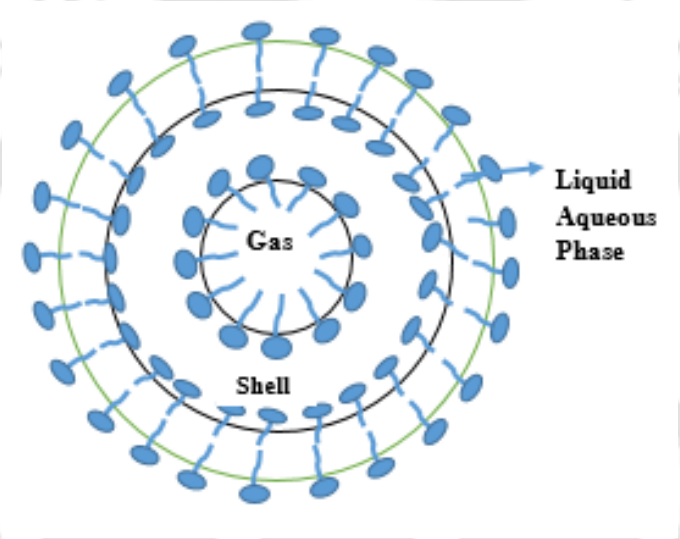

Figure 1.2. Schematic diagram of the structure of charged microbubbles proposed by Sebba (1987).

1.1.4. Generation techniques of colloidal gas microbubble

There are numerous ways to generate colloidal gas microbubbles. A number of researches have been done to build out a generator that is able to produce microbubbles with a minimum amount of power requirement. Initially, Tsuge (2010) described the methods used to generate gas microbubbles. Some important methods of generating microbubbles are as below:

1.1.4.1. Method based on flowing liquid

Rotary liquid flow type: In this method, pressurized water is pumped to create a rotary type of flow of liquid which sequentially causes a reduction in pressure in its central axial part. Gas is automatically induced to the reduced pressure area. The air-liquid mixture then develops microbubbles due to high smashed and shears. Ohnari (2006) developed a cylindrical microbubble generator by this principle, as shown in Figure 1.3.

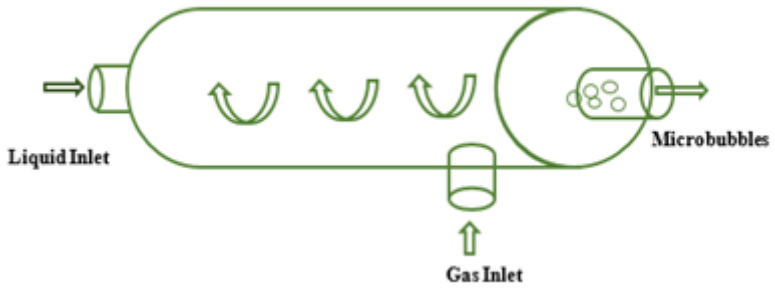

Figure 1.3. Rotary liquid flow type micro bubble generator (Terasaka et al. 2011).

Venturi type: The venturi type system can generate microbubbles using converging-diverging (venture tube) (Fujiwara et al., 2007). A schematic diagram of a venturi-type microbubble generator is shown in Figure 1.4. In this system, the flow of liquid and gas is done through the base simultaneously. It consists of an inlet section, a tubular part, a throat, and a tapered section. Both the fluids are introduced with pressure through the inlet section into the tubular part. Both the fluids are accelerated in the throat, thus, the pressure gets decreased in this part. This helps to generate microbubbles in the system. Fujiwara et al. (2003) generated about 100 μm bubbles by this method.

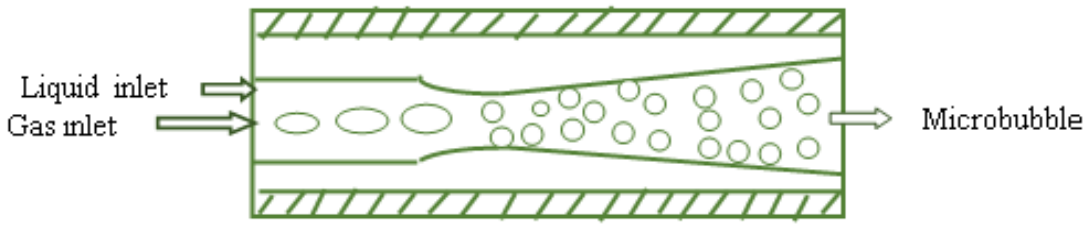

Figure 1.4. Venturi-type microbubble generator (Fujiwara et al. 2003).

Ejector type: This type of generator uses an ejector system (Terasaka et al., 2011). A converging-diverging nozzle converting the pressure energy of a motive fluid to velocity energy creates a low-pressure zone that draws in and entrains a suction gas. The gas-liquid mixer expands, reducing its velocity when the mixer passes through the throat of the ejector, as shown in Figure 1.5. The shearing of the gas-liquid mixture in turbulent flow creates microbubbles. By this method, microbubbles of the size range of about 40-50 μm can be formed. Nakatake et al. (2007) used an ejector-type microbubble generator to generate microbubbles to improve the combustion in diesel engines.

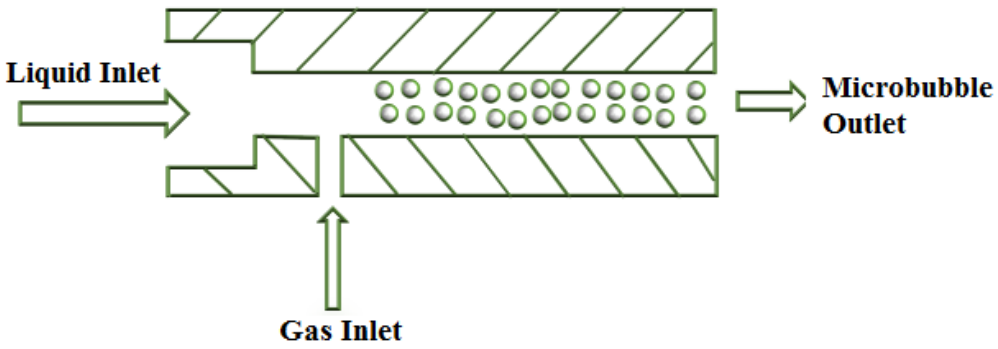

Figure 1.5. Ejector-type microbubble generator (Terasaka et al. 2011).

Pressurized dissolution type: The pressurization type of the microbubble generating system is based on Henry's law. The pressurized water is saturated with gas and then injected into the normal environment with atmospheric pressure through a nozzle; thus, the microbubbles are

formed during the sudden pressure drop. This kind of microbubble generation method has been applied to water and wastewater treatment, known as dissolved air flotation (DAF), where the air is dissolved into the water at elevated pressures of 0.4-0.5 MPa and then released through decompression nozzles to a flotation tank. The pressure difference applied in most DAF systems is at or lower than 0.4 MPa. Theoretically, the concentration of air microbubbles released from saturated water is restricted to be lower than 1/13 at 20ºC. The size range of bubbles generated by the pressurization type is 10 to 100 μm (Han et al., 1998). Moreover, the average bubble size decreases as the saturator pressure increases, but increasing the pressure has a small effect on bubble size above 0.5 MPa (Han et al., 1998).

Multi fluid mixture device: Sadatomi and Kawahara (2008) invented a new device called the multi-fluid mixture device, which can generate microbubbles and mists. As the pressurized water enters the generator, the increased velocity of water is achieved due to the presence of an orifice (Figure 1.6). Thus, the pressure a little downstream becomes negative, which causes automatic suction of air in water from the porous pipe, and creates microbubbles (Sadatomi and Kawahara, 2012).

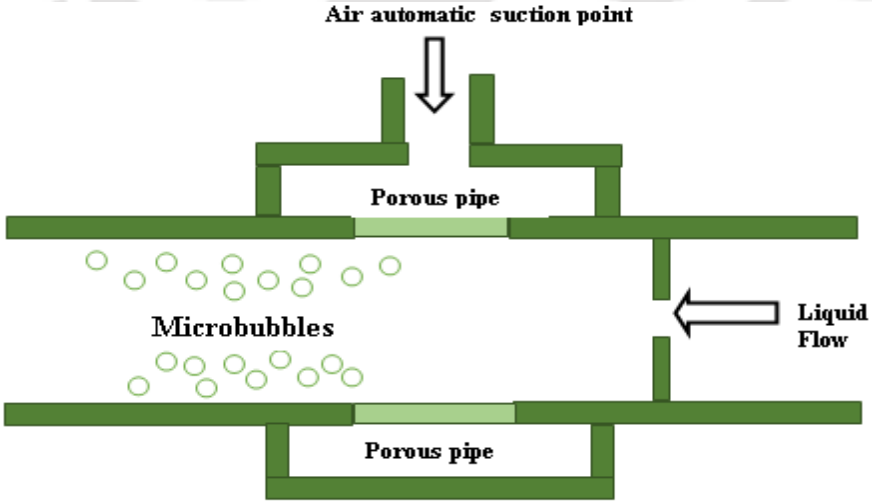

Figure 1.6. Multi fluid mixture device type microbubble generator (Sadatomi et al. 2012).

1.1.5. Characteristics of colloidal gas microbubbles

High internal gas pressure: The internal pressure of the bubble depends on the surface tension and diameter of the bubble. The internal pressure of the bubble increases with decreasing the bubble diameter. The bubble surface feels the pressure from both sides, the inside and outside. The air pressure inside the bubble is always larger than the air pressure from the outside. The magnitude of pressure difference across a curved surface can be calculated according to the Young-Laplace equation

$$\Delta P = \gamma\left(\frac{1}{R_1} + \frac{1}{R_2}\right) \tag{1.1}$$

where γ is the surface tension of the liquid, R_1 and R_2 are radii of curvature and ΔP = Pressure difference across the curve surface. If the bubble is spherical, $R_1 = R_2 = R$, then from Equation (1.1)

$$\Delta P = \frac{2\gamma}{R} \tag{1.2}$$

From Equation (1.2), it can be seen that pressure difference is inversely varying with bubble size. The smaller the bubble's size higher the pressure in inside. So inside-outside pressure difference of microbubble is very high. As the internal pressure of the microbubbles is very high as compared to macro bubbles, bubbles are strongly compressed and shrink very fast.

Bubble rising velocity: The rise of a bubble in liquid is a function of several parameters, viz., bubble size, properties of gas-liquid systems (density, viscosity, surface tension, concentration of solute, density difference between gas and liquid), liquid motion and thermodynamic conditions (temperature, pressure). Reynolds number for microbubbles is significantly less (approximately $Re \leq 1$) due to its small size. The microbubbles are almost spherical solid

spheres where the flow at the gas-liquid boundary is free. Recently most of the studies have shown that the rising speed of microbubbles (U) follows the stoke's equation as

$$U = \frac{\rho_L g D_B^2}{18\mu_L} \tag{1.3}$$

Specific interfacial area: The specific interfacial area is defined as the interfacial area per unit volume of dispersion. The specific interfacial area is related to the mean bubble diameter and the gas holdup, which is represented by

$$a = \frac{6\varepsilon_g}{d_b} \tag{1.4}$$

where a is the specific interfacial area, ϵ_g is the gas hold up, and d_b is the mean bubble diameter.

Charge on microbubbles: Microbubble dispersions are generated by different methods using surfactant solutions. While generating microbubbles, the air gets entrained into the solution, resulting in a white microbubble dispersion.

Microbubbles have the advantage that, unlike conventional bubbles, they form a stable dispersion and can be pumped like a liquid without collapsing. Microbubbles can exhibit a charge depending on whether or not the surfactant carries a charge. For example, anionic surfactants such as sodium dodecyl sulphate (SDS) form negatively charged microbubbles, and cationic surfactants, such as dodecyl trimethylammonium bromide (DTAB), form positively charged microbubbles. The charge exhibited by microbubble suggests that electrostatic interactions can be exploited in order to obtain a selective separation from a mixture of materials. The knowledge of bubble charge in aqueous solutions is important in many areas, namely, food processing, mineral processing, and water and wastewater treatment. The charge of bubbles determines their interactions with solid particles, oil droplets, and other bubbles.

The charge density of the microbubbles and signs depend on the chemistry of the solution in which gas bubbles are formed. The mechanism of charge involves the asymmetric dipoles of water molecules residing at the gas-liquid interface (Engel et al., 1997; Paluch, 2000). Other mechanisms responsible for bubble surface charge may include adsorption of ions, residual surfactants, dissociation of ionic groups, and charge separation (Hunter, 2013). The most likely charging mechanism involves the asymmetric dipoles of water molecules residing at the gas-liquid interface (Engel et al., 1997; Paluch, 2000). Adsorption of ions, residual surfactants, dissociation of ionic groups, and charge separation other mechanisms are responsible for bubble surface charge (Hunter, 2013).

Stability of microbubbles: Stability is the most important feature of colloidal microbubbles, which can be generated externally in accordance with their use and then can be transported by pumping. The effectiveness of colloidal microbubbles in separation processes depends on their stability. For the application of colloidal microbubbles in separation technology, its stability investigation is highly significant for its characterization (Yan, 2005).

Microbubbles are thermodynamically unstable. The stability of conventional aqueous foams is determined by the rate at which liquid drains from foam and the rate of foam breaking (Jacobi et al., 1956), as the stability of colloidal microbubbles can be described by three-phase drainage mechanisms (Feng et al., 2009). Liquid drainage rate is the fundamental parameter for determining stability due to the absence of bubble breakdown prior to the majority of liquid being drained from dispersion (Feng et al., 2009). The stability of microbubbles mainly depends on gas dissolution, bubble size, temperature, and concentration of surfactants due to their influence on liquid viscosity and viscous drag, mechanical properties of lamellar walls, and bubble coalescence.

Zeta potential of microbubble: Zeta potential is a parameter characterizing electrochemical equilibrium on interfaces. It depends on the properties of liquid as well as on the properties of the surface. It plays an important role in the theory of aggregative stability-DLVO theory (Derjaguin and Landau, 1993). Electrostatic repulsion between particles depends on the value of zeta potential. The higher the zeta potential, the stronger the repulsion and the more stable the system becomes. The electrostatic natures of both bubbles and particles are important parameters in particle removal by microbubble flotation (Han and Dockko 1998). Measurements of bubble zeta potential in the presence of polymers are relevant to the flotation of ores and pollutant removal in water and wastewater treatment. The zeta potential is determined by the Smoluchowski equation (Equation (1.5)) (Takahashi, 2005)

$$\zeta \equiv \frac{\mu}{\varepsilon_r \varepsilon_o} \frac{v_e}{E} \tag{1.5}$$

where ζ is the zeta potential (V), μ is the dynamic viscosity of the electrolyte solution (Pa.s), ε_r is the relative dielectric permittivity of the liquid, ε_e is the dielectric permittivity of vacuum, v_e is the electrophoretic velocity (m/s) of particle and E is the strength of the applied electric field (V/m).

1.1.6. Physics of particle attachment and detachment on colloidal gas microbubble

Flotation is a physicochemical process that uses air bubbles to separate particles based on their differences in surface properties involving three phases (solids, water, and froth). Flotation depends on the ability of bubbles to collect particles from the suspension and carry them to the froth phase and the concentrate launder. Usually, the surface of the wanted minerals is rendered water-repellent (hydrophobic), which allows the particles to attach themselves to air bubbles while leaving the surface of the unwanted particles water-wetted (hydrophilic) not attachable

to air bubbles. The attached particles are separated from the suspension of unwanted minerals by the bubble rise.

The bubble–particle encounter interaction is determined by the physics of the particle and bubble motions and the hydrodynamics of liquid flow and has been studied most extensively. The bubble-particle collection determines the attachment of the hydrophobic particles to bubbles by the formation of a finite contact angle at the three-phase gas-liquid-solid contact line. The collection involves a number of bubble-particle interaction sub-processes, which can be divided into as shown in Figure 1.7.

a) Collision

b) Attachment

c) Detachment and stability of bubble-particle aggregates

The capture of particles by rising bubbles is the central process in froth flotation. For efficient capture to occur between a bubble and a hydrophobic particle, they must first undergo a sufficiently close encounter, a process controlled by the hydrodynamics governing their approach in the aqueous environment in which they are normally immersed. They should approach quite closely within the range of attractive surface forces. The intervening liquid film between the bubble and the particle will drain, leading to a critical thickness at which rupture occurs. This is then followed by movement of the three-phase contact line, the boundary between the solid particle surface, receding liquid phase, and advancing gas phase until a stable wetting perimeter is established. This drainage, rupture, and contact line movement sequence constitutes the second attachment process. A stable particle-bubble union is thus formed. The particle may only be dislodged from this state if it is supplied with sufficient kinetic energy to equal or exceed the detachment energy, i.e., the third process of detachment can occur. The capture or collection efficiency E of a bubble and a particle may be defined as

$$E = E_c \times E_a \times E_s \quad (1.6)$$

where E_c is the collision efficiency, E_a is the attachment efficiency, and E_s is the stability efficiency of the bubble-particle aggregate. This dissection of capture efficiency into three process efficiencies was used by Derjaguin and Dukhin (1993) and focused attention on the three zones of bubble-particle capture where, in order, hydrodynamic interactions, interfacial forces, and bubble-particle aggregate stability are dominant, as illustrated in Figure 1.7. We should note that these zones are not completely discrete, rather, they grade into one another. Since surface forces are relatively short range, they do not significantly influence the collision step. This is why collision and attachment may be treated as essentially independent processes.

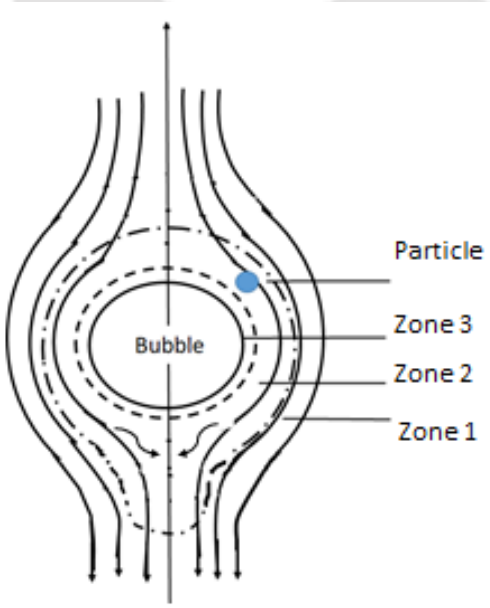

Figure 1.7. Hydrodynamic 1, diffusiophoretic 2, and surface force 3, zones of interaction between a bubble and a particle (Derjaguin and Dukhin, 1993).

Attachment: An intervening liquid film during the bubble–particle attachment is formed in which interfacial forces and micro-hydrodynamic resistance at a short inter-surface separation

distance become important, governing further stability of the liquid film between the gas-liquid and solid-liquid interfaces. The destabilization of the liquid film is caused due to the total interfacial force between a hydrophobic particle and an air bubble. Here the liquid film begins to be unstable and ruptures, which leads to the development of a three-phase contact line and attachment of the bubble. The bubble-particle contact undergoes a continuous change further across the particle surface at a certain rate to form a stable wetting perimeter. The three-phase contact expansion initiated during the rupture of the film leads to an equilibrium state, governed by the dewetting dynamics and the properties of the gas-solid, gas-liquid, and liquid-solid interfaces. The three steps of bubble-particle attachment are illustrated in Figure 1.8.

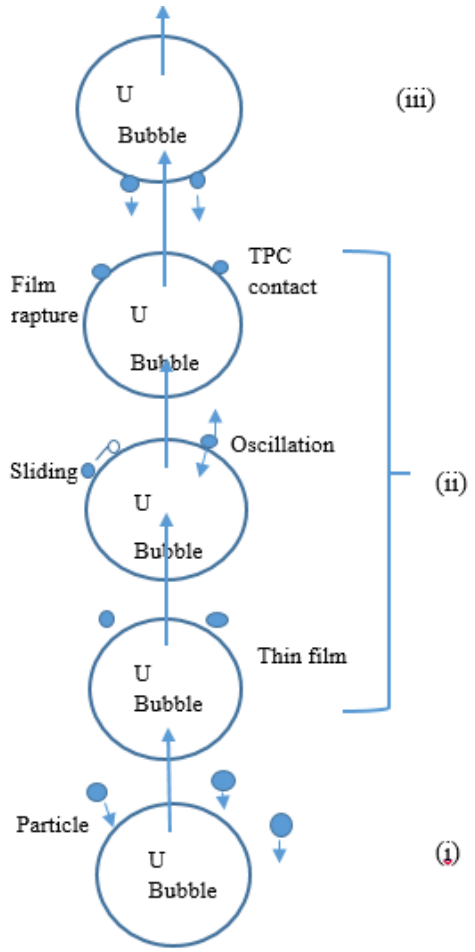

Figure 1.8. Sub-processes of particle collection by an air bubble as it rises through the pulp: (i) collision, (ii) attachment, and (iii) stabilization of particle-bubble aggregates with respect to external stresses.

Stability and Detachment: The stability of gas microbubble is one of its important characteristics. The stability of the gas bubble is determined to know the adhesive force which acts on the attached particle to check the particle detaching from the bubble surface. The dynamic forces which exist in the flotation cell also affect the stability of the bubbles.

1.1.7. Rate of recovery by microbubble flotation based on conventional flotation

The rate of recovery of minerals in flotation relies on the contribution of three factors: (1) the engineering contributions, i.e., the design of the flotation cell, (2) the hydrodynamic conditions inside the flotation cell, e.g., bubble velocity, density, turbulence, and (3) the process of

particle–bubble interaction. To recover minerals, particles need to first collide with a bubble (collision efficiency, *Ec*), secondly, attach to the bubble (attachment efficiency, *Ea*), and finally, form a stable particle-bubble aggregate capable of rising to the top of the flotation cell (stability efficiency, *Es*). These sub-processes, in turn, depend on both the hydrodynamic conditions (*Ec* and *Es*) and the surface chemistry of the mineral particles (*Ea* and *Es*) **(**Duan et al. 2003).

1.2. Importance of the research area

1.2.1. Applications of microbubbles in the field of water and wastewater treatment

Microbubbles have the most remarkable property, their ability to decrease in size and collapse under water, whereas ordinary macrobubbles rapidly rise and burst at the surface. This phenomenon shows the significant capacity to develop the use of microbubbles in different fields with numerous applications. The surface tension causes the increase in the interior gas pressure of the microbubble, along with the shrinkage of microbubbles. While the increase in the ion concentration accumulates on the gas-liquid surface (Takahashi, 2005; Takahashi et al., 2007; Takahashi et al., 2003). Takahashi et al. (2003) demonstrated that microbubbles could be useful in the formation of gas hydrates due to their ability to alter the nucleation conditions and their efficient gaseous solubility. Due to immense human activities, the load of pollutants has increased significantly. This generates huge amounts of nutrient and oxygen-demanding substances, such as organic matter, and brings various negative impacts to the natural environment of rivers and oceans. Microbubble aeration technology can be a countermeasure against water quality problems-for example, to prevent deoxidation in reservoirs and for the treatment of leachates from garbage-dumped landfills.

1.2.2. Application of soil improvement using microbubbles

Soil liquefaction disaster is caused by seismic shocks, which are added to the loose sandy ground under the groundwater level. Soil liquefaction is a major engineering interest for geotechnical engineers in earthquake countries. In Japan, because most of the built-up area is concentrated on the alluvial plain and soft ground, soil liquefaction is one of the latent threats. It is well known that a soil's liquefaction resistance increases as the soil's saturation degree decreases (Yoshimi et al., 1988), so it is reasonable to say that the saturation decreased ground would be able to prevent seismic damage to buildings and infrastructures.

1.2.3. Environment-friendly cleaning technology using microbubbles

The conventional cleaning methods face the challenge of separating the pollutant from the solvent due to the high affinity of the solvent and removed substances. This difficulty can be overcome by the use of the microbubble cleaning method. Miyamoto et al. (2008) have found that the key characteristics of bubbles having hydrophobic surface and buoyancy overcome the fundamental challenge mentioned above. Using the environment-friendly cleaning technology with the help of microbubbles, the following industrial problems can be interpreted:

- For the cleaning purpose of semi-conductor and liquid crystal panel fabrication along with degreasing in electronic fabrication units.
- The reduction of fuel consumption, smoke, and harmful emissions, including PM (particulate matter) of diesel engines using micro and nano air bubbles mixed in gas oil.

In fine-structured equipment manufacturing, cleaning is one of the most important processes to determine the qualities of the materials and products. These processes cause pollutions for which environmentally friendly cleaning technologies are developed and commercialized, such as ionized water cleaning, functional water cleaning, and ultrasonic cleaning. The utilization of ionic microbubbles is a new technique for cleaning and can be used in various fields, which

are summarized in Table 1.1. In the electronics manufacturing cleaning processes, the commercialization of the microbubble method is reported to apply the degreasing process that consumes a large amount of solvent. The development of an environmentally friendly anti-bubble coalescence enables high-density bubbles with high cleaning and separation abilities based on a large surface area.

Table 1.1. Utilization of ionic microbubbles (a new technique) in various areas.

Surfactant	Applications	References
Ethyl-Hexa-decyl-tri-methyl-ammonium bromide and SDBS	The removal of metals (copper, zinc, nickel, chromium, and lead) from wastewater.	Ciriello et al. (1982)
CTAB	Removal of Cu (II) ions and iron hydroxide as a precipitant.	Caballero et al. (1989)
CTAB	Removal of methyl orange.	Caballero et al. (1989)
HTAB	For removal of methyl orange from 2-octanol.	Caballero et al. (1989)
Anionic Surfactant	To clarify a palm-oil-mill effluent that contained fibers and plant-cell debris.	Subramaniam et al. (1990)
CTAB and SDBS	Removal of synthetic dyes (methyl orange, Cibacron-6B, Cibacron-4G, and methylene blue) from wastewater.	Roy et al. (1992)
TTAB, SDS	Removal of organic pesticides (for the removal and mobilization of 2, 4 dichloro phenoxy acetic acid (2,4-D), a synthetic auxin hormone used widely as a herbicide, from contaminated soil).	Roy et al. (1992)
Soapnut solution	Removal of HCB and naphthalene.	Roy et al. (1992)

Sapindusmukurossi	To flush HCB-contaminated soils.	Kommalapati et al. (1998)
SDS	For in situ flushing of subsurface soil to remove oily waste.	Roy et al. (1994)
SDS HTAB	The removal of Naphthalene and hexachlorobenzene (HCB).	Roy et al. (1995)
TTAB	Removal of cellulose fiber from paper-mill wastewater.	Hashim and Gupta (1998)
HTAB and SDBS	The separation of organic dyes from wastewater.	Roy et al. (1992)
Triton SP-190	To remove n-pentadecane from a contaminated.	Chang et al. (2000)
Protein base	For the delivery of microbes, nutrients, and oxygen to treat hydrocarbon-contaminated soil.	Ripley et al. (2000)
HTAB and SDBS	For removal of methyl orange and methylene blue dyes from water.	Basu et al. (2001)
AOT	For separating lactoferrin and lactoperoxidase from sweet.	Fuda et al. (2004)
SDS, HTAB	Removal of suspensions of fine particles from water.	Mansur et al. (2004)
HTAB SDBS	The flotation of magnesium hydroxide (particle size 2.3–9m) and polystyrene.	Elmabruk et al. (2005)
Rhamnolipid	Remediation of heavy metal-contaminated soil.	Mulligan and Wang (2006)
CTAB and SDS	For removing dust composed of fly ash, wheat flour, and powder of polyvinyl chloride from the air.	Jarudilokkul et al. (2008)

SDS	To separate CuO from SiO2 and compare the results with conventional batch flotation using air bubbles.	Waters et al. (2008)
SDS, CTAB	Removal of pentachlorophenol.	Chaphalkar et al. (1994)
CTAB	For recovered astaxanthin, a natural xanthophyll antioxidant, from the cells of Phaffiarhodozyma.	Dermiki et al. (2008)
Saponin	To enhance aerobic biodegradation of phenanthrene in a sand column.	Choi et al. (2009)
CTAB, SDS, TWEEN 60	For the recovery of astaxanthin from an aqueous solution.	Dermiki et al. (2009)
Sapindusmukorossi (Soap nut)	Removal of arsenic from Contaminants soil.	Mukhopadhyay et al. (2015)
Sapindusmukorossi (Soap nut)	To recover pulp fibers from paper machine backwater in a flotation column.	Mukherjee et al., 2015)

1.2.4. Chemical process synthesis

In the engineering field, much research has been done to use microbubbles to enhance the process economically and environmentally friendly. The microbubbles in the engineering field can be used in material production; one micron or less foamed polyurethane can be obtained by mixing with air microbubbles. This polyurethane has obtained a light reflectivity of 90% or larger. Aldehyde microbubbles can be used to obtain novolac-type phenolic resin. Oxygen microbubbles can be used to synthesize rod-like particles made from ferric hydroxide having small size distribution (Daiguji et al. 200). The studies are continued for gas absorption and gas-liquid reaction, where CO_2 has generally been used as microbubbles. The development of

a compact reactor for neutralization of alkaline wastewater and the retaining of carbon dioxide in the ground by the systems has been recently studied.

1.2.5. Food processing

The food industry is constantly looking for functional ingredients to make healthy products that are liked by consumers and have preferred sensorial and textural properties. To attain the consumer's aspects along with the environmental issues, bubble technology is used to fulfill them. The physical properties, appearance, and texture of the food can be maintained even after the use of microbubble or micro-nano bubble (MNB) technology. The various applications of MNB technology in the food industries are (Tsuge H., 2010):

- Control of dissolved oxygen using MB treatment
- Separation or degradation using MB treatment
- Sterilization using MB treatment

1.2.6. Agriculture, marine, and stock-raising fields

The rapidly growing population of our planet brings new challenges to global food security. New and innovative solutions are required in the current agricultural practices to meet the future demand for cheaper and better quality food. Hydroponic agriculture is one of the current agricultural practices which provide high productivity and require limited cultivation space (Tsuge H., 2010). Hydroponic agriculture uses nutrient solutions for agriculture, and their disposal after the usage may result in an environmental imbalance, and thus, it may cause infectious disease via roots.

1.2.7. Application in mineral beneficiation

Flotation is found to be one of the best available techniques for the separation of fine particles. The particle recovery depends on many factors like the solids content of the pulp and the

hydraulic regimes in the cell, particle size distribution, the bubble population, and the concentration of frother (Bergh and Yianatos, 1993; Tuteja et al., 1995). The dominant physical factor in flotation is particle size and bubble size, so microbubbles are desirable for fine particle flotation.

Chapter 2

2. Literature Review and Formulation of Research

This chapter reports the literature review on the hydrodynamics of microbubble flow such as stability, holdup, size distribution, rheology and turbidity behavior, dispersion characteristics and its transport processes like entrainment characteristics, the recovery efficiency of minerals and its kinetics in the mineral beneficiation are described.

2.1. Literature survey

2.1.1. Rheological behavior of the microbubble in particle-laden solution

Various effects govern the rheological behavior of the microbubble during its flow. From the literature, it is found that the microbubble suspension in the liquid behaves like a shear-thinning liquid (Parmar and Majumder, 2014). The rheology is affected by the different physical properties of the liquid in which the microbubble is produced. Larmignat et al. (2008) studied the effect of surfactant concentration and pipe shape and size on the rheological properties of microbubbles. They observed no change in microbubble morphology during their flow in the pipe. They also have reported that the pipe shape and diameter do not affect the microbubble's rheology. Microbubble's were considered a shear-thinning fluid. An increase in the concentration of surfactants caused the shear stress to increase for a given apparent shear rate. They obtained good results with theoretical models and suggested the following correlation

$$\tau^* = C(x)(Ca^*)^{2/3} \qquad (2.1)$$

where τ^* is the dimensionless volume equalized shear stress, $C(x)$ is a constant that $C(x)$ increases with surfactant mass fraction x, and Ca^* is the capillary number. The effective viscosity of microbubbles given by

$$\mu_e = C(x)\mu_1(Ca^*)^{-1/3} \quad (2.2)$$

where μ_e is the fluid effective dynamic viscosity and Ca^* is the capillary number, which was followed by the standard friction factor for microbubbles under laminar flow conditions. $f = 16/\mathrm{Re}_D$. Shams et al. (2014) studied the viscosity and rheological behavior of microbubbles in capillary tubes. They performed the experiments in tubes of different diameters and lengths, with a constant microbubble concentration and viscosities. With a decrease in the tube diameter and an increase in tube length, the viscosity of microbubbles decreases. Furthermore, the viscosities of the suspensions were found to increase with an increase in the bubble void fraction. They concluded that, in the bubble size range of 1–12 μm, the size distribution of bubbles did not influence the viscosity of suspensions and found that the power-law was unable to predict the microbubble's behavior in capillary tubes with different bubble void fractions. They developed a correlation to predict the viscosity of microbubbles flowing through capillary tubes from the experimentally obtained data, which was capable of predicting microbubble viscosity in the range of Re_c <50. Their results showed that the microbubble suspensions were viscoelastic, exhibited power-law behavior, and determined the relationship between the air fraction of the suspension and fluid viscosity. Denkov et al. (2009) reviewed the role of surfactant type and bubble surface mobility in foam rheology. They focused on the viscous friction between bubbles in steadily sheared foams and between bubbles and confining solid walls. With the help of a large set of experimental results, they demonstrated that the two qualitatively different classes of surfactants could be distinguished. One is the synthetic surfactants (such as sodium dodecyl sulfate) showed low surface modulus and fast relaxation of the surface tension after a rapid change of surface area, and the other surfactants (such as sodium and potassium salts of fatty acids, for example, alkyl carboxylic acids) exhibits high surface modulus and relatively slow relaxation of the surface

tension. The authors concluded that the second class of surfactants significantly leads to higher viscous stress and different scaling laws of the shear stress vs. shear rate in flowing foams. They also discussed the process of bubble breakup in sheared foams (determining the final bubble-size distribution after foam shearing).

Tchuenbou-Magaia and Cox (2011) investigated the tribological behavior of micron-sized air cells (microbubbles) coated and stabilized by proteins (0.5-10μm) produced sonochemically using different cysteine-rich proteins (hydrophobin, bovine serum albumin, and egg white proteins). The low-fat emulsion-based products were produced by suspension of air cells termed “air-filled emulsions” (AFEs). This study explored the tribological behavior of AFEs and a triphasic A/O/W emulsion-based prototype salad dressing. Different results were found for BSA-AFE and EWP-AFE for tribological measurement of AFEs, indicating that the very nature of the protein plays a crucial role. No direct conclusive results for AFEs were found, but some indication of their contribution to lowering the friction was seen. It was postulated that AFEs may contribute to lower friction in several ways.

Ziaee et al. (2015) reviewed the Herschel-Bulkley rheological parameters of lightweight colloidal microbubble-based fluids. They stated that it is crucial to understand the rheological characteristics of a colloidal microbubble in the determination of the performance of the fluid in order to maintain the most effective fluid properties for safe, efficient, and economical drilling operation.

A concise investigation was presented on the effect of concentration of the three main components of a novel environmentally friendly lightweight colloidal microbubble-based fluids, i.e., xanthan gum biopolymer, starch, and biosurfactant, to the Herschel-Bulkley rheological model parameters. Yield stress, fluid consistency, and fluid flow index are the three parameters of the Herschel-Bulkley model, which were calculated by fitting the experimental

data of shear stress as a function of the rate of shear to the model. They analyzed that the Herschel-Bulkley model performed satisfactorily and described the rheological behavior of colloidal microbubble-based fluids. The authors concluded that an increment of the amount of the three main components increased the yield stress of the final colloidal microbubble-based fluid as the flow resistance was increased and showed that fluid consistency depends on the presence of xanthan gum and starch. They determined the shear-thinning thinning behavior having a value of fluid flow indices (*n*), i.e., 0.2-0.3, to formulate colloidal microbubble-based fluids, which was also helpful in determining the appropriate procedure for utilizing the colloidal microbubble-based fluids in oilfield operations.

In the various application of microbubbles, it is necessary to understand the rheological behavior associated with its flow in the device. Parmar and Majumder (2014) investigated the rheological behavior of the flow of a microbubble suspension in a surfactant solution through a horizontal pipe and developed a model based on wetting effects in microbubble suspensions. They found that the effective viscosity of the microbubble suspensions decreased with apparent shear rate, indicating that microbubble suspensions behave as shear-thinning non-Newtonian fluids, and an increase in surfactant concentration caused a decrease in shear stress and effective viscosity with shear rate.

2.1.2. Holdup, the size distribution of microbubbles in particle-laden solution

The gas holdup is one of the most important parameters in microbubble transport processes and thus, has been extensively studied. Miller (1980) investigated gas holdup and pressure drop in bubble column reactors diameter was 0.229 m and height of 9.14 m with air and four different liquids in concurrent upflow. The authors used perforated plates with 0.00635 m holes and 2.85% open area inserted at 1.524 m spacing for half of the experiments. They developed

relationships with and without plates for vessel diameters larger than 0.15 m and two-phase Froude numbers under 0.05.

Cheng and Lemlich's (1983) approach was to generate a microbubble of distribution of bubble sizes in a vertical glass column and then examine it photographically at the glass wall. The authors determined the bubble size by planimetric measurement of the area of the contact face at the glass wall of a column containing the homogeneous form and concluded that the unadjusted measure of bubble size at a wetted boundary wall was a reliable way of determining the actual bubble size. A significant error occurred in interpreting the bubble size at a wetted boundary wall.

Engelsen et al. (2002) investigated the bubble size distribution of microbubbles by image analysis and studied the influence of several physical parameters on bubble size. The pictures were taken with a Nikon CCD camera and recorded directly onto a personal computer, and the pictures were analyzed with commercially obtainable software. For the analysis, the parameters such as the nature of the surfactant, liquid viscosity, solid-phase content, and rotational speed of the mixer were varied. The analysis was based upon the shape, location, and dimensions of the individual images. The authors concluded that all the parameters influenced the bubble size and its distribution to a certain extent.

Rodrigues and Rubio (2003) developed a new method to measure the bubble size distribution based on the bubbles capturing an image (with movement) with the combination of a microscope and digital image processor. The authors employed LTM-BSizer to draw bubbles rising in a column through a special viewing chamber and exposed them to a digital camera, which was helpful in overcoming the errors due to the movement of bubbles, focused illumination, photographic speed, and bubbles overlapping. The authors obtained good correlation results with the values reported with the traditional image analysis method and

showed that using this technique, accurate size distributions were produced conveniently and efficiently. The authors concluded that the bubble size measurement technique developed by them assisted in understanding and improvement of the DAF and conventional fines and ultrafine mineral flotation from both theoretical and practical viewpoints.

Coutoa et al. (2008) studied the production and characterization of colloidal microbubbles for subsequent application in the separation process. They studied the generation and characterization by air injection through surfactant solution and by high-speed stirrer when surfactant solution was submitted to a high shear rate in the presence of air. They found that the colloidal microbubble contained gas (gas hold-up) in the range of 30-60%, while conventional foams contained up to 90%.

Parmar and Majumder (2014) investigated the gas holdup in microbubble-aided aeration systems and found that the volume of the liquid before and after bubbling did not change markedly when the gas holdup was measured by the phase isolation method. Due to this reason, they used the electrical conductivity method to measure the gas holdup with more accuracy at different concentrations of surfactants. They found that the concentration of surfactants played an important role in the microbubble suspension and concluded that gas holdup increases with surfactant concentration.

2.1.3. Stability and zeta potential of microbubble

Yoon and Yordan (1986) investigated the zeta potential of microbubbles of size range 40 to 80 μm by means of a simple micro-electrophoresis technique. The authors used a Rank Brothers particle micro-electrophoresis apparatus to determine the mobilities of microbubbles. Generally, the sign of the bubble charge is determined by the polar head of the surfactant when an ionic surfactant is used, while in the presence of non-ionic surfactants, bubbles' charge can be either positive or negative depending on the pH. They concluded that an increase in the

concentration of ionic surfactants results in an increase in bubble charge due to a change in zeta potentials, while with nonionic surfactants, the zeta potentials change little with the concentration and hence the charge of the bubble does not change significantly. Lye and Stuckey (1998) investigated the structure and stability of microbubbles using different experimental techniques, i.e., cryo-TEM, DSC, and light scattering. The structural model proposed by Sebba (1987) was supported by their findings. Microbubbles were termed as colloidal gas aphrons (CGAs) when gas was used to get encapsulated inside the bubble and colloidal liquid aphrons (CLAs) when liquid was used to get encapsulated inside the bubble. They investigated the stability of CLAs dispersed in a stirred vessel over a range of continuous phase ionic strengths, pH, and temperatures by the first-order half-life method for the first time. These enabled them to compare the stability of CLAs when dispersed under various conditions and the influence of including various concentrations of lipase or erythromycin-A in the aphron formulation. They proposed a mechanism for the breakdown of dispersed CLAs structure, which involved destabilization and loss of the “soapy shell.” The authors applied the light scattering technique to the study of dispersed CLAs and found that the most stable CLAs were formed from relatively non-polar solvents (decanol>octanol>butyl acetate) and non-ionic surfactants having high HLB numbers (Atlas G1300>Softanol 120 Softanol 30). Matsushita et al. (1992) and Sebba (1987) studied the influence of pH, surfactant type, the concentration of surfactant, stirring speed, and duration on the CGAs' half-life and found that stable polyaphron had half-lives of the order of months or even years. At the same time, Chaphalkar et al. (1993) applied a light scattering technique to investigate the influence of surfactant type and its concentration in the continuous phase on the stability of dispersed CGAs and analyzed that the CGA half-lives vary between 4 and 10 min.

Han and Dockko (1998) investigated the zeta potential variation of bubbles and floc with pH. In dissolved air flotation, the effects of several operational parameters were investigated. The

effect of pH and mixing time on the removal efficiency was also presented. During the investigation, it was found that all the phenomena could be explained primarily from the electrostatic nature of bubble and particle and secondarily from the effect of particle size. Dai and Deng (2003) studied the stability and characterization of colloidal microbubble dispersions. Colloidal microbubbles have been characterized with various techniques in terms of the stability and size distribution of microbubbles in solution. The stability of colloidal microbubble was studied by measuring the drained volume of liquid CGAs with respect to time (Longe, 1989). The rate of rise of bubbles was analyzed in a measuring cylinder and showed that it was equivalent to that of the hindered rising of a 35-μm spherical bubble with a 0.75-μm outer shell (Amiri and Woodburn, 1990). Jauregi et al. (2000) made a modified model to account for the variation in microbubble diameter with time.

Takahashi (2005) investigated the electrical properties of the gas-water interface electrical charge. The authors investigated the zeta potential of microbubbles in aqueous solutions and revealed that the bubbles were negatively charged under a wide range of pH conditions. They found positive potential under strongly acidic conditions, and the inorganic electrolytes decreased the potential by increasing the number of counterions within the slipping plane. The authors found that OH(-) and H(+) are crucial factors for the charging mechanism of the gas-water interface, while other anions and cations had secondary effects on the zeta potential because counterions were attracted by the interface charge. They added a small amount of propanol and butanol, considering the mechanism of the gas-water interface charge, which provided significant information. Knowing that the alcohols have no electrical charge even though they found the alcohols had a strong effect on the gas-water interface charge and dispersed the zeta potential of the microbubbles in the aqueous solution. The alcohols tended to get adsorbed to the interface and affected the hydrogen-bonding network at the interface, which enabled the author to conclude that the gas-water interface electrical charge must be

related to the difference in the construction of the hydrogen-bonding network between the bulk water and the gas-water interface. Shen et al. (2008) investigated the stability, and rheological behavior of concentrated monodisperse food emulsifier coated microbubble suspensions. The authors produced nearly monodispersed populations of microbubbles in the size range of 120-200μm using flow focusing with a food-grade emulsifier. They controlled the size of the microbubbles by changing the relative flow rates of the gas and the liquid. The emulsifier used consisted of a mixture of monoglycerides, diglycerides, and sodium stearoyl lactylate in combination with polyethylene glycol (PEG)-40 stearate. The emulsifier formed a thin shell that stabilized the microbubbles. The microbubbles are stable over time, with their sizes remaining roughly constant over two hours. Such stability allowed suspensions of microbubbles to be formed and their rheological properties to be tested. The sizes of the microbubbles were monitored offline while testing, examining the effect of shearing on the bubble sizes, as well as their stability over time. Moshkelani and Chalkesh (2008) investigated the electrical conductivity (EC) of colloidal gas aphron (CGA) suspensions for anionic and cationic surfactants (Sodium Dodecyl Sulfate (SDS) and Tetradecyl Trimethyl Ammonium Bromide (TTAB)). Experiments were done for different concentrations of SDS (6, 8.1, 10 mM) and TTAB (2, 3.51, 5 mM). The authors measured the EC using a 1 litre measuring cylinder and observed CGA drainage. They observed the drainage process has a four-phase mechanism in place of three conventional phases. The drainage process was divided into absorption, macroscopic, bubble, and microscopic phases instead of surfactant concentration and type of surfactant. The authors found no change in the drainage rate at the end of the bubble phase, with the maximum value at the end of the absorption phase. They concluded that electrical conductivity was a more sensitive property for studying microbubble characterization. Hasegawa et al. (2008) investigated the electrical potential of microbubbles generated by shear flow in a pipe with slits. The authors developed a compact and low-power microbubble

generator in which microbubbles were generated by inducing local shear stress in the flow of water through a pipe with slits. The authors used three types of models in order to investigate the effect of slit angle on the purification technique. They found that the proposed microbubble generator with the slit angle $\theta = 60^{\circ}$ showed superior performance for the water purification technique in comparison with the other two models. The authors concluded that microbubble generation was affected by slit angle and also investigated the electrical property of the gas–water interface and the ζ-potential of microbubbles by electrophoresis. They show the results of the floatation experiments were affected by the ζ-potential of the microbubbles. Oliveira and Rubio (2011) studied the zeta potential of microbubbles in the presence and absence of different polyacrylamides. The microbubbles were generated by injecting pressurized air into water or solutions of cationic, anionic, amphoteric, or nonionic polymers at a constant pressure of four atmospheres. A modified micro-electrophoresis glass cell was used to measure the charge of the bubbles at the shear-zeta plane at varying pH (2.0–12.0). The authors found the anionic, amphoteric, and nonionic polymers increased the negative charge of the bubbles, but the isoelectric point (IEP) remained constant at about pH 2.0, whereas in the presence of the cationic polymer, the bubbles exhibited positive surface charges between pH 2.0 and 8.0 and an IEP of pH 8.0. The authors concluded the existence of an important interaction mechanism between air bubbles and polymeric macromolecules, especially in the treatment of wastewater by flocculation followed by dissolved air flotation (DAF).

The zeta potential of microbubbles has been determined experimentally, and many studies have been published reporting bubble charges in different electrolytes and frother solutions. The results of several of these important contributions are summarized in Table 2.1.

Table 2.1. Zeta potential of bubbles at the air/water interface-a summary and a brief description of selected studies.

Authors	Brief description
Collins et al. (1977)	Zeta potential of very small gas bubbles generated by electrolysis in a microelectrophoresis cell in the presence of cetyltrimethylammonium bromide (CTAB) and sodium sulphate solutions.
Usui et al. (1981)	Measurements of the sedimentation potential (Dorn effect) of argon bubbles generated by fritted-glass-sphere gas diffusers dispersers were used to evaluate the effects of bubble size on their zeta potential in sodium hexadecyl sulphate, butanol, aqueous solutions, and distilled water.
Kubota et al. (1983)	Determination of the zeta potential of air bubbles, generated by a DAF method, in surfactant solutions (sodium dodecyl benzene sulphonate, sodium dodecyl sulphate, and cetylpyridinium chloride).
Yoon and Yordan (1986)	The zeta potential of microbubbles (microelectrophoresis), generated by a microfoam method, was measured in different concentrations of anionic, cationic, and nonionic surfactants in aqueous solutions over a wide pH range.
Han and Dockko (1998)	Zeta potential of air microbubbles, formed as in a DAF technique, using a microelectrophoresis cell with a video camera. The study investigated the effect of bubble charge on the removal efficiency of solid particles using a coagulant over a wide pH range.
Yang et al. (2001)	The Microelectrophoresis technique coupled to a video camera was used to measure the zeta potentials of oxygen and hydrogen bubbles generated by electrolysis in different electrolyte solutions (NaCl, $CaCl_2$, and $AlCl_3$).

2.1.4. Entrainment characteristics of microbubble

Ross (1989) investigated the contributions made by true flotation and the entrainment of mineral particles during batch flotation tests. The author conducted laboratory-scale tests,

during which various amounts of floatable gangue materials from three different sources were substituted for the feed (a pyritic dump residue). He observed that, as the degree of feed substitution increased, the ratio of floated to entrained particles decreased, while the transfer factor and the stability and mobility of the froth increased. The author concluded that the trends obtained were independent of the origin of the gangue material and reported that an excessively stable froth increases the amount of material recovered by entrainment.

George et al. (2004) studied the entrainment in the flotation of submicron particles by fine bubbles and assessment of true flotation. Entrainment can make an important contribution to recovery in the flotation of fine particles. The authors carried out the flotation experiments in a small laboratory column-type cell with fine bubbles of about 150 µm. Cetyltrimethylammonium bromide and Dowfroth 250 were used as the collector and frother, respectively. The particle concentration in the pulp was about 1% by weight. The authors found that the total recovery of particles was low, i.e., 54% after 50 min. The authors used a new technique along with the three previously described in the literature, i.e., the method of Warren (1985), the method of Trahar and Warren (1976), and the method of Ross and Van Deventer (1988), to assess the true flotation due to the bubble-particle collection mechanism, and the entrainment. They found that the proportion of the colloidal particles recovered by true flotation was quite high, varying from about 79–86% of the total recovery. The authors also discussed the mechanisms of minimising the entrainment of the colloidal particles in the laminar flow flotation regime with fine bubbles. The authors concluded that the high efficiency of true flotation was obtained with colloidal silica due to fine bubble size. A smaller bubble size has a smaller associated wake, and hence fewer particles are entrained into the froth.

Cilex (2009) studied the effect of hydrodynamic conditions on true flotation and entrainment in a complex sulphide ore flotation by using a fractional factorial experimental design. The author used the method previously described in the literature that was applied to determine the

contributions of true flotation and entrainment in the flotation of complex sulphide ore. He conducted the kinetic flotation tests under various hydrodynamic conditions defined by some physical variables to apply the methods used earlier. Also, some of these tests were conducted in the presence and absence of a collector to evaluate the self-induced floatability. The selectivity index of the mineral species for entrainment was seen to be a suitable evaluation of the non-selectivity and efficiency of the entrainment. The author observed that the results of the size-by-size analysis of the froth products indicated the presence of the self-induced hydrophobic particles in the feed, which is important as the presence of very fine particles for accurate estimation of true flotation and entrainment in the flotation of complex sulphide ore. He concluded that a new approach would be necessary to determine the contributions of true flotation and entrainment in the flotation of a complex sulphide ore as the estimated results for entrainment in the flotation of the complex sulphide ore were misleading.

Taki and Unal (2012) studied the statistical evaluation of flotation and entrainment behavior of an artificial ore. They investigated the role of several parameters on gangue recovery in froth and the effects of frother type and collector dosage on flotation performance at pH 10. The result evaluation was done statistically by two-way analysis of variance without replicates, sample range, and sample standard deviation. The hydrophilic mineral was recovered mainly by entrainment through hydrophobization of Ca-activated quartz from tap water in the presence of Sodium oleate as collector, entrapment, and slime coating were also proposed as recovery mechanisms in the minority. The degree of gangue entrainment in froth product increases by the reduction in liberation size. On the basis of experimental results, the authors concluded that selectivity would be improved by increasing collector concentration and reducing the flotation time.

Wang et al. (2015) reviewed the entrainment mechanisms, contributing factors, and modeling in flotation. In flotation, entrainment is a mechanical mass transfer process by which particles

suspended in the water between bubbles enter the flotation froth from the top pulp region and are transferred to the concentrate. The recovery by entrainment is influenced by a number of factors such as water recovery, solids percentage in the cell, particle size distribution, slurry viscosity, froth height, froth structure, gas rate, particle density, froth retention time and flotation cell design, but the relative significance of these factors on entrainment in a flotation cell still needs to be explored. Both hydrophobic and hydrophilic mineral particles suspended in water can experience entrainment. They discussed the essential factors affecting entrainment and identified the methods for the quantification of entrainment. They reviewed the literature on entrainment models and identified their significance and usefulness in industrial applications. They concluded after going through the literature that there is a need to develop a more general model of entrainment since the current models available could not be used to predict entrainment at a changed operating or feed condition. Abidi et al. (2015) investigated the contribution of entrainment and true flotation in the overall recovery by the laboratory tests performed on a natural complex sulfide ore, provided by la Compagnie Minière des Guemassa (Morocco), and the effect of two different collectors, Potassium Amyl Xanthate (PAX) and Sodium di-isobutyl di-thiophosphinate (Aerophine 3418A), on the two contributions. The authors fitted to first kinetic model for overall recovery and true recovery and calculated modified flotation parameters to measure the flotation separation selectivity of chalcopyrite, galena, and sphalerite over gangue and pyrrhotite. The authors concluded that for the entrainment estimation, the Ross method was the most suitable in the case of complex sulfide ore with high content of pyrrhotite, whereas Trahar's (1981) method overestimates the effect of entrainment.

2.1.5. Separation kinetics of fine particle by microbubble flotation

Yoon (1993) studied the possibility of predicting the probability of bubble-particle collision over a range of bubble sizes employed in flotation practice. To predict the probability of

bubble-particle collision, stream functions are derived for the intermediate flow regime. It also predicts the probability of adhesion based on induction time measurements and the power relationship between flotation rate constant and bubble size. The rate constant obtained using smaller bubbles tended to decrease, while those obtained using larger bubbles were increased under more turbulent conditions. He suggested that the benefits of using small bubbles are best exploited under relatively inactive conditions, which are more readily obtained with columns than with mechanically agitated cells. Matis et al. (1993) inspected that many industries generate fine particles along with the product, which may cause potential environmental problems if released into the environment. These fine particles generally range from 1 to 100 μm in size, which was more complicated and consequently difficult if selective separation of fines was needed. He investigated good results for particles of a size range less than 120 μm by use of dissolved-air flotation and electrolytic flotation. Waters et al. (2008) investigated the flotation of fine particles using charged microbubbles. They generated microbubbles using a high-speed impeller and produced microbubbles of the size 50 μm using anionic surfactant SDS. Separation of copper oxide and silica powder (-10μm) was conducted using microbubbles which resulted in a CuO grade of 81.8% and a recovery of 76.5%. Mansur et al. (2006) studied the flotation of magnesium hydroxide (particle size 2.3-9μm) and polystyrene (particle size 24-300μm) by microbubbles. Optimum particle size and bubble size that gave high removal efficiency were known, along with the effect of particle size on the removal efficiency. The microbubbles formed from ionic surfactants (HTAB, SDBS) were more efficient than microbubbles formed by non-ionic surfactants (Tween 20) for the removal of fine particles. Surfactant concentration, which gave high removal efficiency, was equal to the critical micelle concentration (CMC), yielding more than 50% of magnesium hydroxide and 97% of polystyrene. Hashim et al. (2012) reviewed the microbubble's properties, generation techniques, and applications. Microbubbles have high stability due to their very small size and

thick surfactant shells, which made its application in the clarification of particles and microorganisms, protein separation, gas and nutrient transfer, and pollutant separation from water and soil matrices. Mineral separation processes by microbubble flotation have been reviewed because of their importance to contaminant removal processes. The microbubbles were found to function on the principles of bubble entrained floc flotation, electrostatic and ionic interaction, diffusion of entrapped gas, and hydrophobicity of the pollutant particles.

2.2. Formulation research

2.2.1. Scope of the research

The problem of processing fine particles is a serious concern in the mineral processing and chemical industries. Because current technology is unable to satisfactorily treat these fine particles, large amounts of valuable materials are routinely discarded as waste. For example, nearly one-third of the Florida phosphate, one-fifth of the world's tungsten, and one-half of the Bolivian tin are discarded as unrecoverable slimes. The flotation of fine particles has become particularly important in recent years as advances in grinding are allowing low-grade mineral deposits to be economically exploited. Froth flotation is a method for processing fine particles, but it becomes less efficient in making a clean separation between the desired particles and the undesired particles as the particle size is decreased. The poor recovery of fines by flotation can be attributed to the low probability of bubble–particle collision, which decreases with decreasing particle size. The decreased probability of collision between particles and bubbles can be improved by a reduction in bubble size. For this reason, various types of bubble generators have been developed that incorporate the production of microbubbles. The phenomenon of bubble formation decides the primitive bubble size in the system (which later attains an equilibrium size), whereas the rise velocity decides the characteristic contact time between the phases, which governs the interfacial transport phenomena as well as mixing.

Considerable research efforts have been devoted to advancing microbubbles technology due to various potential applications using microbubbles. However, the characteristics and behavior of microbubbles have not been completely clarified yet, because microbubbles exhibit various unique chemical and physical characteristics in engineering applications. Microbubbles expose a large interfacial area per unit volume for the adsorption of particles and can be separated easily from the bulk liquid phase because of their buoyancy and their stability enhance mass transfer. And these properties help researchers to consider its applications in various fields and flotation separation technique. However, bubble–particle interactions such as electrostatic and hydrophobic forces are important in determining the selectivity of separation. Thus, it is of practical interest to investigate the rheology, hydrodynamic characteristics, entrainment characteristics, and separation efficiency of microbubbles to enable optimum process design. There is a lack of studies on the characterization, such as stability, bubble size distribution, gas holdup, rheology, entrainment, and tribological behavior of the microbubble particle-laden solution and their effect on the fine particle separation efficiency.

2.2.2. Objective of the work

The scope of the current research work is on mineral-based colloidal microbubble and its subsequent application in the separation of fine mineral particles. The following objectives are proposed for the present research:

(1) Study the holdup characteristics and size distribution of microbubbles produced in particle-laden solution.

(2) Study the surface-active molecule adsorption characteristics of the microbubble in particle-laden solution.

(3) Study the stability of the microbubble produced in solution and its kinetic model.

(4) Study the stability of the microbubble produced in particle-laden solution and its kinetic model analysis.

(5) Study the entrainment characteristics of the submicron particle by microbubble in particle-laden solution.

2.2.3. Significance of the formulated work

The most important characteristic of microbubbles is their high stability compared to conventional foams. The stability of microbubbles significantly affects its application in various processes such as wastewater treatment, oil recovery, mineral flotation, and many other applications. Microbubbles have been used as a source for extreme temperatures in sonochemical reactions and to increase oxygen delivery in the fermentation process, to drive mixing on a chip in micro electromechanical devices, and to develop for use as ultrasound contrast, drug/gene delivery agents. A certain degree of stability is required to use them in such applications.

Zeta potential is one of the important characteristics of microbubbles as they have attracted considerable attention due to their wide potential in practical applications to a variety of advanced technologies. Suspended solids are effective in the purification of polluted water in rivers, lakes, seas, and aquariums because microbubbles dissolve in water, and the gas components of the bubble can be effectively supplied. Electric potential or zeta potential significantly affects the selectivity of the particle in the suspension, which indirectly affects the efficiency of the separation process.

Gas hold-up and bubble size distribution are important parameters that strongly influence the hydrodynamic behavior of microbubbles and its characteristics in the bubble columns. Gas hold-up depends mainly on the superficial gas velocity. The large gas bubbles rise more quickly through the column than the small bubbles. Therefore, the gas residence time decrease and cause a reduction in the total gas hold-up. The relation between superficial gas velocity and gas

sparger type with gas hold-up is important in designing parameters for predicting the hydrodynamic behavior of slurry bubble column flotation.

Rheology of microbubbles enables optimum process design. Besides their stability, the increase in viscosity due to their presence in aqueous solutions can result in an increased sweep efficiency, which has been exploited in water flooding enhanced oil recovery instead of polymer injection. These microbubbles have been found to preserve the pressure inside of the reservoir and, thus, increase oil recovery. Most of the applications mentioned involve microbubble flows in capillary environments; therefore, it is important to understand their behavior in capillary flows.

Entrainment can contribute to recovery in the flotation of fine particles. The recovery of fine particles is a function of true flotation, entrainment, and entrapment. The advances currently being made in grinding technology are allowing large, complex low-grade mineral deposits to be exploited economically. To fully exploit these deposits, however, considerable research needs to take place in the area of ultrafine particle flotation. While the optimum P_{80} of many ores is substantially less than 10 μm, the optimum particle size for flotation still ranges between 10 and 100 μm in diameter (Jameson, 1984). Techniques such as carrier flotation, agglomerate flotation, emulsion flotation, and oil-in-water flotation have been suggested to increase ultrafine flotation rates. However, all of these methods were found to have their limitation. It is observed that instead of developing a new process, it is more feasible to use a modified advanced ultrafine flotation technology which is more well-established than the conventional flotation method (Sivamohan, 1990).

Fine particles can be significantly recovered by using microbubbles. Microbubble flotation has been used efficiently for the recovery of heavy metals, the separation of bacteria, yeast, or algae suspensions, and fine particles.

2.2.4. Novelty importance of the proposed project in the context of the current status

Research does not always lead to new equipment but new ways of processing, thus improving the economics or environmental impact. Some of the active areas of process research include methods of selective removal of valuable metals from a solution containing numerous metals, some valuable and some considered waste. Another area is focused on increasing the recovery of water from waste tailings to minimize the need for new fresh water to sustain operations. In conjunction with increased water recovery from tailings, the research will also lead to methods for faster environmental reclamation of tailing deposits and lower the costs of tailings management. The present work leads the above points to develop a process that enhances the flotation separation process for the separation of fine particles by microbubbles. The present work can be used in mineral industries where fine particles produced while mining or communition process of the bigger lump of ores are discarded as waste. These fine particles are huge in amount, and if we are able to recover these fines economically, this will enhance the economic and sustainable development of the country.

Chapter 3

3. Holdup Characteristics and Mean Size of Ionic Microbubbles

This chapter deals with the investigation of the gas holdup of the ionic microbubbles in the presence and absence of particles and their size. The effects of surfactant type, surfactant concentration, and temperature on the holdup and size of the ionic microbubbles have been reported. The size of the ionic microbubbles is determined by the rise velocity of the microbubbles and the photography technique. Correlations have been developed to interpret the bubble size of microbubbles at different variables.

3.1. Introduction

Ionic microbubbles are bubbles having colloidal properties and consist of spherical bubbles with a size range of 25-100 µm. Continuous research has been done on generating ionic microbubbles over the past few decades, along with improving the efficiency of gas-liquid phase processes. Researchers have been focusing on the generation methods, bubble size measuring techniques, and categorizing of bubbles based on their characteristics (Temesgen et al., 2017). However, it's still a challenge to generate uniform-size bubbles in bulk and let the bubble resist its size for the time being. Due to this reason, ionic bubbles have no precise classification, and their type can't be defined. Microbubble size is one of the key factors with a significant impact on its application. Hence, many researchers continually enlisted the category of bubbles based on their size. Based on the differences in their size, bubbles were categorized as macrobubbles, microbubbles, sub-micro or nanobubbles for conventional or big bubbles, fine bubbles, and ultrafine bubbles. Every researcher gave their size range to define the bubble categories. Agarwal et al. (2011) mentioned that microbubbles have a size range of 10-50 µm, and nanobubbles have a size range of less than 200 nm. They reviewed that the

microbubbles have an environment-friendly technique for the oxidation of organic compounds, water disinfection, and fouling control as they can generate free radicals without the use of any toxic chemical. While Yasuda et al. (2008) scaled microbubbles in the range of 10 μm to 100 nm and nanobubbles in the range of less than 100 nm. Similarly, different researchers defined different ranges for specific bubbles produced with varying methods of generation.

Gas holdup and bubble size are also important characteristics, which will vary depending on the values of the operating parameters. Large gas holdup and small bubble sizes are generally desirable in order to maximize the interfacial area. It has been found that gas hold-up increases with the time of stirring. In general, gas holdup also increases with an increase in surfactant concentration, tending to a maximum at concentrations near the CMC of the surfactant. However, Bredwell et al. (1995) found that surfactant concentration had no effect on the gas holdup. Chapalkar et al. (1993) found that higher gas hold-ups are obtained with non-ionic surfactants than with ionic surfactants, and Save and Pangarkar (1993) found that gas holdup increased with the length of the alkyl chain of the surfactant when comparing different anionic and cationic surfactants.

Through literature, it is noted that photographic techniques have been the most used techniques for measurement of the microbubble size in gas-liquid dispersions (Graham, 1976). Bee et al. (1986) used a light microscope combined with photographic and image-analysis techniques for the measurement of bubble size in the microbubbles of high viscosity, stressing the difficulty of obtaining reliable measurements for dispersed gas phases. Ronteltap and Prins (1989) reported the use of an optical glass-fiber probe method to study the stability of the microbubbles by measuring bubble-size changes with time. A microscope connected to a CCD camera was used by Jauregi et al. (2000) to determine the size distributions of the microbubbles. Basu and Malpani (2001) took photomicrographs with a stereo-zoom microscope to estimate the microbubble diameter through Sauter mean diameter method. Through earlier investigation, it

was found that over certain ranges of gas flowrate, uniform bubbles can be formed. Cheng and Lemlich (1983) described an apparent method for measuring the size distribution of the microbubbles and claimed that the size of the bubbles unchanged and eliminated distortions were caused by the wall effects of the container.

The work carried out in this chapter is to study the hydrodynamic parameters such as bubble size distribution and rise velocity of microbubbles in various liquids. The microbubble size distribution became narrow with decreasing surface tension. At low viscosity, the microbubble size is found to be dependent on the surface tension of the liquid. Microbubble systems are dynamic and change continuously, which results in bubble breakage, coalescence, and disproportionation [i.e., transfer of core air from smaller bubbles (higher pressure) to the larger bubbles (lower pressure)]. This limits its stability and the other features of microbubbles. Its other features depend on the bubble size and its holdup.

3.2. Theoretical background

3.2.1. Ionic microbubble holdup

The important variables that affect the holdup are gas and liquid velocities, liquid viscosity, liquid surface tension, design of the gas distributor, solid concentration, and column diameter. Knowledge of gas holdup is necessary for the estimation of the interfacial area, which influences the efficacy of microbubble-aided fine particle separation. The gas holdup depends on the gas flow rate, physic-chemical properties of the liquid and gas phase, operating temperature, and pressure (Kantarci et al., 2005). The gas holdup also depends on the number of bubbles generated, average bubble size, and the bubble rise velocity (Josm et al. 1998). The various methods to estimate gas-phase fraction are phase isolation, conductivity, pressure drop, gamma-ray attenuation, electrical resistant tomography (ERT), and dynamic gas disengagement (DGD).

3.2.2. Rise velocity of ionic microbubbles

Physicochemical phenomena affect the hydrodynamics of microbubbles, and conventional bubble sizes similarly. As we know that the forces that define the bubbles' rise velocity are gravity, drag, and buoyancy, and their rise velocities get affected by the force balance. However, the hydrodynamics of microbubbles are more affected than conventional bubbles (Pérez-Garibay et al., 2018). Surfactant reduces the terminal velocity of floating bubbles because of two reasons (i) they reduce the surface tension of the solution, thus reducing bubble size, and (ii) because they increase the friction between the bubble surface and the liquid side (Maldonado et al., 2013).

Generally, three main theoretical approaches are available in the literature to calculate the rise velocity of bubbles, namely the force balance approach, dimensional analysis, and the wave Analogy approach (Kulkarni and Joshi, 2005). In the force balance approach, the terminal velocity is calculated from the balance of buoyancy and drag force. Under this approach, it is assumed that the bubbles are perfectly spherical, with no internal circulation within the bubble and no slip existing at the boundary. Fan and Tsuchiya (1990) developed a correlation to determine the terminal rise velocity of bubbles applicable for the pure and contaminated system. If the equivalent radius of the bubble is smaller than 100 μm, the shape of the bubble remains almost spherical, and the bubble behaves like a solid sphere. If the equivalent radius of the bubble increases, a change in bubble shape from spherical to ellipsoidal to the spherical cap can occur. The radius at which these transitions occur depends on the physicochemical properties of the liquid (Haberman and Morton, 1953). When the size of the bubble reaches to micron level, i.e., the Reynolds number approaches zero, and bubbles can be considered as a rigid spherical bodies. Thus, the terminal rise velocity of microbubble (u_{mb}) can be described by Stokes' law (Takahashi, 2005).

3.3. Experimental Procedure

3.3.1. Estimation of ionic microbubble gas holdup

In the present work, the phase isolation method is used to estimate the gas holdup of the ionic microbubbles. The method proposed by Amiri and Woodburn (1990) is used to determine the size of ionic microbubbles based on the rise velocity of the microbubbles as a function of gas holdup in the ionic microbubble dispersion. The change of gas holdup (ε_g) with time in the ionic microbubbles solution can be expressed as

$$\varepsilon_{g,t} = \frac{V_{g,t}}{V_t} \tag{3.1}$$

where $V_{g,t}$, and V_t are the volume of gas in the microbubbles solution and volume of microbubbles solution at time t, respectively. The volume of gas at time t is

$$V_{g,t} = V_t - V_{d,t} \tag{3.2}$$

where $V_{d,t}$ is the volume of liquid drained at time t. Therefore, from Equations (3.1) and (3.2), one can write:

$$\varepsilon_{g,t} = \frac{h_t - h_{d,t}}{h_t} \tag{3.3}$$

At $t=0$ of drainage, $h_t = h_o$, $h_{d,t} = h_{d,o}$ and $\varepsilon_{g,t} = \varepsilon_{g,o}$. Hence one can write

$$\varepsilon_{g,o} = \varepsilon_o = \frac{h_o - h_{d,o}}{h_o} \tag{3.4}$$

where h_t is the total height of the microbubble and liquid, and $h_{d,o}$ is the height of liquid drainage at t = 0. Dividing Equation (3.3) by Equation (3.4) one can write,

$$\frac{\varepsilon_{g,t}}{\varepsilon_o} = \frac{h_t - h_{d,t}}{h_t} \times \frac{h_o}{h_o - h_{d,o}} \tag{3.5}$$

After rearranging Equation (3.5) it becomes

$$\varepsilon_{g,t} = \frac{h_o\left(h_t - h_{d,t}\right)}{h_t\left(h_o - h_{d,o}\right)}\varepsilon_o \tag{3.6}$$

Ionic microbubbles solution is filled in the transparent glass cylinder, and the camera is used to record the change in the height of the clean liquid with time. After a certain time, the bubbles at the top start disappearing as they are in contact with the atmosphere directly. Few snapshots of the ionic microbubble's height or volume taken at different times are shown in Figure 3.1.

3.3.2. Estimation of ionic microbubble size from its rise velocity

The rise velocity of ionic microbubbles, $u_{mb}\,(t)$, can be calculated from understanding the velocity of the bubbles rising in solution. According to Stokes' theory, the rise velocity can be expressed as

$$u_{mb} = \frac{d_{mb}^2(\rho - \rho_g)g}{18\mu} \tag{3.7}$$

The Equation (3.7) is used to calculate the size of the microbubble as

$$d_{mb} = \sqrt{\frac{18\mu_l}{(\rho - \rho_g)g}u_{mb}} \tag{3.8}$$

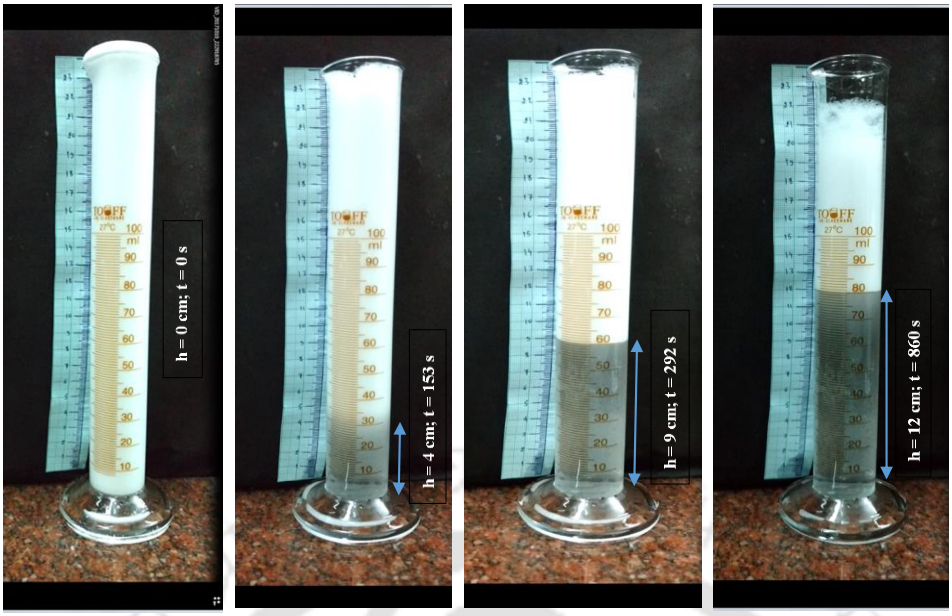

Figure 3.1. Experimental photographs of drainage process at room temperature with 500 ppm of SDS.

where d_{mb} is the diameter of the microbubble, μ_l is the viscosity of the liquid or slurry, g is the gravitational acceleration, ρ is the density of the liquid-microbubble mixture, and ρ_g is the density of microbubble gas. The velocity of ionic microbubbles in liquid is estimated experimentally from the change of height of the liquid drainage with respect to time, as shown in Figure 3.1. The assumptions made for the execution of this principle are (i) the microbubbles do not coalesce or burst, and (ii) Eqs. (3.7) and (3.8) for a single microbubble are applied to a swarm of microbubbles, and (iii) the microbubbles are assumed to be monosized and spherical.

3.3.3. Determination of ionic microbubble size by photographic method

The size of the ionic microbubble is also determined by using the photographic method, as shown in Figure 3.2. In this case, ionic microbubbles generated in the mixture are filled in a glass cell. A CCD camera (PCO Ltd., model-PCO Pixelfly-USB, Germany) having a resolution of 1360×1024 pixels in conjunction with a macro zoom lens (Navitar) was used to capture the images of microbubbles inside the cell. The images are recorded with a frame rate of 19 frames

per second and stored in a computer. The digital photographs are further processed and enhanced using Image Processing Software (Image J 1.48v). The same software estimates the size of the bubble, and a total of 150-200 bubbles are examined to determine the size. A typical snapshot of the microbubble is shown in Figure 3.3, along with its size distribution. The mean bubble diameter is calculated as the volume-to-surface mean bubble diameter, which is called Sauter mean bubble diameter. The Sauter mean diameter of microbubble (d_{bs}) is mathematically expressed by

$$d_{bs} = \frac{\sum_{i=1}^{n} n_i d_{bi}^3}{\sum_{i=1}^{n} n_i d_{bi}^2} \tag{3.9}$$

where n_i is the number of bubbles of diameter d_{bi}.

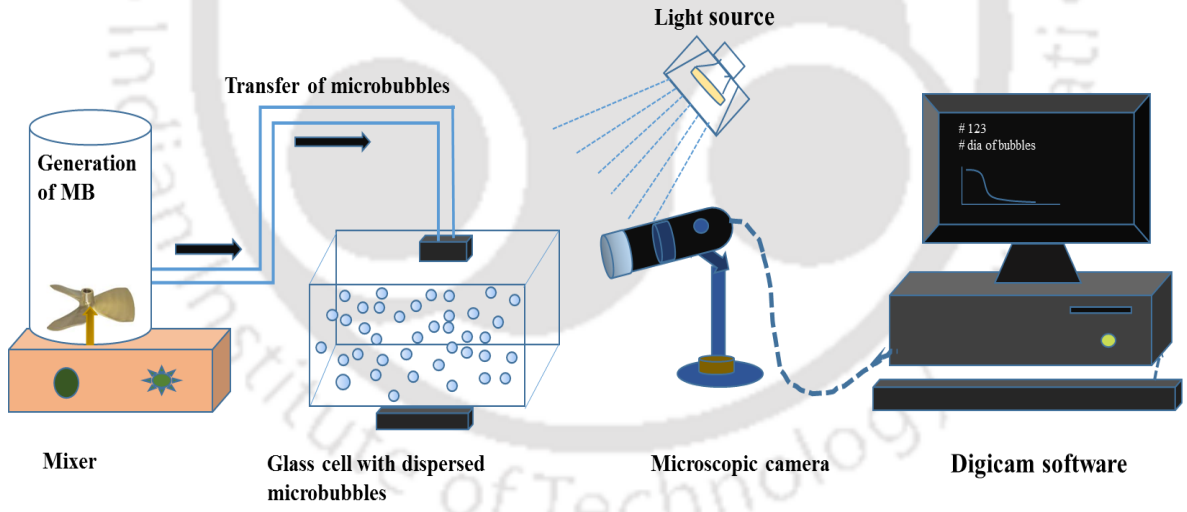

Figure 3.2. Schematic diagram of the photographic method to determine the bubble size.

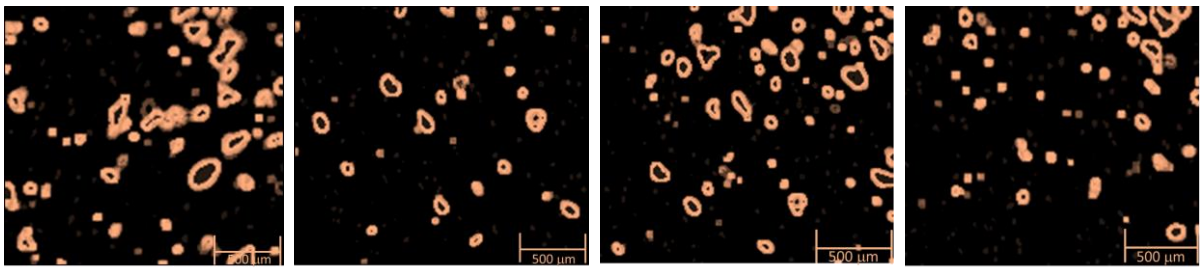

(i) SDS 100 ppm (ii) SDS 200 ppm (iii) SDS 300 ppm (iv) SDS 400 ppm

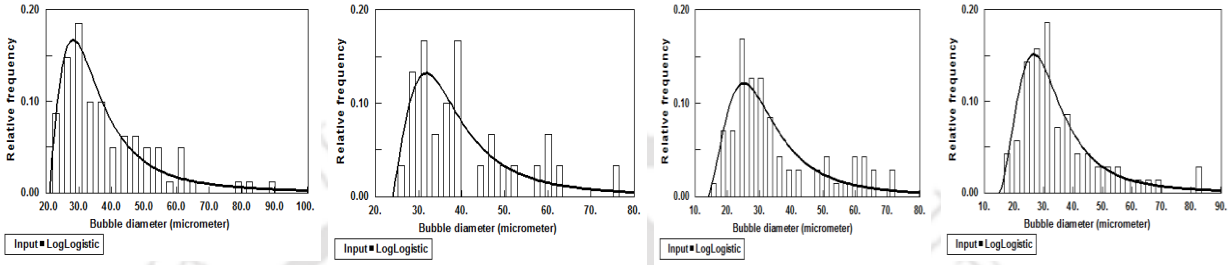

SDS 100 ppm SDS 200 ppm SDS 300 ppm SDS 400 ppm

Figure 3.3. Typical snapshot of ionic microbubble after editing it by image processing software and its distribution.

3.3.4. Properties of the system

In the present work, sodium dodecyl sulfate (Sodium Lauryl Sulfate, anionic), and cetyl trimethyl ammonium bromide (CTAB, cationic), nanoclay a surface modifier containing 25–30 wt.% trimethyl stearyl ammonium, and a bio-surfactant saponin (non-ionic) and alcohol (glycerol) are used to study the effect of different factors on the stability of the microbubbles. The various properties of the surfactants and materials used in the present study are shown in Tables 3.1.–3.3. All the experiments in the present work were carried out at 25° C.

Sodium chloride (99.9%, Himedia laboratories, India), lithium chloride, and cesium chloride (Min. assay 99% and 99.5% respectively, Spectrochem, India) were used as a salt for their effects on the characteristics of the microbubble. The properties of the salts present in this work are described in Table 3.4.

Table 3.1. Properties of surfactants.

Surfactant	SDS	CTAB	Saponin
Molecular formula	$C_{12}H_{25}OSO_2ONa$	$C_{19}H_{42}BrN$	$C_{45}H_{73}NO_{15}$
Molar Mass (g/mole)	288.37	364.46	868.06
Appearance	White powder	White powder	white crystalline solid
Melting point (ºC)	204-207 ºC	248-251 ºC	271-273 °C
Solubility in water	2 g/l at 20˚C	36.4 g/l at 20˚C	74 g/l at 30 °C

Table 3.2. Physical properties of glycerol.

Properties	Value
Density	1.26 g/cc (20˚C)
pH value	5 (100 g/l, H_2O, 20˚C)
Vapour pressure	< 0.001hPa (20˚C)
Molar mass	92.1 g/mol

Table 3.3. Properties of the micro and nano particles.

Type of mineral	Copper Oxide	Aluminum Oxide (Nanosize)	Zinc Oxide	Aluminum Oxide
Density (g/cm^3)	6.31	3.95	5.61 g/cm^3 (20˚C)	3.94 g/cm^3 (20˚C)
Size (µm)	<50 nm (TEM)	13 nm (TEM)	4.47	19.6
Molar mass (g/mol)	79.55	101.96	81.37	101.96
Boiling point		2980 °C	2360˚C	2980 °C (1013 hPa)
pH value	-	-	7 (50 g/l, H_2O, 20 °C) (slurry)	6.8 - 7.8 (10% suspension)

Melting point		2050˚C	1975˚C	2050˚C
Surface area (m^2/g)	29 m^2/g	85-115 m^2/g (BET)		

Table 3.4. Properties of different salts.

Type of salt	Lithium Chloride	Sodium Chloride	Cesium Chloride
Density (g/cm^3)	2.07	2.16	3.988 (25˚C)
Assay	99 %	99.9 %	≥ 99.5 %
Molar mass (g/mol)	42.39	58.44	168.36
Melting point	605-614 °C	801°C	646 °C
Boiling point	1382 °C	1413°C	1297 °C
Solubility in water (25°C)	84.25 g/100ml	359 g/L	1910 g/L
Chemical formula	LiCl	NaCl	CsCl
Ionic radius (Å) (Conway and Ayranci, 1999)	0.060	0.095	0.169
Hydrated radius (Å) (Wang and Weinstock, 2012)	3.40	2.76	2.28

3.4. Results and Discussion

3.4.1. Holdup of the ionic microbubbles at different variables

The effect of surfactant concentration is presented in Table 3.5. It is observed that the holdup of ionic microbubble increases with surfactant concentration, and it is maximum around the CMC value of the solution. It also depends on other parameters like time of stirring, temperature, and the addition of surfactants and nanoclays. Jauregi et al. (1997) reported that the holdup depends on time, the concentration of surfactant, and the concentration of salt. Their

experimental result showed no significant dependence on pH and temperature. They also reported that the hold-up tends to a maximum at about 25 mM of SDS. Roy et al. (1992) found that the holdup increases with increasing stirring time. They found that a concentration of 25% lower than the CMC leads to only a slight decrease in the holdup. As per the present experimental observation, the variation of a gas holdup at different temperatures for two different types of surfactant is shown in Figure 3.4 (a).

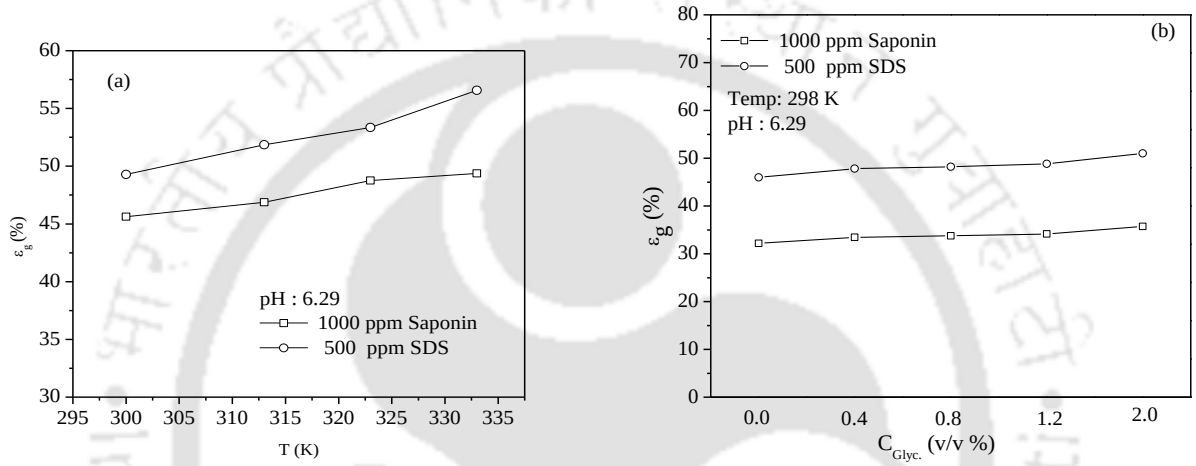

Figure 3.4. Variations of the holdup of microbubbles, (a) with temperature and (b) with glycerol concentration.

Table 3.5. Holdup and half-life of microbubble at different parameters with ionic surfactant (SDS 500 ppm).

Surfactant type	Concentration of surfactant (ppm)	Experimental data		
		Holdup	$t_{1/2}$	V_{max}
SDS	100	56.32	84	16.6
	200	58.95	88	15.6
	300	61.05	93	14.8
	400	64.21	98	13.6
	2333 (CMC)	79.74	251	7.7
	2500	81.32	259	7.1

It is found that with an increase in temperature, the holdup of microbubble is increased for both the surfactants SDS and Saponin. It is observed that higher microbubble holdup results in SDS (ionic surfactant) than Saponin (non-ionic) (Figure 3.4 (a)). However, Chapalkar et al. (1994) found that a higher holdup of microbubble is obtained with non-ionic surfactants than with ionic surfactants. In Figure 3.4 (b), the variations of microbubble holdup with the addition of different concentrations of glycerol to the solution are shown. It is observed that the addition of glycerol slightly increases the holdup. The addition of glycerol to the solution not only increases the viscosity but also reduces the surface tension of the solution and results in the formation of smaller microbubbles (Parmar and Majumder, 2015). The addition of glycerol also increases the density of the solution, which increases the holdup of the microbubbles

(Parhizkar, 2014). It is observed that the charged microbubble tends to rise due to the density difference between the ionic microbubble and the bulk liquid phase. In addition, drainage of the liquid within the charged microbubble dispersion takes place. As a result, charged microbubble-liquid interface height rises. Interface rise velocity is equal to charged microbubble rise velocity, which depends on gas holdup and ionic microbubble diameter. As the ionic microbubble continuously undergoes changes resulting from creaming, bubble breakage, coalescence, and disproportion, the number density of the ionic microbubble changes with time as drainage proceeds.

3.4.2. Size of the ionic microbubbles at different variables

It is observed that mean bubble size decreases with increasing surfactant concentration, as shown in Figure 3.5. Within the low range of viscosity, the microbubble size depends on gas-liquid interfacial tension (Parmar and Majumder, 2015). Surfactants lower the surface tension of the gas-liquid interface and thus help to create a small bubble. The bubble size decreases with surfactant concentration as per Equation (3.10):

$$d_b(\text{in } \mu\text{m}) = 56.41 - 0.0193 C_s(\text{in ppm}) \tag{3.10}$$

Without surfactant, the typical bubble size at 298 K is 56.41 μm. Since there is a significant decrease in surface tension with an increase in temperature, the bubble size changes accordingly. Figure 3.6 shows the variation of bubble size with the temperature at a fixed concentration of SDS and Saponin surfactants. It is observed that bubble size decreased almost linearly with increasing temperature, which can be expressed as

$$d_b - d_b^0 = m\Delta T^{\alpha} \tag{3.11}$$

where, d_b^0 is the bubble diameter at 298 K, which is found to be 47.55 μm from the present experiment in the case of SDS, whereas its value for Saponin, is 43.29 μm. The term ΔT is the

temperature deviation from 298 K. The coefficients *m*, α are 0.1063, 0.9857, and 0.1174, 0.8978, respectively, for SDS and Saponin. Figure 3.7 shows the variation of bubble size with the addition of glycerol. It is observed that bubble size decreases with the addition of glycerol for both the surfactants. With increasing glycerol concentrations, viscosity and density of solution increase, whereas surface tension decreases. A decrease in surface tension produces a smaller bubble.

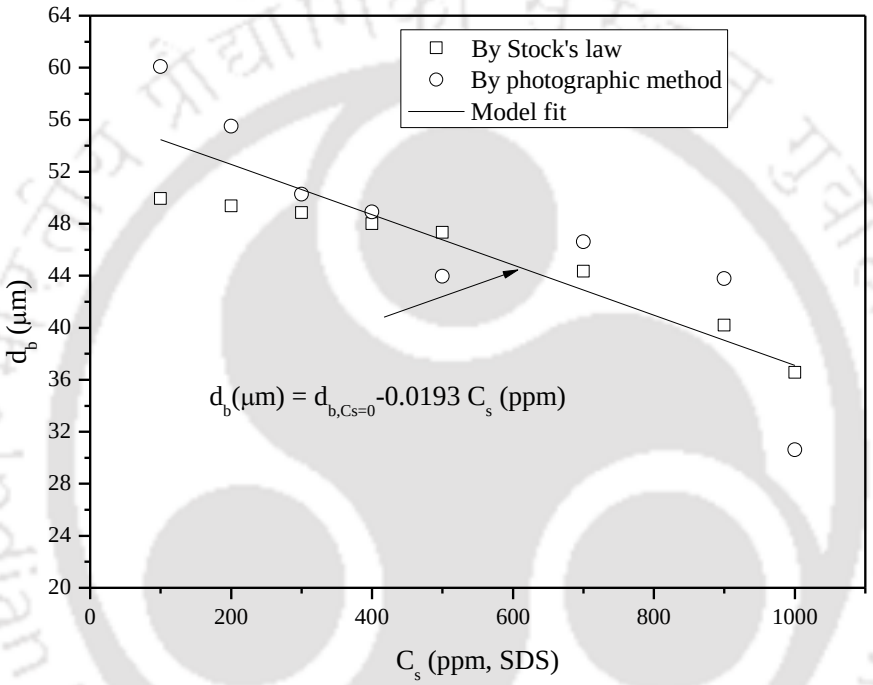

Figure 3.5. Effect of SDS surfactant concentration on bubble size at stirring speed of 20000 rpm for 15 s in the absence of particles at temperature 298 K and pH = 6.29.

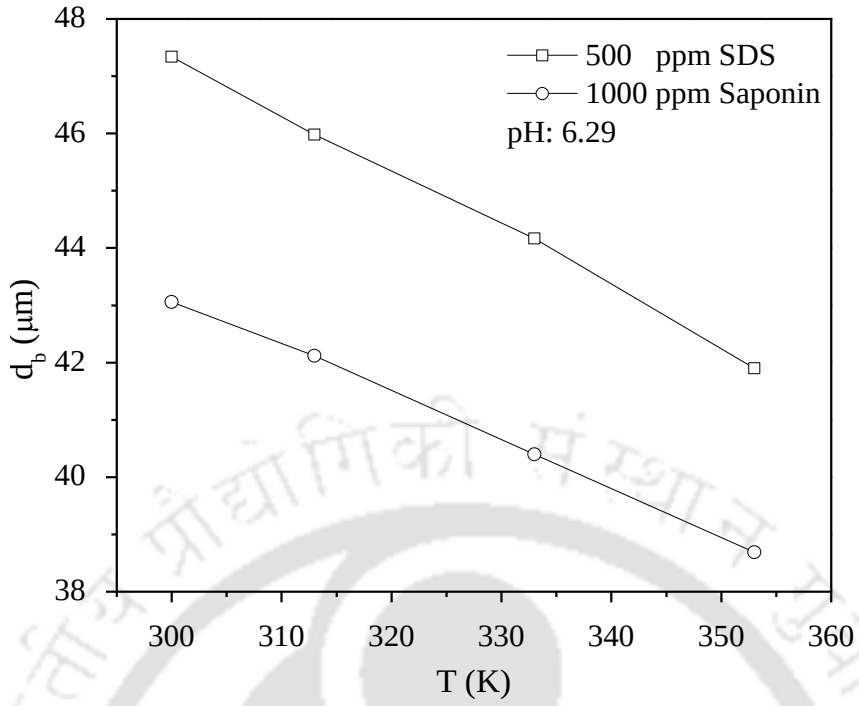

Figure 3.6. Variations of bubble size with temperature at different doses of surfactant.

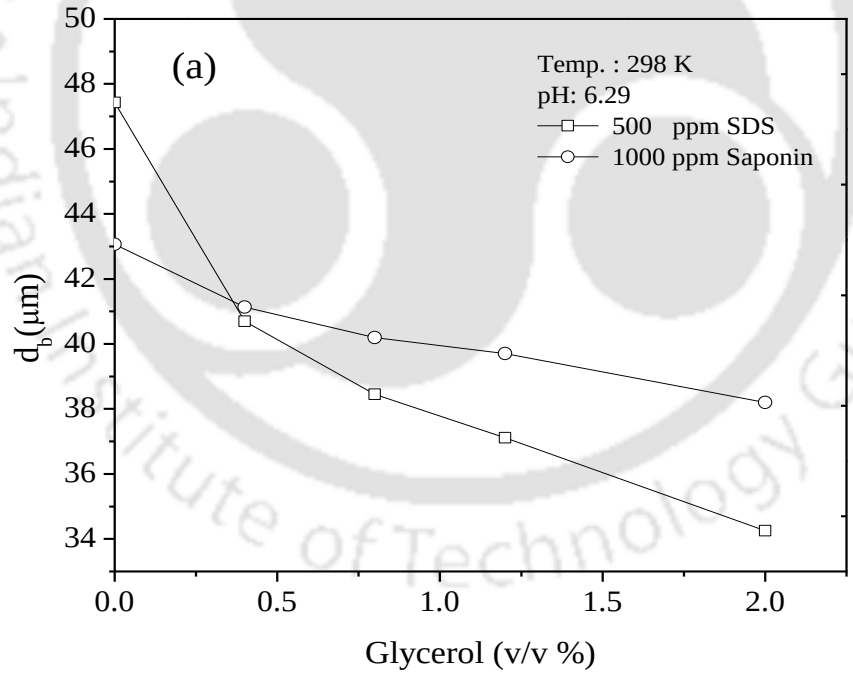

Figure 3.7. Variations of bubble size with the concentration of glycerol at different doses of surfactant.

Jamaialadi and Miiller-Steinhagen (1992) also reported the reduction of bubble size with the addition of alcohol and organic acid to water. Han et al. (2002) found a reduction in bubble size with an increase in the concentration of isobutanol which reduces the bubble coalescence by accumulating at the gas-liquid interface, orienting their hydrophilic group into liquid film surrounding the gas bubble and thus creating repulsive electric forces when two bubbles come close to each other. Nanoclays are surface modifiers that modify the surface of the bubble. Additions of nanoclays to the surfactant solution affect the size of the microbubble. Figure 3.8 shows the variation of bubble size with an increase in nanoclays concentration. It is observed that with an increase in the concentration of nanoclays, bubble size is decreased. Nanoclays attach to the bubble surface and modify its surface properties (Hunter et al., 2008). The size of anionic microbubbles decreases ~14 % with an increase in pH from 7-9 at a fixed concentration of SDS surfactant, whereas it is observed that only ~3% decrease in size with an increase in pH from 5-7 of the acidic medium, as shown in Figure 3.9.

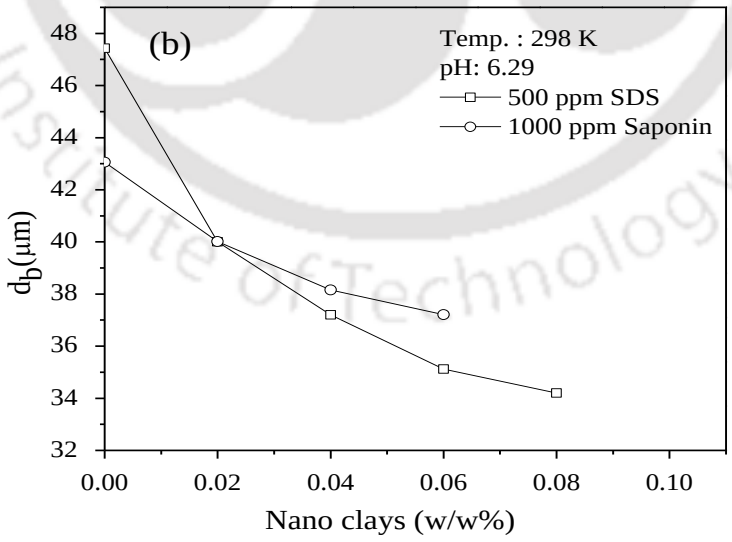

Figure 3.8. Variations of bubble size with the concentration of nanoclays.

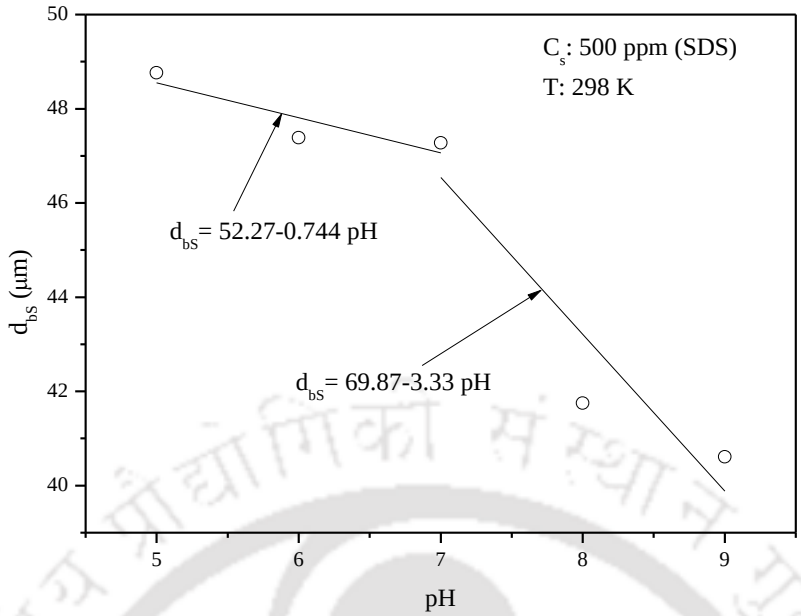

Figure 3.9. Variation of microbubble size (Sauter mean bubble diameter) with pH.

The variation is assumed to be related to the change in the surfactant molecular structure. Sodium-ion replaces the potassium ion if potassium hydroxide is added to change its pH, as shown by scheme 1 as

$$CH_3-(CH)_{11}-O-SO_4-Na+KOH \rightarrow CH_3-(CH_2)_{11}-SO_4-K+NaOH \quad \text{(Scheme 1)}$$

(Sodium dodecylsulfate (SDS)) (Potassium dodecylsulfate (PDS))

Since the sodium ion has more activity than the potassium ion, the pH increases gradually and continuously as the concentration of the SDS-KOH system increases (Topallar and Karadag, 1998). According to literature, "the surface viscosity shows a remarkable decrease with the concentration of added base (i.e., with pH) till the critical micelle formation. Further addition of base increase the surface viscosity (Poskanzer and Goodrich,1975)". However, the surface tension gradually decreases with the increase of the dose of base (i.e., pH), which results in more reduction in bubble size. In the case of pH < 7, by addition of HCl results in a fraction of

the SDS molecules protonated to form dodecyl sulfonic acid (DSA) (Cistola and Small, 1990). Under such conditions, SDS and DSA combine to form acid–surfactant crystals (Cistola et al., 1986; Cistola et al., 1988) which added an additional phase to the system due to the reaction of hydrogen ions with negative SDS micelles, which increases the surface viscosity and forms relatively bigger bubbles as compared to that at pH > 7 as shown by scheme 2 as

$$CH_3-(CH)_{11}-O-SO_4-Na+HCl \rightarrow CH_3-(CH_2)_{11}-SO_4-H+NaCl \quad \text{(Scheme 2)}$$

(Sodium dodecylsulfate (SDS)) (Dodecylsulfonic acid (DSA))

The size distribution of the microbubble in SDS solution is found to follow the log-logistic distribution for all pH which can be expressed as

$$f(x)=\frac{p\left(\frac{d_b-d_{b,\min}}{\beta}\right)^{p-1}}{\beta\left[1+\left(\frac{d_b-d_{b,\min}}{\beta}\right)^{p}\right]^2} \quad (3.12)$$

The parameters p, β can be obtained from the experimental conditions. The parameter $d_{b,min}$ is the minimum bubble diameter at a particular experimental condition. From the present experimental conditions, variations of parameters for a typical operating condition are given in Table 3.6.

3.4.3. Effect of Salt on the Size of Microbubbles

The formation of finer bubble sizes at low surface tension is observed. The lower the surface tension, the higher the quantity of free surface on the surface-active molecules adsorbing at the gas-liquid interface of bubbles (Pandey et al., 2003; Xu et al., 2009). It is observed that the mean bubble size decreases with the increasing concentration of the surface-active molecules.

The microbubble size at different concentrations of salt and surface-active molecules are enlisted in Table 3.7.

Table 3.6. Experimental values of parameters of Eq. (3.12) at pH = 6.29.

Parameters	100 ppm (SDS)	200 ppm (SDS)	300 ppm (SDS)	400 ppm (SDS)
$d_{b,min}$	21	20	14	15
p	1.69	2.08	2.29	2.47
β	11.35	16.16	16.82	16.51

Table 3.7. Microbubble size and surface tension in the presence of salt (NaCl).

Concentration		Surface tension, γ (mN/m)	Microbubble diameter d_{mb} (μm)	Solution density (kg m^{-3})
NaCl(mol m^{-3})	SDS (mol m^{-3})			
5	0.5	41.20	61.68	999.98
10	0.5	32.78	59.86	1000.13
50	0.5	32.62	58.79	1001.39
100	0.5	32.12	56.92	1002.94
5	1	38.28	63.34	1000.11
10	1	32.27	55.89	1000.27
50	1	31.39	52.68	1001.52
100	1	31.03	40.26	1003.08
5	3	31.89	56.42	1000.68

10	3	31.98	36.44	1000.83
50	3	31.45	38.85	1002.09
100	3	31.63	37.57	1003.65
5	5	31.49	45.06	1001.29
10	5	31.94	31.51	1001.45
50	5	32.34	33.95	1002.70
100	5	32.95	47.48	1004.26

A typical histogram of the bubble size distribution along with a snapshot of the microbubbles generated with SDS in the presence of salt is shown in Figure 3.10.

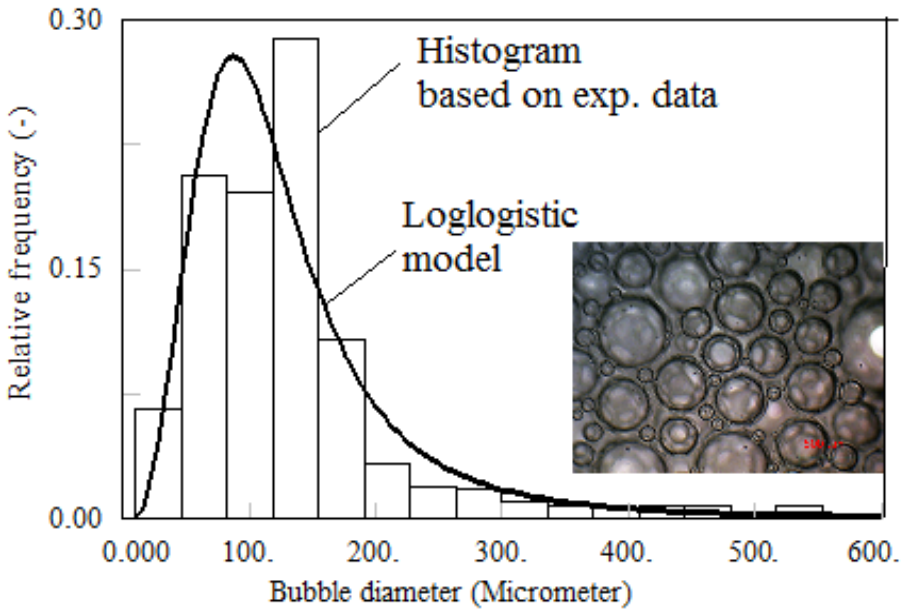

Figure 3.10. Bubble size distribution Optical microscopy images of microbubble generated with SDS only, (b) histogram of the bubble size distribution for SDS, (c) Optical microscopy images of microbubble generated with SDS and NaCl.

Figure 3.11 (a) shows the diameter of the microbubble changes drastically, whereas the addition of nanoparticles at the same specification shows slight variations. In this case, microbubbles were formed with SDS by adding a fixed concentration of salt (10 mol m^{-3}) and nanoparticles (CuO 0.79 w/w %). At the lowest SDS concentration, the size of the microbubble formed was 98.18 µm. As shown in Figure 3.11 (a), the stable microbubble is produced at an SDS concentration of 10 mol m^{-3}, which is beyond the CMC, in the presence of CsCl salt. The salt has a synergistic effect on SDS even beyond CMC. Xu et al. (2009) found that the bubble diameter decreases as the SDS concentration increases, reaching a minimum diameter at the SDS concentration above the CMC. This is similar to the results found here. The size of microbubbles not only depends on the concentration of SDS or salt but also depend on the presence of particles, as shown in Figure 3.11 (b). The effect of types of salts and their concentration on the size of microbubbles is demonstrated in Figures 3.12 (a) and (b), respectively. The size of the microbubble reduces with the addition of salt. At a higher concentration of SDS, the effect of salt addition on the size of microbubbles is significant.

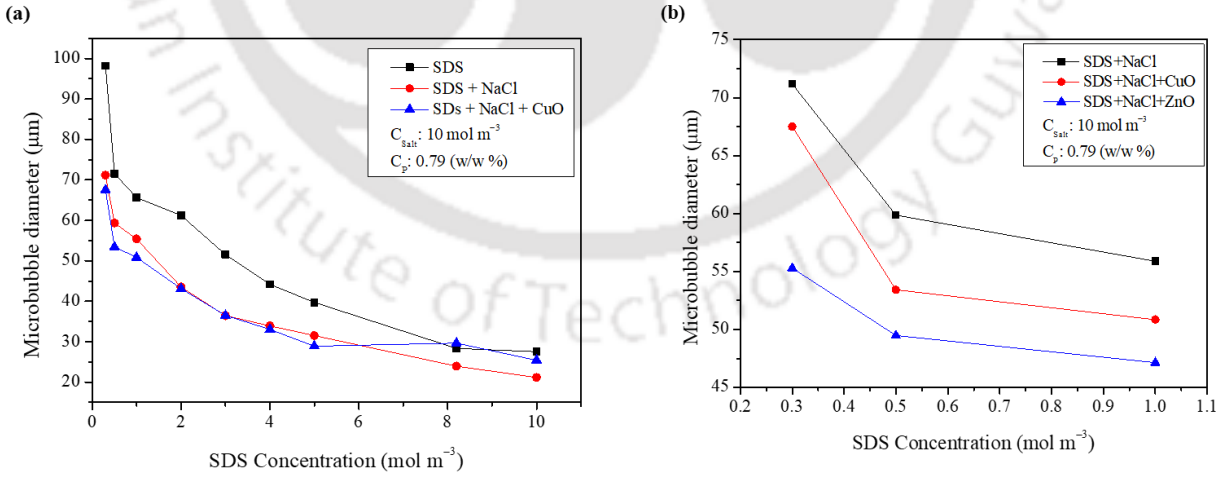

Figure 3.11. Variations of bubble size with (a) increasing concentration of SDS only, the addition of salt NaCl (10 mol m^{-3}) at same concentrations of SDS and with addition CuO (0.79

w/w %) nanoparticle at the same concentration of SDS and salt and (b) Effect of different size of the particle on the bubble diameter of microbubbles.

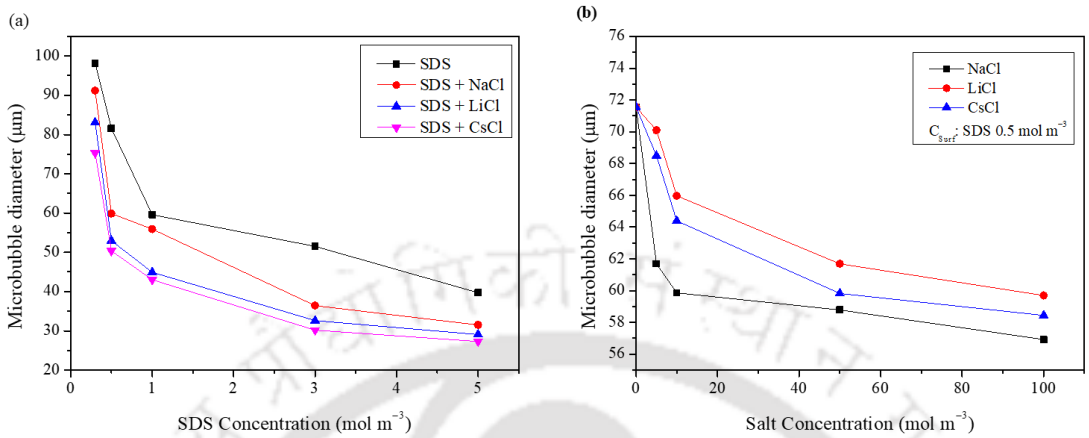

Figure 3.12. (a) Effect of different salt on the size of microbubbles at 10 mol m^{-3} concentration of salt with varying concentration of SDS and (b) Effect of varying concentrations of different salt on the size of microbubbles at 0.5 mol m^{-3} concentration.

3.4.4. Salt Effect on the Holdup of Microbubbles

Figure 3.13 presents the experimental results for the gas holdup, ε, as a function of particle and salt concentrations. It is observed that the increase in gas holdup is more in the CsCl solution than that with other salt solutions, as shown in Figure 3.13 (a). The variation in bulk liquid properties causes this result. The variation of the holdup of microbubble with the addition of nanoparticles to the solution is shown in Figure 3.13 (b). The addition of nanoparticles slightly increases the holdup of the microbubble.

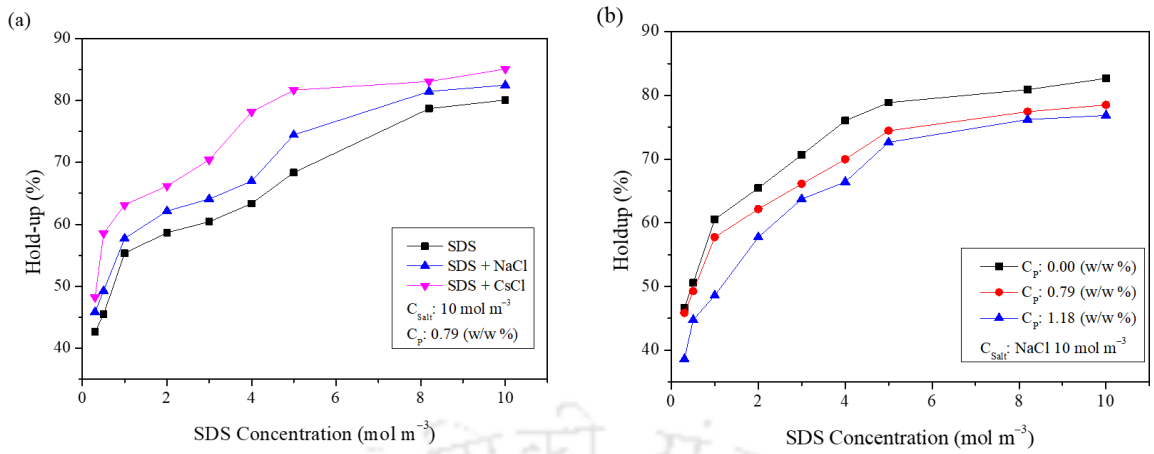

Figure 3.13. Variations of the holdup of microbubbles. (a) with different salt at different concentrations of surfactant and constant concentration of salt & particles, and (b) at different concentrations of particles with a constant amount of salt.

3.5. Conclusions

The effect of various conditions such as the types of surfactant, the concentration of surfactant, glycerol, temperature, and pH on holdup and size of the microbubbles were investigated experimentally. The holdup of microbubble increases with surfactant concentration, and it is maximum around the CMC value of the solution. It was found that with an increase in temperature, the holdup of microbubble increased for both the surfactants SDS and Saponin and found that higher microbubble holdup for SDS (ionic surfactant) than Saponin (non-ionic). The addition of glycerol to the solution not only increases the viscosity but also reduces the surface tension of the solution and results in the formation of smaller microbubbles. Addition of glycerol also increases the density of the solution, which increases the holdup of the microbubbles. As per experimental data, correlations were developed for different conditions like temperature, surfactant concentration, and pH to determine the microbubble diameter for the given limits.

CHAPTER 4

4. Interfacial Adsorption Phenomena of Microbubble

This chapter discussed about the investigation of the interfacial adsorption phenomena at air-water and liquid-solid interfaces with prominence on the systems containing surfactants and micro- or nanoparticles. The effect of different salt on the physicochemical properties of the solution is enunciated.

4.1. Introduction

Adsorption of surfactant at the solid-liquid interface is substantial in the separation of particles by flotation. The surface-active molecules get adsorbed at the interfaces of solid-liquid and liquid-liquid interfaces and attach to the microbubbles, moving along with the microbubbles for effective separation. Some of the commercial implementations incorporate the addition of salt in the presence of a surfactant and solid particles. Surfactants are used in the applications of mineral beneficiation, water purification, dye removal, deinking wastewater from the paper recycling plant, water removal from petroleum, liquid-liquid separation, seaward oil renewal, disinfection, and conservation of food items and medicinal products. The presence of salt and solid particles influences the adsorption and coalescence of ionic microbubbles. Studies on the monodisperse surfactants, co-surfactants in the presence of salt, show adsorption and desorption immediately at the interface. In such cases, the surfactants below their critical micelle concentration (CMC) demonstrate no observable sorption-activation barriers on time scales of layout a minute (McCaffrey et al., 2017; Svitova et al., 2003).

Microbubbles coated with surface-active molecules are utilized in various applications depending on its characteristics, that is, the stability of the microbubbles. Challenges to stabilizing the microbubbles are required to cover up yet. On the basis of previous studies, the

structure of microbubbles figured out by various researchers consists of air/gas encapsulated inside the layers of molecules of a surfactant, which restrict the coalescence of the ionic microbubbles throughout raising their stability compared to conventional bubbles (Ma et al., 2008a; Mohamedi et al., 2012). The interaction between the surfactant molecules and particles is a miscellaneous phenomenon. Adsorption of a surface-active molecule at the surface of the particle depends on the properties of the particles, the surfactants involved, and the condition at which the process was performed, such as temperature and pH. The effectiveness of Polytetrafluoroethylene particles causing the film to collapse is analogous to the size and shape of the particles and the receding contact angle. The presence of particles modifies the stability of ionic microbubbles in three different ways: (i) adsorption loss (getting adsorbed on the surface of particles) caused by reduction of surfactant concentration, (ii) increase in the viscoelastic property of the microbubbles, and (iii) increase in the viscoelastic property of the liquid films.

Adsorption is a phenomenon driven by numeral forces such as electrostatic attraction, bonding between two non-metal atoms, that is, covalent bond, hydrogen bonding, and nonpolar interactions. The stabilization of any matter in the base solution is due to an interaction between them. Solvation and desolvation are the lateral interactive forces that govern on the adsorption at the interfaces (Somasundaran and Grieves, 1975). Specific characteristics of surfactants on adsorption behavior to solid surfaces are obvious. Electrostatic interaction is responsible for the fast adsorption of surfactants on a charged surface (Fuerstenau and Jang, 1991). At low concentrations, that is, below CMC, the surfactant gets adsorbed and accumulates on the surface. This accumulation of surface-active molecules is named as micelles and is affected by the length of the surface-active molecules chain. These are essential characteristics which sharply distinguish the adsorption of surface-active agents on hydrophobic and hydrophilic surfaces (Koopal and Ralston, 1986).

Furthermore, at a higher concentration of surfactants, adsorption phenomena can have four regions. In the first region, the interaction between the adsorbed monomers is absent; the second region is associated with the number of hydrogen and carbon atoms present in the molecule of the surface-active compound adsorbed at the interface named Stern plane. In the third region, the electrostatic force does not favor the adsorption, and the potential is reversible (Fuerstenau and Jang, 1991). The magnitude of the adsorption of any surface-active ion can be measured at the interface and named as "surface excess." This magnitude can be estimated in two ways, first by measuring the surface tension of the sample at different concentrations of the surfactant in the presence and absence of particles. The surface tension measurement indirectly helps to estimate the magnitude of the adsorption by using the equation of state (EOS). The changes in the surface tension of experimental data are helpful in assessing the surface excess by the Gibbs adsorption equation. Several models are present in the literature to determine surface excess indirectly. The Langmuir adsorption isotherm and the Frumkin isotherm are very often used to estimate the magnitude of adsorption. The other method is the experimental one, which directly determines the density of the adsorbed surfactant molecules at the surface. Several techniques used by the researchers are radiotracer (Lu et al., 1995), neutron reflection (Tajima et al., 1970), and infrared-reflection-absorption spectroscopy (Flach et al., 1997). The soluble chloride ion controls fluid equilibrium at the interface of the gas-liquid mixture. The chloride ion also controls fluid equilibrium and pH levels in metabolic systems. It is especially important to monitor the microbubble/nanobubbles characteristics used for medical applications like gene delivery (Huang et al., 2017) and drug delivery (Wang et al., 2013). The present research is to study the effect of various salts on the adsorption of sodium dodecyl sulfate (SDS) at gas-liquid and liquid-solid particles interfaces. Sodium chloride, lithium chloride, and cesium chloride were used to generate counterions. These counterions affect the stability of microbubbles, and this effect was studied in the presence of particles.

4.2. Theoretical background

4.2.1. Adsorption of surfactants at the bubble-liquid interface.

The effects of ions in gas-liquid two-phase phenomena depend on the increment of the molar surface tension in aqueous solutions. These phenomena are important to evaluate the increment of the surface tension of individual ions from the measurable surface tension data of complete electrolyte solution differs from that of pure water, which is referred to as a surface tension increment. It may be positive or negative depending on the electrolyte concentration (proportional to the electrolyte concentration) from high dilutions up to at least 1 mol dm^{-3}. The smaller concentration of ions results in a positive increment. From the ionic surface tension increment, it is possible to obtain the enrichment or depletion of the ions in the surface layer of the solution relative to their bulk concentrations. This is governed by the Gibbs adsorption law, which can be expressed as (Ghosh, 2009)

$$\Gamma = -\frac{1}{\nu RT}\frac{d\gamma}{d\ln\alpha} \tag{4.1}$$

where α is the thermodynamic activity of the electrolyte. The low concentration of the electrolyte is set equal to its activity. In general, for the surface-active compound, the Gibbs adsorption equation is used to interpret the surface excess concentration (Γ). Hence, Equation (4.1) is expressed as

$$\Gamma = -\frac{1}{\nu RT}\frac{d\gamma}{d\ln c} \tag{4.2}$$

where γ is the surface tension, and c is the concentration of the surfactant in bulk. Here, ν is a constant, and its value is 1 for a nonionic surfactant and 2 for 1:1 ionic surfactant or a univalent electrolyte (such as SDS or cetrimonium bromide). The Langmuir isotherm relates the concentration of the surfactant in the bulk solution in terms of surface excess as

$$\Gamma = \frac{\Gamma_\infty K_L c}{1 + K_L c} \tag{4.3}$$

Here, Γ_∞ is the adsorption capacity, which depends on the minimum surface area per adsorbed surface-active molecule. The equilibrium constant, K_L, is the ratio of the rate constants for adsorption and desorption. The surface EOS can be derived from Equations (4.2) and (4.3), as

$$d\gamma = -\nu RT\Gamma_\infty \left(\frac{K_L c}{K_L c} \right) d \ln c \tag{4.4}$$

For a pure solvent without the surfactant, the surface tension is γ_o. For this condition, Equation (4.4) can be integrated to obtain

$$\gamma = \gamma_o - \nu RT\Gamma_\infty \ln(1 + K_L c) \tag{4.5}$$

Equation (4.5) is the simplest surface EOS, known as the Szyskowski equation (Ghosh, 2009), that correlates the surface or interfacial tension with the concentration of the surface-active compound in the bulk of the sample. The parameters Γ_∞ and K_L are unknown and can be estimated by fitting the experimental data obtained from surface tension versus concentration profile. A limitation of this model is that it may not be accurate for the adsorption of ionic surfactants. When the ionic surfactant molecules adsorb at the interface, a potential is developed. The Langmuir model is not accounted for this potential.

4.2.2. Adsorption of the surfactant in the presence of salt

When a single-valence salt of the same counterion as the surfactant is added to the solution, it significantly affects the adsorption of ionic surfactant (Giribabu et al., 2007). Surface or interfacial tension decreases with the addition of salt concentration, which affects the degree of adsorption of ionic surfactants significantly more than nonionic surfactants. The electrostatic double-layer repulsion force between the surfactant head groups decreases with an increase in

the concentration of salt because of the enhanced electrostatic screening (Giribabu et al., 2007). Electrostatic screening develops further adsorption of the surfactant molecules at the interface. Giribabu et al. (2007) found that the salts containing divalent counterions (e.g., $MgCl_2$) are more functional than the salts containing monovalent counterions (e.g., NaCl) in the reduction of the surface tension of the solution, while salts containing trivalent counterions (e.g., $AlCl_3$) are more effective. For the investigation of the salt adsorption on the surfactant, Equation (4.4) can be modified as (Ghosh, 2009)

$$d\gamma = -RT\Gamma_{\infty}\left(\frac{K_L c}{1+K_L c}\right)\left[d\ln(c+c_s)+d\ln c\right] \tag{4.6}$$

where c_s is the concentration of salt. Integrating Equation (4.6), the surface EOS can be expressed as:

$$\gamma = \gamma_o - \left(\frac{RT\Gamma_{\infty}}{K_L c_s - 1}\right)\left[(K_L c_s - 2)\ln(1+K_L c)+K_L c_s \ln\left(\frac{c+c_s}{c_s}\right)\right] \tag{4.7}$$

This equation for the surface EOS does not account for the electrostatic and intermonolayer interactions and causes variations in the parameters K_L and Γ_{∞} with salt concentration.

The two crucial inferences that were made for deriving Equation (4.7) are as follows: first, the activity coefficients were taken to be unity, which corresponds to ideal solutions. The second assumption is that the salt is undistinguished to the adsorption at the interface. The parameters are obtained based on experimental data at high surfactant concentrations.

4.2.3. Adsorption behavior in the presence of particles

The microbubbles are thermodynamically unstable systems (Zhang et al., 2015). These microbubbles can be kinetically stable in the presence of the surfactant, as the surfactant molecules get adsorbed at the air-water interface and reduce the interfacial energy. The

drainage of liquid through the aqueous film of microbubbles is slowed down because of the Gibbs–Marangoni effect, which develops in the presence of the surfactant molecules at the interface (Jeelani and Hartland, 1994). The difference between the pressure inside the microbubble and its periphery is the capillary pressure which governs the drainage of liquid from the film of the microbubble. As the thickness of the film reduces to less than ~100 nm, the stability of microbubbles is governed by the DLVO (Derjaguin-Landau-Verwey-Overbeek) and the non-DLVO forces (Verma et al., 2018). These forces are dependent on the properties of the surfactant. The total disjoining pressure in the film of the microbubbles (Π_T) can be expressed by (Joye et al., 1992)

$$\Pi_T = \Pi_{vdW} + \Pi_{EDL} + \Pi_{Sr} \tag{4.8}$$

The first component of the disjoining pressure is van der Waals force of attraction, which refers to the film thinning, and the second is electrical double-layer-repulsive force, which resists the flow of liquid. Disjoining pressure is positive when it resists film thinning. The total pressure Π_T can be expressed by incorporating the components of the disjoining pressure (Joye et al., 1992)

$$\Pi_T = -\frac{A_H}{6\pi\delta^3} + 64RT_c \tanh^2\left(\frac{ze\psi}{4kT}\right)\exp(-\kappa\delta) + C_1\exp(-C_2\delta) \tag{4.9}$$

where n is the number of counterions per cubic centimeter in the bulk solution, δ is the thickness of the adsorbed monolayer, z is the valence, e is the electronic charge, ε is the dielectric constant for the solvent, k is Boltzmann′s constant, ψ is the electrical potential at the interface, and κ^{-1} the Debye–Huckel characteristic length, which can be expressed as

$$\kappa^{-1} = \left(\frac{2e^2z^2n}{\varepsilon kT}\right)^{-1/2} \tag{4.10}$$

Equation (4.10) is valid for flat bubble films but can be applied to the spheres as well. The van der Waals force dominates when the separation between the surfaces is small and is insensitive to the sample with electrolytes. If the separation between the surfaces is significant, electrostatic double-layer repulsion is stronger and more sensitive to the solution with electrolytes. The Debye–Huckel parameter is being controlled by the concentration of salt directly; thus, if the concentration of salt is increased, it will increase and affect the electrostatic double-layer-repulsive force inversely. Therefore, the presence of salt can alter the magnitude of the electrostatic double-layer force.

The behavior of microbubbles is related to an increase in adsorption with a decrease in dynamic surface tension. The surface tension of microbubbles changes with time until a final equilibrium is reached depending on various factors such as the physic-chemical property of the surfactant molecules and the surface composition. The dynamic behavior of the adsorption is governed by first the interchange of molecules between the surface layer and the subsurface layer and second by the interchange of molecules between the subsurface and the bulk solution. The most straightforward controlling equation for the prediction of surface concentration $\Gamma(t)$, given by Chang and Franses (1995), can be expressed as

$$\Gamma(t) = 2c_o\left(\frac{Dt}{\pi}\right)^{1/2} - \left(\frac{D}{\pi}\right)^{1/2}\int_0^t \frac{c(0,\tau)}{(t-\tau)^{1/2}}d\tau \qquad (4.11)$$

where τ is a dummy variable, c_o is the initial concentration, t is the time, and D is the diffusivity in the bulk solution.

Salt addition in the solution facilitates the adsorption on the interface and increases the repulsion between the surfaces, maybe because of steric or osmotic pressure. For stabilizing the microbubbles, surface modifiers of low molecular weight or high molecular weight can be used. Solid particles having such properties can also be used to stabilize the microbubbles. The

adsorption ability of surfactants vigorously affects the microbubble stability and controls its stability along with its formation (Denkov and Marinova, 2006).

4.3. Experimental procedure

4.3.1. Determination of CMC

Measurement of surface tension is one of the methods for the determination of CMC of surface-active solutions. In the present study, the surface tension of the anionic surfactant is measured in the presence and absence of the different types of salts at their different concentration. The CMC of the surface-active solutions was determined from the profile of surface tension versus surfactant concentration. The Wilhelmy plate method (Ghosh, 2009) tests were performed using the KYOWA automatic surface tensiometer (model: DY-300, S/N: 021-00368, made in Japan) to determine the effect of salts on the CMC as well as the critical association concentration. Each test was repeated four times, and the value was noted with a standard deviation not exceeding ± 0.2 mN/m.

Ionic microbubbles were generated using a mixture having a maximum speed of 20,000 rpm (Butterfly Matchless 750 W Mixer) based on the design recommended by Sebba (1987), as described in Chapter 3. The significant variables chosen were surfactant concentration, salt concentration, different salts, different particles, and particle concentrations. Distinct levels (low, medium, and high) were studied for each variable. The description of the levels considered in the present study is given in the following sections.

Surfactant concentration: Low – 0.1 mol m^{-3}, medium – 1 mol m^{-3}, and high – 10 mol m^{-3}. These levels were fixed corresponding to the value of the CMC of the surfactant used, that is, SDS. The solution condition is chosen because the CMC strongly depends on the presence of salt.

Salt concentration: Low–10 mol m^{-3}, medium–50 mol m^{-3}, and high–100 mol m^{-3}. These levels were chosen for all three salts (NaCl, LiCl, and CsCl) as a variable for the fact that it affects the electrostatic interactions between surfactant molecules and between particles and surfactant molecules when particles are present in the system.

Particle concentration: Low – 0.79 w/w %, medium – 1.57 w/w %, and high – 3.84 w/w %. These levels of particle concentration were chosen as the concentration of particles exceeded the high level.

4.4. Results and Discussion

4.4.1. Effect of salts on adsorption

Salt addition plays a supportive role in affecting the surface tension property of the surface-active solution. The significant change observed during salt addition was a reduction in the CMC of the surfactant. It is also observed that lithium chloride (LiCl) is significantly stronger than sodium chloride (NaCl). Significant changes occurred in the aqueous surface-active solution (SDS with water) in saturating the air-water interface at a low concentration of the cesium chloride. The change in the bending pattern of the curve represents the CMC for a specific salt in the surface tension versus concentration (surfactant) profile, as shown in Figure 4.1. The salt concentration is varied between 10 mol m^{-3} and 100 mol m^{-3}. It was observed that adding 50 mol m^{-3} of NaCl reduced the CMC to 2 mol m^{-3}, which was 7 mol m^{-3} initially in the absence of salt. Adding more NaCl enhances the adsorption properties. The surface is found saturated at the concentration of 2 mol m^{-3} when the salt concentration was at 100 mol m^{-3} (Figure 4.1 (a)) in the presence of the surfactant, which was a quarter fraction of the CMC of the surfactant when there was no NaCl present. An abrupt change in surface tension and CMC

is observed with an increasing salt concentration. Similar changes were also seen in the presence of LiCl in Figure 4.1 (b), but CMC was attended at around 0.6 mol m^{-3} concentration of SDS with 100 mol m^{-3} of LiCl salt, which is very low. As shown in Figure 4.1 (c), the CMC was at 2 mol m^{-3} of the surfactant solution at 10 mol m^{-3} of salt of CsCl, which reduced to 0.4 mol m^{-3} at 100 mol m^{-3} concentrations of CsCl. Figure 4.1 (d) shows the variation in the surface tension of each salt at 10 mol m^{-3} with a change in the concentration of SDS. Saturation was achieved at the air-water interface for levels which was from 50 mol m^{-3} to 100 mol m^{-3} for NaCl and CsCl, respectively, and produced curtailment in surface tension values to a smaller extent. But in the presence of LiCl, there is a massive difference between the CMC at 50 mol m^{-3} and 100 mol m^{-3}; therefore, more salt can be added as the saturation is not attended.

The salt efficiency in reducing the CMC is reported in the following progression as CsCl > NaCl > LiCl. Figure 4.2 represents the changes in CMC with salt concentration. The CMC of a surfactant solution depends on the polar head group, which repels each other because of the mutual charge-repulsive nature, and if the repulsion is giant, no micelles are formed. Hydrophobic interaction is the other factor that attracts the surface-active agent tails. The addition of salt decreases the attraction force and reduces the charge density, thus reducing the CMC of the surfactant solution.

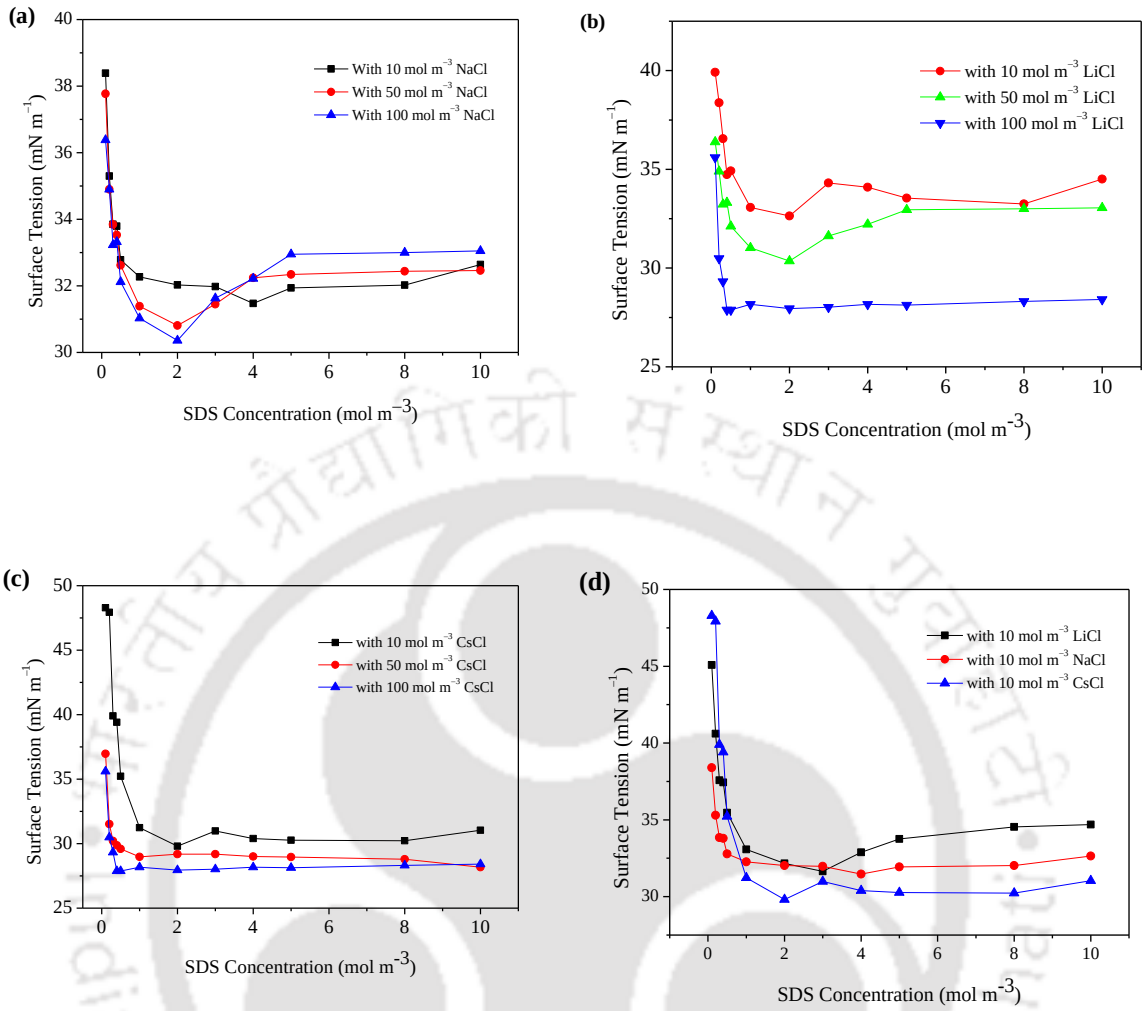

Figure 4.1. Variation of surface tension with varying concentrations of SDS at 0, 50, and 100 mol m^{-3} concentration of salts (a) in the presence of NaCl, (b) in the presence of LiCl, (c) in the presence of CaCl, and (d) in the presence of different salts with 10 mol m^{-3} of its concentration.

4.4.2. Effect of salt on critical micelle concentration

The interfacial behavior of surface-active molecules at the interfaces is essential for a variety of colloidal phenomena such as surface tension, thin-film stability, and micellization. Counter-ions play a significant role in the interfacial properties of surface-active molecules. Depending

on the counterions, the CMC changes for any surfactant in the presence of electrolytes. For example, the CMC of dodecyl sulfate follows the rule $CMC_{Cs} < CMC_{K} < CMC_{Na} < CMC_{Li,}$ that is, it increases with the effective radius of the hydrated counterion (Mukerjee et al., 1967). This example shows that the smaller the hydrated radii, the higher is the interaction, which produces a lower degree of dissociation and more compact double layers. When an ionic micelle is formed from these monomeric ions, the hydrophobic interactions are balanced between the hydrophobic part of the amphipathic micelle-forming ions and the electrostatic interactions between their hydrophilic charged components, as well as among the counterions. These interactions depend on temperature, ionic strength, properties of the ions involved; concentration and structure of the resulting micelle; and the compactness of its electrical double layer (Boström et al., 2005). The ranking of the ions, according to their efficiency, is called the

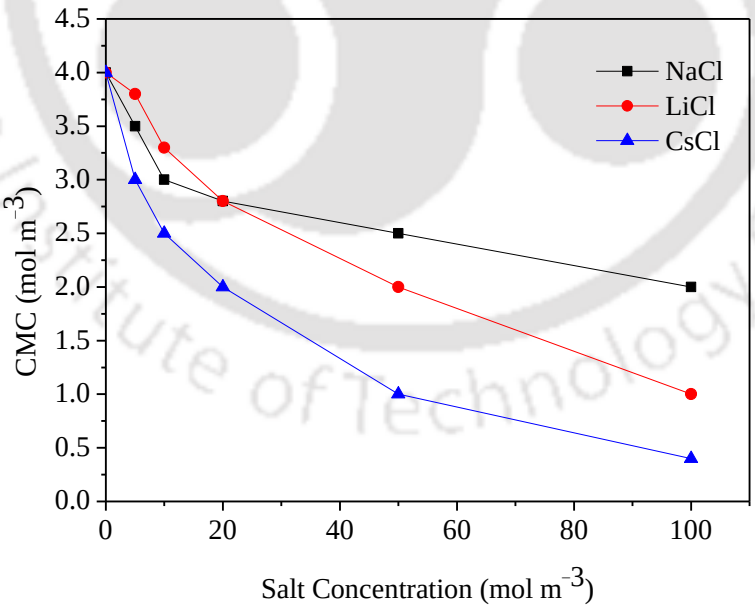

Figure 4.2. Variation of CMC with a salt concentration in an aqueous solution of SDS

Hofmeister series. The Hofmeister effect is related to many phenomena besides the solubility of surfactant and the surface tension of electrolyte solutions. It is vital for colloidal stability, including bubble-bubble interaction (Weissenborn and Pugh, 1996).

4.4.3. Effect of different salts on the film thickness around the interface

In ionic surfactant solutions, the stability of microbubbles is dependent on the interface being repelled by the double-layer force (Ghosh, 2004; Ghosh and Juvekar, 2002). The film thickness between the microbubble and the interface reduces with time. At a level when the film thickness becomes adequately small, the film gets ruptured because of van der Waals forces, which lead to coalescence. Increasing salt concentration reduces the thickness of the ionic atmosphere present between surfaces (i.e., the Debye length, κ^{-1}). The thickness called Debye length is expressed as (Giribabu et al., 2007):

$$\frac{1}{\kappa} = \sqrt{\frac{\varepsilon \kappa_B T}{N_A e^2 \Sigma_i z_i^2 c_i}} \tag{4.12}$$

The degree of film thickness reduction follows the progression as CsCl > LiCl > NaCl at a specific salt concentration. The double-layer-repulsive response is affected by the ion binding, which tends to reduce the surface potential.

4.4.4. Effect of salt and particles on adsorption

Langmuir is one of the simplest adsorption isotherms, which is a two-parameter equation relating the adsorbed surface density to the bulk surface-active agent, as briefly described in the earlier section. The maximum experimental number of molecules adsorbed for a soluble surfactant approach is the theoretical limiting value, $\Gamma_{m,L.}$ $\Gamma_{m,L}$ (mol m^{-2}) for SDS is about 8×10^{-6} (upper limit value) and 6×10^{-6} (lower limit value). The Langmuir isotherm is modeled as a dynamic equilibrium on adsorption and desorption. The experimental surface tension data

were used to calculate the model outputs at different parameters, as summarized in Tables 4.1 and 4.2. For a larger value of $K_{L,}$ a smaller bulk surfactant concentration is needed to affect the same degree of surface coverage. The parameters strongly depend on the salt concentration because of the electrostatic and intramonolayer interactions.

Table 4.1. Parameters of Adsorption of SDS at the Air-Water Interface.

SDS (mol m^{-3})	γ (mN m^{-1})	$\Gamma \times 10^6$ (mol m^{-2})	K_L (m^3 mol^{-1})
0.3	51.34	–1.52	–0.10
0.5	47.93	0.38	–0.51
1	43.13	1.89	–1.00
2	40.21	2.07	–2.01
3	31.85	1.59	–3.01
4	30.72	1.00	–4.02
5	31.13	0.38	–5.08
8.2	32.50	–1.46	–8.17
10	33.43	–2.38	–9.97

Table 4.2. Best fit parameter values to the Langmuir model.

c_s (mol m^{-3})	Parameters fit	$10^6\,\Gamma_{m,L}$ (mol m^{-2})	K_L(m^3 mol^{-1})	$\Delta\gamma$ (mN m^{-1})
		For NaCl		
5	$\Gamma_{m,L}$, K_L	0.13	0.13	0.72
10	$\Gamma_{m,L}$, K_L	0.29	0.03	1.10
50	$\Gamma_{m,L}$, K_L	–0.02	–0.02	1.10
100	$\Gamma_{m,L}$, K_L	–0.01	–0.01	1.14
		For LiCl		
5	$\Gamma_{m,L}$, K_L	0.03	–0.09	0.82
10	$\Gamma_{m,L}$, K_L	0.04	–0.05	0.89
50	$\Gamma_{m,L}$, K_L	0.01	–0.02	0.92
100	$\Gamma_{m,L}$, K_L	0.01	–0.01	0.94
		For CsCl		
5	$\Gamma_{m,L}$, K_L	0.14	0.12	0.62
10	$\Gamma_{m,L}$, K_L	0.42	0.02	0.78
50	$\Gamma_{m,L}$, K_L	-0.02	-0.02	1.35
100	$\Gamma_{m,L}$, K_L	-0.01	-0.01	1.42

4.5. Conclusions

An understanding of the presence of electrolytes at different concentrations in the aqueous surfactant solution and their effect on the characteristics of ionic microbubbles is of great interest. The behavior of the microbubbles formulated at different parameters with salts and particles has been studied in this work. As we know, the degree of micellar growth varies in the reverse order of the hydrated radius of the counterions; here, it was found that the hydrated caesium ions interact more strongly with the oppositely charged heads, as the hydrated Cs^+ ions have the smallest hydrated ionic size than other ions in the present study. Consequently, these strong interactions favor micelle formation and binding to the Cl^- at the surface. The present results show that with an increase in the size of the hydrated counterion, the CMC increases, whereas the degree of counterion binding decreases. It has also been observed that salt addition affected the CMC of the surfactant up to the critical concentration of the particular salt until saturation was achieved. This study is useful for further analysis of the stability of microbubbles in the presence and absence of salt and mineral particles.

CHAPTER 5

5. Stability of Ionic Microbubbles and Its Kinetics

This chapter presents the generation of ionic microbubbles and their stability. The degree of stability of ionic microbubbles is estimated by measuring the drained volume of liquid with respect to time. The effects of types of surfactants, surfactant concentration, temperature, and pH of the solution on the stability of colloidal microbubbles are examined. The investigation of the kinetic mechanism of the microbubble in the presence and absence of particles is studied. A correlation has been developed to predict the stability parameters.

5.1. Introduction

Microbubble structure and its stability are known to play a significant role in determining the grade and recovery by its flotation. Sebba (1971 and1987) first described the microbubble as having some colloidal properties with a size range of 25-100 µm. He proposed that microbubbles consist of a gaseous inner core surrounded by a shell composed of two surfactant layers in addition to the third layer of surfactant that stabilizes its structure. Numerous studies are presented in the literature on microbubble generation (Parmar and Majumder, 2013) and applications such as removal of pulp fiber (Mukherjee et al., 2015), pre-dispersed solvent extraction of dilute products (Matsushita et al., 1992), protein recovery (Amiri and Valsaraj, 2004; Jauregi et al., 1997), clarification of suspensions (Roy et al., 1992; Subramaniam et al., 1990), separation of organic dyes from wastewater (Roy et al., 1992), removal of heavy metals from aqueous solutions (Ciriello et al., 1982), separation of fine particles (Chalkosh Amiri, 1990; Mansur et al., 2004), removal of methyl orange and methylene blue dye from water (Basu and Malpani, 2001), removal of hazardous oily waste from a soil matrix (Roy et al., 1994), fractionation of a red grape marc extract (Dahmounea et al., 2013), extraction of erythromycin

(Lye and Stuckey, 2000), removal of pyrene (Maske et al., 2012), etc. The microbubble indicates a large interfacial area per unit volume which increases the adsorption of molecules on its surface. Its holdup enhances the probability of particles to attach on its surface (Roy et al., 1992).

Conventional flotation has been incorporated with microbubbles for application in the recovery of fine mineral particles (below 13 μm) and in solid/liquid separation to remove pollutants (Amiri and Valsaraj, 2004). Surface forces and electrostatic forces are two main interactive forces present in dispersed microbubbles, which direct their application in various fields (Maske et al., 2012). Microbubbles formed by the use of ionic surfactants contribute electrostatic interaction to the stability of its dispersion, which is governed by the charged or polar groups in the surfactant molecules at the gas-liquid interface (Tsuge, 2010). Microbubbles in non-ionic surfactants are governed by steric forces, which also play an important role in stabilizing their dispersions (Amiri and Sadeghialiabadi, 2014). The literature reports stability of microbubbles depends on many variables (Parmar and Majumder, 2013). Lamentably, there is a knowledge gap on hydrodynamic characteristics of microbubbles in various liquids in the presence and absence of fine solid particles and its stability. Modifying the surface tension of liquid can not only shift the bubble size distribution it also influences the stability. But there are no significant studies available in the literature that can correlate the stability of microbubbles with the concentration of surfactant in the presence of micro and nano particles. Also, there is no such quantitative research available in the literature that can demonstrate the effect of particle concentration and other effects like temperature and pH on the stability of microbubbles. Based on this scope of the study, the objective of the present work is to study the effects of micro-nano particle concentration, temperature, pH, and surfactants on the stability of microbubbles, its holdup, and size. The present work is also aimed to develop an empirical model to interpret the effect of variables on them.

The stability of microbubbles has been determined by two different occurrences, first is the rate at which liquid drains from a bubble, and the second is the rate at which the body of the bubble breaks down (Jacobi et al., 1956). The former is the gas disengagement method, and the latter is the gas dissolution method. In the present work, the previous process has been used to study the stability of the microbubbles generated with different specifications. The microbubbles have been formulated with surfactants, which are stable, and there is no perceptible breakdown of the colloidal microbubbles until after the majority of the liquid has drained from the microbubbles. The microbubbles are very close together, so they coalesce; they do not coalesce by disruption of the interface but at the expense of smaller bubbles. The coalescence happens due to the pressure difference between the bubbles, but when a limiting size of the order of microns in diameter is reached, further reduction ceases. After a while, the larger bubbles grow and increase in buoyancy until they overcome the surface forces retaining them in colloidal dispersion, and it rises to the surface to be part of conventional bubbles. Thus, this describes the stability of a microbubble in terms of half-life, the time required to clear the half volume of bubbles and become milky to transparent. Sebba (1970) observed a half-life of 5 min or more and concluded that the half-life could be increased by reducing temperature or increasing viscosity by adding additives and suggested that microbubbles have enough half-life for a photographic method to study the behavior of microbubbles and the mechanism of the coalescence.

Xu et al. (2008) reported that the properties of the microbubbles depend on the generation method and the type of surfactant used. Therefore, the selection of a suitable method of bubble generation and a suitable surfactant is essential for the application of microbubbles in any area. There is a wide range of choices to meet the specific property of the microbubble for a particular application. However, based on the literature review, it is observed that the stability of microbubbles can be enhanced by using different types of surfactants, even by changing the

temperature of the system or pH of the system, the stability of the microbubble can be enhanced. So, to know the behavior of the microbubbles in a different system, the present study has been done. The purpose is to study the stability of microbubbles generated with different surfactants like anionic, cationic, and bio-surfactant at different temperatures and a wide range of pH.

5.2. Experimental

5.2.1. Generation of ionic microbubbles

The ionic microbubbles are generated with a high-speed stirrer (Butterfly Matchless 750 W Mixer, max 20,000 rpm), similarly to Sebba's (1987) defined microbubbles created by the intense stirring of a surfactant solution. The details of the experimental setup and procedure for the generation of microbubbles are described in chapter 3.

5.2.2. Stability measurement of ionic microbubbles

Generally, the stability of the ionic microbubbles is determined by two different methods. The first method is based on the rate at which liquid drains through the bubbles, and the second is based on the rate at which the bubbles break down (Jacobi et al., 1956). Based on the first method, the volume of liquids drained through the ionic microbubbles is observed in three phases. The first phase constitutes the rapid increase in the drainage of the liquid with time, the second phase constitutes the sharp decrease in the drainage of the liquid with time, and the third phase constitutes a very less liquid volume of the liquid to drain with time. Initially, liquid drains invariably, and the drainage of liquids is influenced by the distribution of the liquid between the microbubble films and the plateau border (Wang and Narsimhan et al., 2004; Narsimhan and Ruckenstein, 1986). The first phase is governed by the gravitation force, which allows water to drain through the plateau border and the upward creaming of microbubbles. The microbubbles increase in size with time due to the disproportion of the liquid and the gas

diffusion between bubbles (Sebba, 1987). The stability of ionic microbubbles can be defined as the length of time over which the number of bubbles and their size distribution remains constant. It can be measured with respect to the time for half the liquid of the ionic microbubbles are drained (Jauregi et al., 1997). The degree of stability of ionic microbubbles is estimated by measuring the drained volume of liquid with respect to time, as proposed by Longe (1989). The schematic diagram of the stability analysis is shown in Figure 4.1 (a).

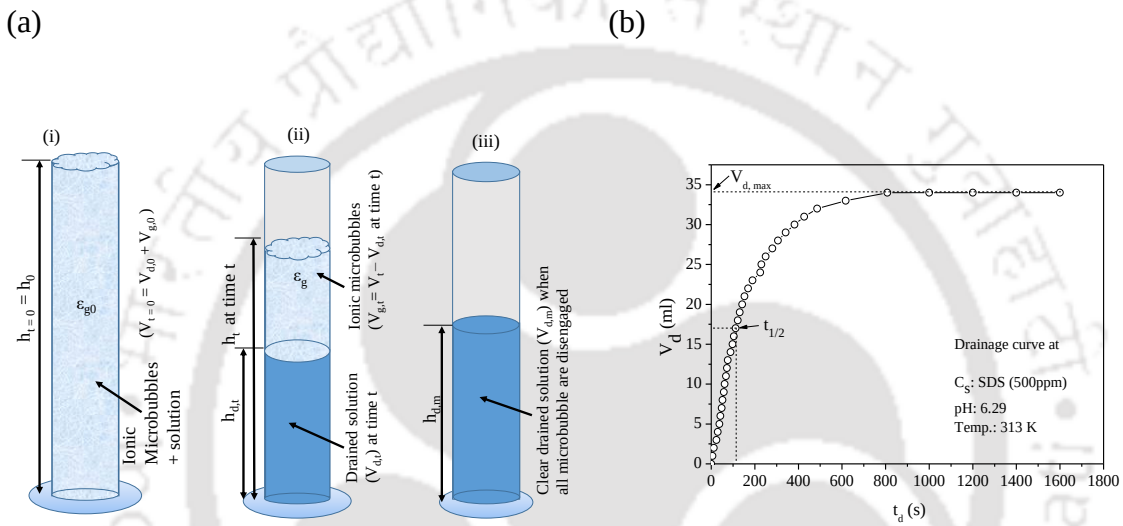

Figure 5.1. Pictorial representation of the subsequent steps in the drainage process. (a) (i) Maximum dispersion volume of microbubbles immediately poured into the cylinder just after stirring at t = 0, start of drainage process; (ii) progress of drainage at time (iii) clear liquid after drainage, and (b) Typical outline to estimate the half-life of ionic microbubbles.

After preparing the ionic microbubble, it is transferred to a measuring cylinder, which is kept in a constant temperature bath. A circulating water bath (ANM Industries Pvt. Ltd., Thane, Model No.: WB 2000) is used to maintain a constant temperature. A video camera (Nikon, Coolpix L340) is used to record the drainage of liquid for different concentrations with various

operating parameters. The measurement is done immediately just after the preparation of ionic microbubbles to avoid an error. Figure 5.1 (a) illustrates the drainage process of microbubbles; the freshly generated microbubbles were poured into a 50 ml measuring cylinder, and the total height of the microbubble with a solution was recorded as (h_t), as well total volume of the cylinder at the same time (V_t). With a span of time, the total height/volume of the microbubbles will decrease as the liquid through the microbubble lamella drains through them and accumulate at the bottom, which gives clear liquid noted as $h_{d,t}$ or $V_{d,t}$. After the complete drainage of liquid through microbubbles, the final height/volume of the liquid is recorded as $h_{d,max}$ or $V_{d,max}$. The stability of the microbubbles was quantified according to Sebba (1987), as the time taken for half the liquid to drain through the microbubbles is referred to as half-life ($t_{1/2}$). The volume drainage of liquid (V_d) as a function of time (t_d) was plotted for different parameters. The plotted curve was used to estimate the time taken to drain half of the liquid from the colloidal microbubbles suspension, as shown in Figure 5.1 (b). The ratio of half-life to the total time of liquid drainage is referred to as a degree of stability.

5.2.3. Properties of the system

The sodium dodecyl sulfate (Sodium Lauryl Sulfate, anionic), cetyl trimethyl ammonium bromide (CTAB, cationic), nanoclay, a surface modifier containing 25–30 wt.% trimethyl stearyl ammonium, and a bio-surfactant saponin (non-ionic) and alcohol (glycerol) are used to study the effect of different factors on the stability of the ionic microbubbles. All the experiments in the present work are carried out at 25° C unless the effect of temperature is studied. The various properties of materials used in the present study are shown in Tables 3.1–3.3 in Chapter 3.

5.3. Results and Discussion

5.3.1. Drainage kinetics

Ionic microbubbles are thermodynamically metastable systems, and their stability is apprehensive for its practical application, for which lots of research has been done. The stability of the microbubbles depends on the collapsing of the bubble with time, which occurs by two phenomena: disproportionation of the bubbles and film breakage. Film breakage can be hindered by the use of viscous liquids and by using suitable surfactants, which may stabilize the films when the ionic microbubbles are in dry form (Vignes-Adler and Weaire, 2008). The stability of ionic microbubbles can be measured directly from the rate of liquid drainage. The drainage process for SDS and CTAB is shown in Figures 5.2 and 5.3, respectively. It is seen from Figures 5.2 and 5.3 that the various formulation of ionic microbubbles tested results in drainage curves are of the same trend.

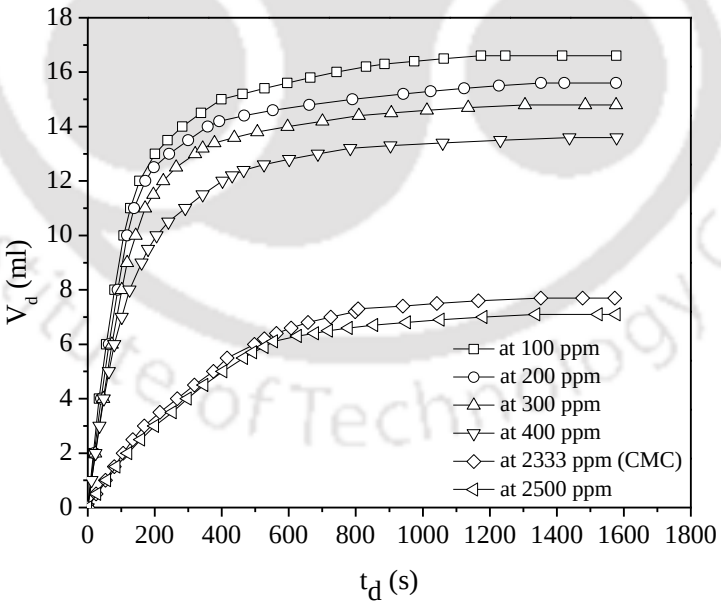

Figure 5.2. Effect of different concentrations of surfactant (with anionic surfactant (SDS) without particles) on drainage at room temperature.

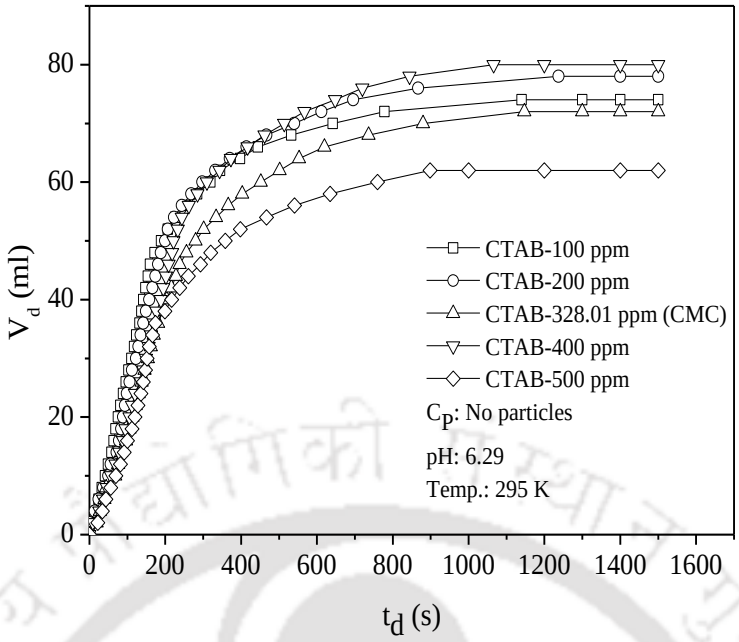

Figure 5.3. Effect of different concentrations of surfactant on drainage at room temperature with cationic surfactant (CTAB) without particles.

The microbubbles are not possible to be formed using only pure water, so a minimum concentration of surfactant is required for its formation. The flow behavior of the microbubbles is like those of water, so microbubbles can be pumped easily, without collapsing, from one location to another. Liquid drainage curves of the colloidal microbubbles follow the "S"–shaped profile, with an increase in the rate of drainage at the initial stage followed by a decrease in the rate of drainage at later times. It is seen that the most stable microbubbles are formed at the critical micelle concentration (CMC) of the surfactant. Beyond CMC, Moshkelani and Amiri (2008) also reported that the most stable microbubbles could be produced at critical micelle concentration (CMC) in the absence of particles or any other additive. The stability of microbubbles is decreased when the concentration of surfactant is more than CMC (Yan et al., 2005). The drainage curves of various ionic microbubbles in the presence of nanoclay are shown in Figures 5.4 and 5.5.

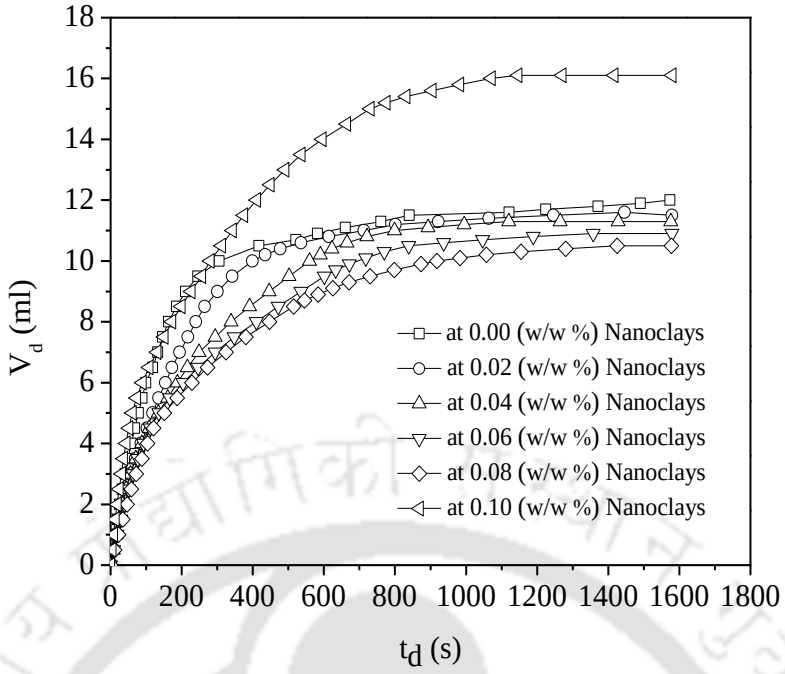

Figure 5.4. Effect of nanoclay addition on stability of charged microbubble with an anionic surfactant SDS (500 ppm) at room temperature.

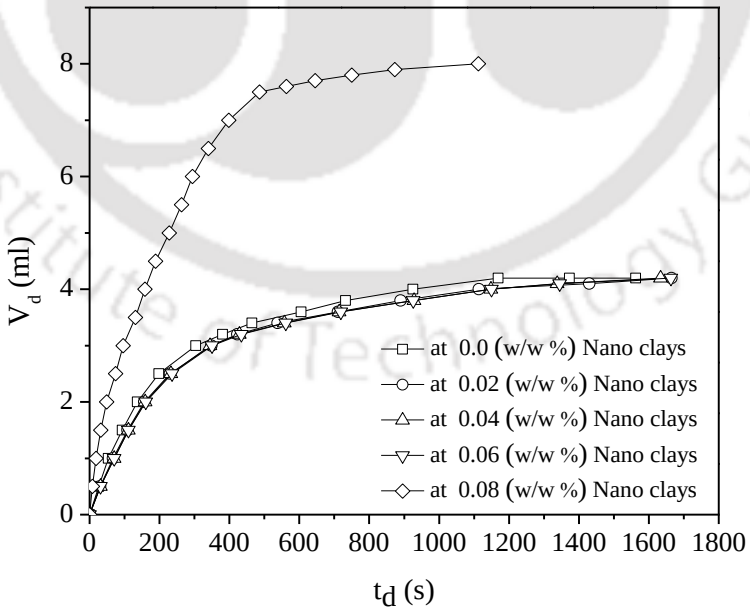

Figure 5.5. Effect of nanoclay addition on stability of charged microbubble with the Saponin (non-ionic surfactant, 1000 ppm) at room temperature.

It is observed that with an increase in the concentration of nanoclay, the rising velocity of microbubbles decreases up to a certain concentration of 0.08 wt. % of nanoclay. After that sudden increase is observed with more amount of nanoclay. The nanoclays are encapsulated around the microbubbles, which inhibit the gas diffusion and coalescence, thus improving the stability of the microbubble. But increase in nanoclays also increase the density of microbubbles, so the addition of more nanoclays would not lift the bubble and so break down. The new behavior of the surface tension plot with surfactant in the presence of nanoclay was found by Amiri and Sadeghailaliabadi (2014). They found that above CMC, the surface tension of microbubbles has no consistency. The CMC of surfactant solution shifts to a lower value in the presence of nanoclay. They also concluded that with the concentration of nanoclay, the stability of microbubbles does not significantly change. The surface tension is decreased initially, and then an increase is seen with the increase in the concentration of nanoclay to 72.9 mN/m, and then a fall of surface tension is seen. The effective surface tension of systems containing both surfactants and nanoparticles depends on their affinity for each other, as reported in the literature (Ma et al., 2008).

The profiles of liquid drainage as a function of time at different temperatures for constant surfactant concentration are shown in Figures 5.6 and 5.7. It is observed that as an increase in temperature of the surfactant solution half-life of the liquid drainage increases. The degree of stability is found to increase with the increase in temperature. There are two reasons for changing stability with temperature: (i) with an increase in temperature larger microbubble breaks into a smaller bubble which rises slowly as compared to a larger microbubble, and (ii) the liquid temperature reaches near saturation where phase change rate is increased due to increase in vapour pressure (Yan et al., 2005). Jianhong et al. (2009) reported that with an increase in temperature, the viscosity of liquid reduces and make a thin liquid film, resulting in

an increase in the rate of liquid drainage, which results in a decrease in stability with an increase in the half-life of the ionic microbubble.

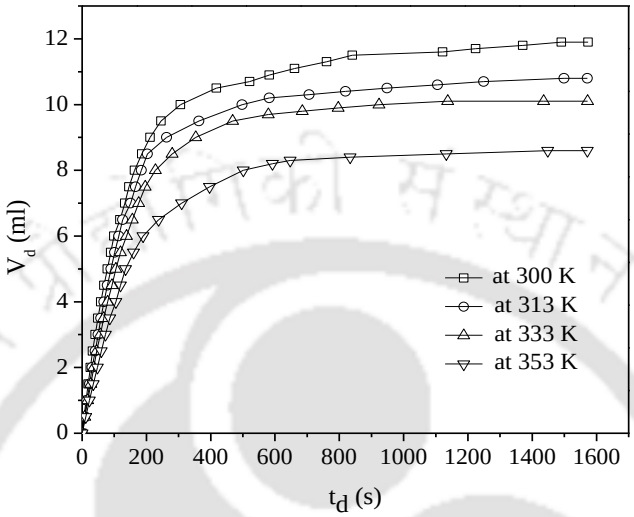

Figure 5.6. Effect of temperature on the stability of charged microbubbles with an anionic surfactant SDS (500 ppm).

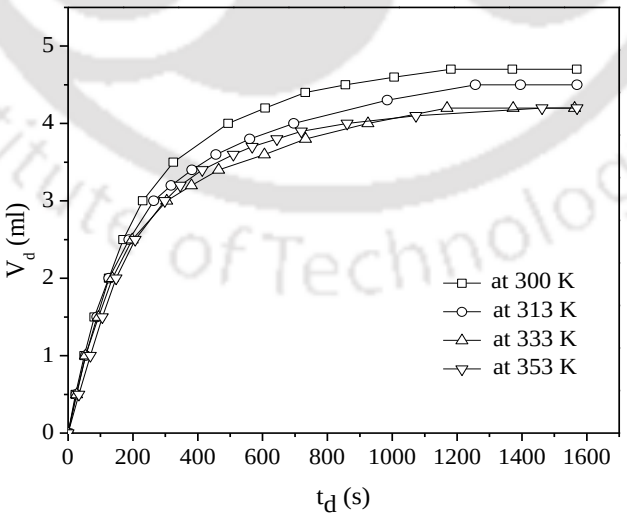

Figure 5.7. Effect of temperature on the stability of charged microbubbles without particles and with non-ionic surfactant Saponin (1000 ppm).

5.3.2. Half-life of ionic microbubble at different pH

The stability of ionic microbubble is calculated by measuring the half-life ($t_{1/2}$) (i.e., the time taken to drain half of the initial volume of the liquid) of the liquid drainage. More half-life represents more stable ionic microbubbles. Figure 5.8 shows the effect of pH on the stability behavior of anionic surfactant (SDS) solution.

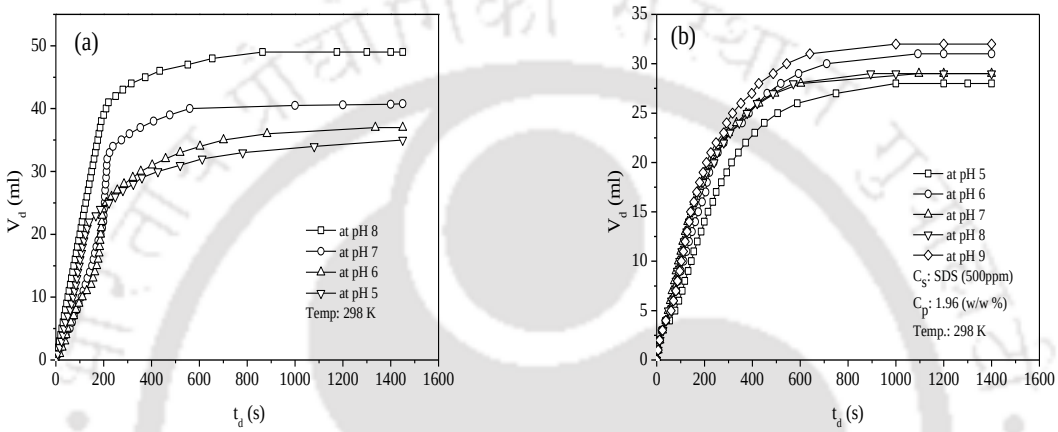

Figure 5.8. Effect of pH on drainage profile (a) with anionic solution (500 ppm SDS) in the absence of particles and (b) with aluminum oxide particles at a concentration of 1.96 (w/w %) with anionic surfactant at (SDS) room temperature.

The half-lives of microbubbles in the absence of particles are higher (160 and 180 s) for the given pH range, while in the presence of particles, it reduces from 140 to 150 s, as shown in Figures 5.8 (a) and Figure 5.8 (b) respectively. It is also observed that at different concentrations of particles, the stability of microbubbles depends on the concentrations of particles. In the absence of particles, the stability of the microbubbles generated by the anionic surfactant SDS decreases by about 8% for pH changing from 6 to 8, while at lower pH < 6, the stability decreases further. The half-life value increases at pH 9 both in the absence and presence of particles with the same anionic surfactant solution, as shown in Figure 5.9.

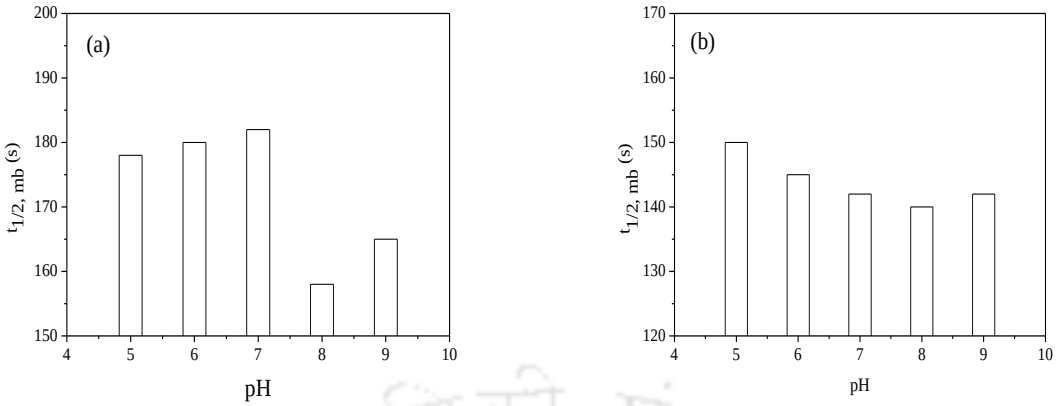

Figure 5.9. Effect of pH on the half-life of colloidal microbubbles, (a) microbubbles without particles in the presence of SDS (500 ppm) and (b) microbubbles with Al_2O_3 particles in the presence of SDS (500 ppm) at room temperature.

At a fixed concentration of anionic surfactant (SDS) and particles, a similar trend is observed with pH varying from 6-8. The same trend of influence of pH on stability has been reported for anionic surfactant SDS by Lye and Stuckey (2000), which suggests a declining trend as the continuous phase becomes more acidic. The excess hydrogen ion concentration by changing pH leads to the addition of a proton (H^+) to an atom, molecule, or ion of the sulphonate head-groups of the SDS molecules located at the surfaces of microbubbles. This effect the microbubble stability in two ways: one is that it would reduce the surface charge on the microbubbles and hence the energy barrier to their coalescence, which can be seen for 500 ppm SDS solution in the presence of copper oxide particles as its zeta potential falls from –40.01mV at pH 9 to –23.75mV at pH 7.5 as shown in Figure 5.10. The other effect is the reduction in the polarity of the surfactant monomers making it energetically less favorable for the hydrophobic tails of the surfactant molecules to remain in the polar environment.

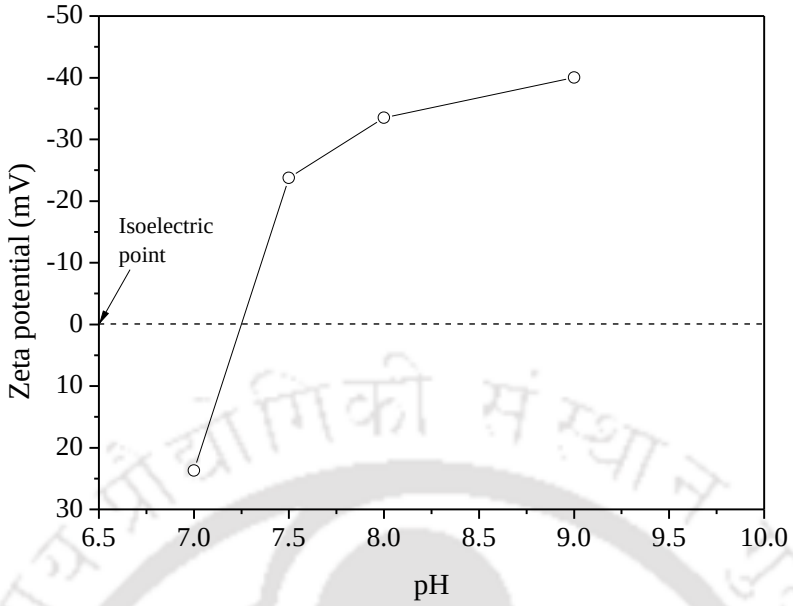

Figure 5.10. Effect of pH on the zeta potential of CuO particles in the surfactant (SDS 500 ppm) solution.

The reason for the stability change (either increases or decreases) is that the solution presents in the ionic form, which would have contributed to the stabilization of the microbubbles, but the degree of ionisation that changes with pH does not appear to affect the stability of the system. These consistent observations are reported by other authors (Save et al., 1993; Subramaniam et al., 1990). Feng et al. (2009) concluded that at higher pH, ionization of the surfactant's functional group increases, which can change the stability of the microbubbles, depending on the effect of ionization on bubble charge density and the repulsion between bubbles. The significant influence of pH on stability has been reported by Roy et al. (1992) for other ionic microbubbles formed by anionic rhamnolipid, while the stability of microbubbles of the non-ionic surfactant Tergitol remains unaffected. Some investigators reported that pH has no significant effect on ionic microbubbles stability (Sharma et al., 1985).

5.3.3. Mechanism of liquid drainage through ionic microbubbles

From the present experimental results, it is found that, for SDS, when the surfactant concentration is equal to or near the CMC (8.7 mM), the half-life ($t_{1/2}$) is higher than those of other surfactant concentrations excluding CMC value. Although the drainage curve shows a similar trend for the different surfactants, wide variations were observed in the drainage rate. This variation is mostly because of parameter n'-the higher value of n' results in higher stability of ionic microbubble. Initially, a rapid increase in the drainage rate is seen as per the present experiment at a particular variable to a maximum and then decreases as the power-law decay with increasing time, as shown in Figure 5.11. The initial increase in the drainage rate is due to the uniform water distribution in the ionic gas microbubbles throughout the tube just after its preparation. The distribution of the microbubbles changes with time. As soon as the liquid starts draining through the microbubbles, this liquid may redistribute, which results in increasing the liquid concentration at the trailing of bubbles. A consecutive increase in the liquid drainage increases the size of the microbubbles up to the drainage rate reaching its maximum value. The liquid drainage of the microbubble dispersions occurs in three distinct phases, as shown in Figure 5.11. Initially, in the first phase, the drainage rate increases with time due to a combination of up-flow migration of bubbles and downward liquid drainage under gravity. The drainage rate then decreases with time, dominated by liquid flow under gravity in the second phase. The dispersion behavior of this phase is similar to conventional wet foam. In the third phase, the drainage rate is low due to the slow liquid released from films under capillarity suction. From the drainage rate, it is observed that the height of the clear liquid reached a value of 40 mm within 883 s at 500 ppm of SDS at 298 K. Figure 5.12 is represented to show the change in drainage rate as a function of temperature. In contrast, when the temperature is increased to 313 K, 323 K, and 343 K, the clear liquid observed after the dispersion phase has completely disappeared at 727 s, 520 s, and 472 s, respectively. The total

height of the clear solution is decreased at a slower rate with increasing temperature, which affects the stability of the microbubbles. The stability is reduced with increasing temperature as the viscosity of the solution decreases with the increase of temperature.

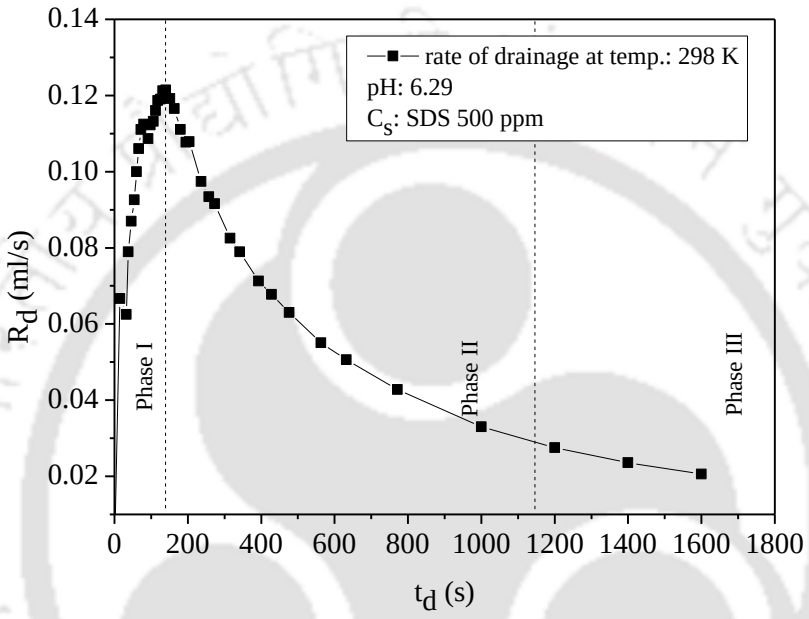

Figure 5.11. Variations of drainage rate of microbubbles in the absence of particles at 298 K temperature at 500 ppm SDS.

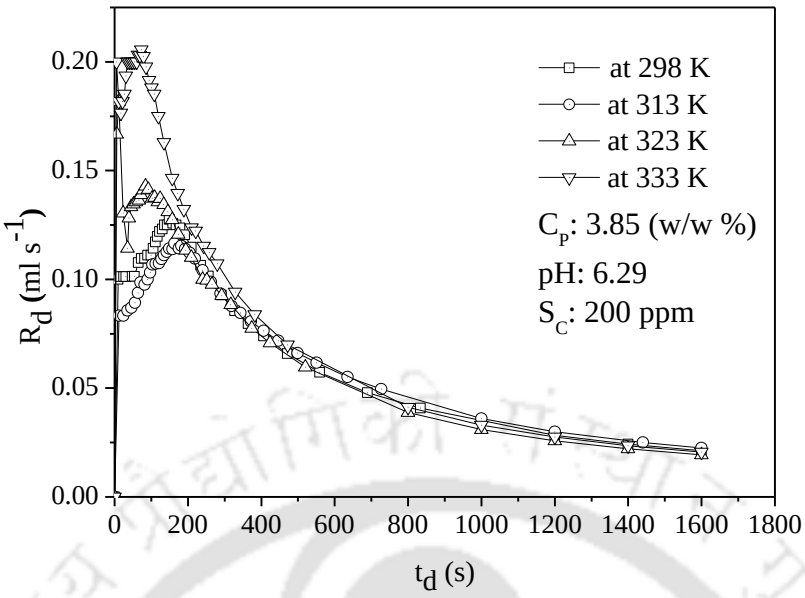

Figure 5.12. Effect of temperature on drainage rate for microbubbles with cationic surfactant CTAB in the presence of CuO particles.

5.4. Model kinetics of ionic microbubbles

Many investigators tried to develop a model for predicting liquid drainage rates. Amiri and Woodburn (1999) proposed a predictive model for the liquid drainage rate of colloidal microbubbles. Save and Pangarkar (1994) interpreted the drainage mechanism through the mathematical model for colloidal microbubble drainage. While Yan et al. (2005) developed an empirical model to study the rate of liquid drainage as a function of time. The unsteady liquid drainage from the charged microbubble can be empirically expressed by (Yan et al., 2005)

$$V_{d,t} = V_{d,\max} \frac{t_d^{n'}}{t_{1/2}^{n'} + t_d^{n'}} \qquad (5.1)$$

where $V_{d,t}$ is the volume of drained liquid at time t_d, $V_{d,max}$ is the final drained liquid volume, $t_{1/2}$ is the half-life of liquid drainage, and n' describes the growth character of the drainage

curve. These parameters are observed to vary with the concentration of surfactant, type of surfactant, temperature, and pH value of the solution. The stability of charged microbubble can be measured directly from the rate of liquid drainage. The rate of liquid drainage (R_d) can be derived by differentiating Equation (5.1) with respect to time which can be expressed as:

$$R_d = \frac{dV_{d,t}}{dt_d} = \frac{n' V_{d,\max} t_{1/2}^{n'} t_d^{n'-1}}{(t_{1/2}^{n'} + t_d^{n'})^2} \tag{5.2}$$

After rearranging Equation (5.2) the relationship between t_d and $V_{d,t}$ could be expressed as

$$t_d = t_{1/2} \left(\frac{V_{d,t}}{V_{d,\max} - V_{d,t}}\right)^{1/n'} \tag{5.3}$$

Substitution of Equation (5.3) into Equation (5.2) yields

$$R_d = \frac{dV_{d,t}}{dt_d} = \frac{n'}{t_{1/2} V_{d,\max}} V_d^{(1-1/n')} (V_{d,\max} - V_{d,t})^{(1+1/n')} \tag{5.4}$$

The modified model better fits the measured data compared to the original model in terms of smaller residual values and a more accurate prediction for the parameters' half-life and maximum drained volume.

The parameters of the drainage rate equation (Equation (5.1)) $V_{d,max}$, $t_{1/2}$, and n' were estimated using nonlinear least square regression. A plot of experimental data and the least square fit curve as per model Equation (5.1) is shown in Figure 5.13.

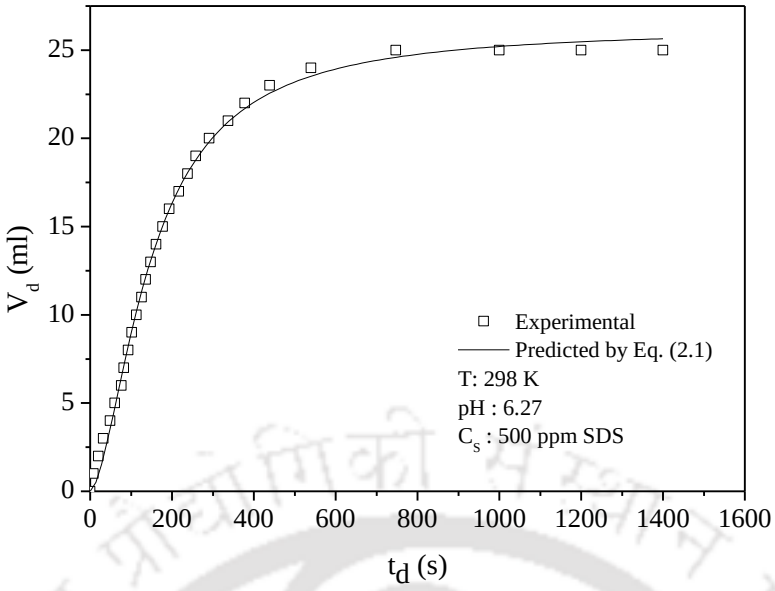

Figure 5.13. Comparison of experimental liquid drainage data and model data at 500 ppm of SDS in the presence of 3.85 w/w % of Al_2O_3 particles at room temperature.

The values of the parameters $V_{d,max}$, $t_{1/2}$, and n' as per different operating variables are shown in Table 5.1. It is observed that the value of n' increases with increasing the concentration of surfactant, temperature, and glycerol concentration. As n' increases, the half-life of the bubble increases, which corresponds to a more stable charge microbubble. To predict the stability parameters ($V_{d,max}$, $t_{1/2}$, and n'), correlations for those are developed based on the present experimental data as a function of different operating variables. The general correlations can be expressed as follows:

$$Y = \lambda\left(\frac{T_{\exp}}{T_{room}}\right)^{c_1}\left(\frac{\sigma_{\exp}}{\sigma_W}\right)^{c_2}\left(\frac{pH_{\exp}}{pH_w}\right)^{c_3}\left(\frac{\mu_{sl}-\mu_{sol}}{\mu_{sol}}\right)^{c_4}\left(\frac{\rho_{sl}-\rho_{sol}}{\rho_{sol}}\right)^{c_5}\left(\frac{d_p}{d_b}\right)^{c_6} \qquad (5.5)$$

where Y represents $V_{d,max}/V_{d,t}$, $t_{1/2}/t_{max}$, and n'. The notations λ, c_1, c_2, c_3, c_4, c_5, *and* c_6 are coefficients that are obtained by fitting the equation (Equation (5.5)) with the present

experimental data as shown in Table 5.2 with respective goodness of fit by expressing correlation coefficient (R^2) and standard error (SE). The validity ranges of the correlations are:

$$1 < \frac{T_{\exp}}{T_{room}} \le 1.12; \qquad 0.61 < \frac{\sigma_{\exp}}{\sigma_w} \le 0.84; \qquad 0.79 < \frac{pH_{\exp}}{pH_w} \le 1.43; \qquad 1 < \frac{\mu_{sl} - \mu_{sol}}{\mu_{sol}} \le 1.07;$$

$$1 < \frac{\rho_{sl} - \rho_{sol}}{\rho_{sol}} \le 1.06 \; ; \; 3.55 \times 10^{-4} < \frac{d_p}{d_b} \le 14.1$$

Table 5.1. Parity of experimental and model parameters.

Parameters Chosen	Concentrations and other variables	Experimental data		Model outputs		
		$t_{1/2}$	V_{max}	$t_{1/2}$	V_{max}	n'
Surfactant conc.	100 ppm	84	16.6	86	16.90	1.45
	200 ppm	88	15.6	90	15.80	1.49
	300 ppm	93	14.8	95	14.70	1.58
	400 ppm	98	13.6	99	13.90	1.60
	2333 ppm	251	7.7	247	7.80	1.79
	2500 ppm	259	7.1	252	7.19	1.83
Temperature	500 ppm at 313 K	102	10.8	100	10.80	1.59
	500 ppm at 333 K	104	10.2	105	10.20	1.63
	500 ppm at 353 K	118	8.9	123	8.90	1.67
Nanoclay conc.	500 ppm + 0.02 (w/w %)	135	11.6	138	11.60	1.50

	500 ppm + 0.04 (w/w %)	160	11.3	162	11.30	1.54
	500 ppm + 0.06 (w/w %)	167	10.9	168	10.90	1.56
	500 ppm + 0.08 (w/w %)	172	10.5	175	10.50	1.57
	500 ppm + 0.10 (w/w %)	170	16.1	172	16.10	1.20

Table 5.2. Coefficients of Equation (5.5).

	Y Without solid			Y With solid		
Parameters	V_{max}/V_d	$t_{1/2}/t_{max}$	n'	V_{max}/V_d	$t_{1/2}/t_{max}$	n'
λ	0.595	2.397	3.872	0.241	1.199	1.058
c_1	0.105	0.296	-0.888	0.222	-1.389	2.057
c_2	0.009	0.061	0.069	0.139	-0.576	0.336
c_3	0.381	0.088	0.288	0.024	-0.039	-0.006
c_4	0.092	2.560	0.553	-0.009	-0.098	-0.289
c_5	0.015	-0.024	0.007	-0.112	0.096	0.162
c_6	-	-	-	-0.002	0.022	0.019
R^2	0.963	0.938	0.931	0.930	0.900	0.920
SE	0.013	0.039	0.029	0.051	0.022	0.033

5.5. Conclusions

In the present work, the effect of temperature, pH, and surfactant concentration on the stability of microbubbles are investigated. Increasing the surfactant concentration enhances colloidal microbubble stability both in the presence and absence of particles in the solution. Microbubbles generated in the presence of particles behave similarly as it behaves in the absence of particles with varying pH from 5-9 as per present work. At a fixed concentration of surfactant (SDS 500 ppm), the half-life of colloidal microbubbles at different temperatures was 102 s at 313 K, 104 s at 333 K, and 118 s at 353 K. A general correlation is developed based on the wide range of experimental conditions to predict the degree of stability of the colloidal microbubble which may be useful for the design of a plant prototype for microbubble aided chemical and biochemical processes.

CHAPTER 6

6. Effect of Salt on Stability of Ionic Microbubbles

This chapter presents the stability of the microbubbles based on the assemblage at air-water and liquid-solid interfaces with prominence on the systems containing surfactants and micro- or nanoparticles. The effect of different salt on the physicochemical properties of the solutions is enunciated. Three salts with different ionic radii are used to study the stability of the microbubbles in the presence and absence of micro-and nanoparticles.

6.1. Introduction

Many industries use various inorganic salts in the froth flotation process, where ions produced by these salts are of discrete valence in the medium. The outcome of these ions of discrete valences on the stability of microbubbles occurs in the presence or the absence of surfactants. Some of the work from the literature reported critical information on the study of the stability of microbubbles in the presence of electrolytic ions of discrete valences in the exclusion of surfactant in the process (Craig et al., 1993; Lessard and Zieminski, 1971; Prince and Blanch, 1990). Reportedly the stability is hindered in the succession of sodium > magnesium > aluminium all in the chloride form of salt. The hindrance to the stability of the microbubbles is due to some of the characteristics such as hydrophobic interaction (Craig et al., 1993), hydration effect (Israelachvili, 1997), and double-layer repulsion (Marcelja, 2006). Pandey et al. (2003) studied the impact of counter-ions of surface-active agents on interfacial properties by assessing microbubble formation, microbubble stability, and other interfacial properties. They found that the surface tension and the stability of bubbles decrease in the succession of Lithium > Sodium > Caesium > Magnesium and denominated the dissimilarity in micellar solidity and dispersion of identical molecules.

Microbubbles coated with surface-active molecules are utilized in various applications depending on its characteristics, that is, the stability of the microbubbles. Challenges to stabilizing the microbubbles are required to cover up yet. On the basis of previous studies, the structure of microbubbles figured out by various researchers consists of air/gas encapsulated inside the layers of molecules of a surfactant, which restrict the coalescence of the ionic microbubbles throughout raising their stability compared to conventional bubbles (Ma et al., 2008; Mohamedi et al., 2012). Various parameters affect the stability of microbubbles; one of them is the presence of nanoparticles, for which limited studies are found in the literature. The presence of particles modifies the stability of ionic microbubbles in three different ways: (i) adsorption loss (getting adsorbed on the surface of particles) caused by reduction of surfactant concentration, (ii) increase in the viscoelastic property of the microbubbles, and (iii) increase in the viscoelastic property of the liquid films. In this chapter, the stability of the microbubbles based on the assemblage at air-water and liquid-solid interfaces with the systems containing surfactants and micro- or nanoparticles were investigated. The effect of different salt on the physicochemical properties of the solution are enunciated. Three salts with different ionic radii are used to study the stability of the microbubbles in the presence and absence of micro-and nanoparticles.

6.2. Experimental

The characteristic factors of stability were estimated using the volume drainage method proposed by Longe (1989), which is given in detail in Chapter 5. The same procedure was followed by adding different salts. A typical snapshot of the bubble drainage at 293 K, with SDS (1 mol m^{-3}), CuO (0.79 w/w %), and salt NaCl (10 mol m^{-3}) is shown in Figure 6.1.

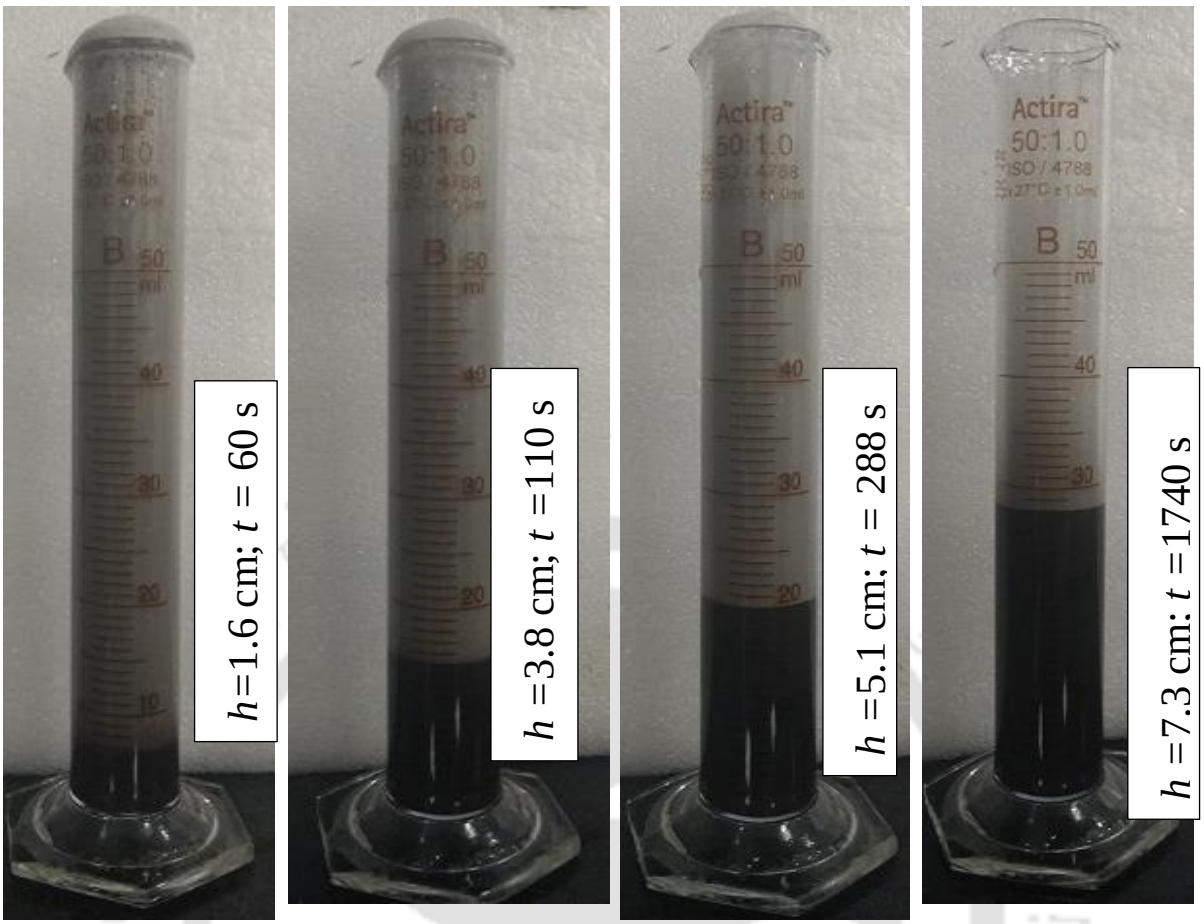

Figure 6.1. Experimental representation of microbubble drainage at 293 K, with SDS (1 mol m^{-3}), CuO (0.79 w/w %), and salt NaCl (10 mol m^{-3}).

6.3. Results and Discussion

6.3.1. Effect of different salts on microbubble stability when the particles are absent

Increasing salt concentration (which decreases the stability of the ionic microbubbles) can be demonstrated by the electrostatic response, which is an essential factor in deciding the stability of the microbubbles (Amiri and Woodburn, 1990; Jauregi et al., 1997; Save and Pangarkar, 1994). The addition of salt increases the electrostatic interactions, which leads to the formation of less stable microbubbles.

Figure 6.2 shows the effect of the concentration of salt (NaCl) on the stability of charged microbubble prepared at different levels of SDS. At low concentrations of surfactant, the addition of salt has no significant effects, as shown in Figure 6.2 (a), and the half-life remains around 80 s at 0.3 mol m^{-3} SDS with 10, 50, and 100 mol m^{-3} NaCl. As the concentration of surfactant is increased, the variation of half-life shows a tremendous difference with the increase in salt concentration. Figure 6.2 (b) shows that maximum stability can be observed at the highest concentration of surfactant and the lowest concentration of salt. Figure 6.2 (c) again shows no significant variation in the half-life of the microbubbles; this indicates that the stability of microbubbles can be significantly varied at some critical concentration of the surfactant in the presence of salt. The experimental results of half-life ($t_{1/2}$) and maximum dissolution time (t_{max}) at different variables are shown in Table 6.1 and Table 6.2.

Table 6.1. Half-life, gas holdup, and maximum dissolution time data of microbubbles with ionic surfactant (SDS).

Salt (mol m^{-3})	Surfactant conc^n (mol m^{-3})	NaCl			LiCl			CsCl		
		$t_{1/2}$(s)	ε(–)	t_{max}(s)	$t_{1/2}$(s)	ε(–)	t_{max}(s)	$t_{1/2}$(s)	ε(–)	t_{max}(s)
10	0.3	120	43.66	801	90	36.62	775	60	50.70	753
50	0.3	90	50.70	810	80	49.30	1550	70	50.20	778
100	0.3	80	50.70	791	80	43.66	1422	83	49.30	650
10	0.5	120	60.56	700	90	49.3	844	110	54.93	889
50	0.5	105	56.34	775	110	54.93	1548	120	54.93	979

100	0.5	120	56.34	913	110	54.93	1342	110	53.52	671
10	1	118	60.56	903	130	66.2	1282	140	63.38	999
50	1	140	54.93	905	150	59.15	1772	123	68.73	890
100	1	125	76.06	812	120	59.15	1102	130	67.61	731
10	3	160	74.65	1260	155	66.2	1506	115	50.70	970
50	3	135	74.65	1156	160	76.06	1285	170	73.24	584
100	3	140	73.24	750	130	69.01	780	150	69.01	667
10	5	180	78.87	730	165	70.85	1278	105	84.79	429
50	5	125	80.28	464	150	80.28	1119	160	77.46	502
100	5	142	59.15	1326	160	71.83	867	140	74.65	745

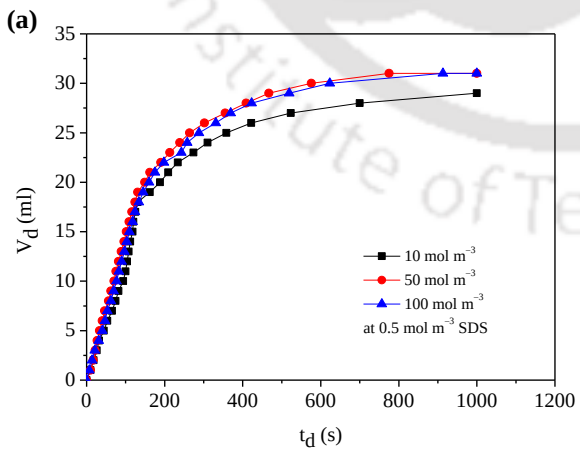

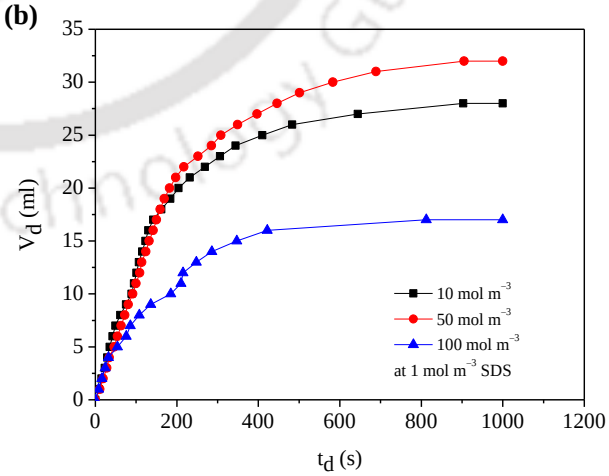

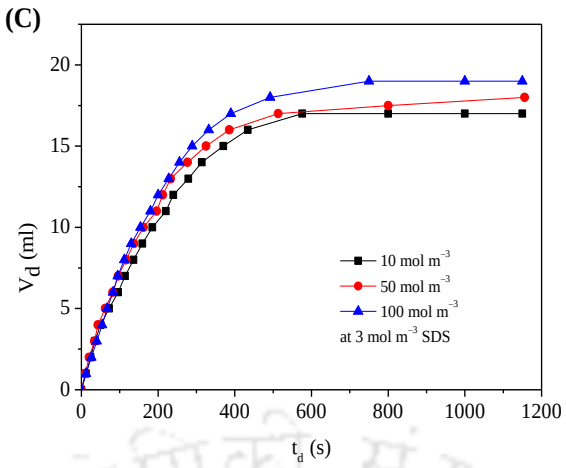

Figure 6.2. Effect of varying concentrations of salt NaCl on the stability of charged microbubble prepared with different concentrations of anionic surfactant SDS (a) at 0.5 mol m^{-3}, (b) at 1 mol m^{-3}, and (c) at 3 mol m^{-3}.

The lowered electrostatic repulsive response between the microbubble surfaces, which is caused by the contraction of the double layer because of the increased ionic concentration, results in a decrease in the stability of the microbubbles (Amiri and Woodburn, 1990). Chalphalkar et al. (1993) also reported that ionic microbubble dispersion with salt addition decreases the life span of ionic microbubbles formulated with ionic surfactants, whereas no change was found at the same condition with microbubbles formulated with nonionic surfactants. At high ionic strength, bovine serum albumin (BSA) molecules were in a native and more compact conformation, resulting in a higher number of microbubbles (Noskov et al., 2010). Rovers et al. (2016) found that the addition of salt led to a higher yield and stability with increasing ionic strength. Tchuenbou-Magaia et al. (2009) reported no formation of microbubbles with aqueous BSA in 0.2 M (sodium phosphate) ionic strength at 7 pH, whereas when buffer concentration was reduced to 0.01 M, microbubbles were obtained at the same pH which was much less than those obtained at 5 pH. A decreased stability and a yield of polyglutamate sodium microsphere were observed with an increase in ionic strength on the

solution > 0.4 M by Dibbern et al. (2006). Some authors described that relatively high surface coverage and an adequate air-water interface are attributed to the charge and confirmation of the molecules (Cascão Pereira et al., 2003; Noskov et al., 2010). The decrease in the repulsion pattern between molecules provides higher and free coverage at the air-water interface (Cascão Pereira et al., 2003).

Table 6.2. Half-life, gas holdup, and maximum dissolution time data of microbubbles with ionic surfactant (SDS) in the presence of particles.

Salt (mol m^{-3})	Surfactant Conc^{n} (mol m^{-3})	**NaCl** in presence of ZnO particles (0.79 w/w %)			**LiCl** in presence of ZnO particles (0.79 w/w %)			**CsCl** in presence of ZnO particles (0.79 w/w %)		
		$t_{1/2}$(s)	ε (–)	t_{max}(s)	$t_{1/2}$(s)	ε(–)	t_{max}(s)	$t_{1/2}$(s)	ε(–)	t_{max}(s)
5	0.3	60	33.80	900	15	25.35	540	40	30.99	568
10	0.3	95	58.03	706	40	21.13	212	20	48.17	484
50	0.3	95	54.37	755	46	35.21	692	15	32.39	780
100	0.3	140	63.38	951	50	54.93	633	100	59.15	840
5	0.5	120	63.38	819	120	59.15	684	80	54.93	764
10	0.5	140	57.75	959	20	46.48	958	100	58.56	883
50	0.5	160	63.38	725	160	60.56	837	130	61.97	796

100	0.5	130	57.75	692	170	60.56	710	180	63.38	869
5	1	135	64.79	707	140	64.08	710	120	64.79	890
10	1	145	60.56	623	142	59.15	790	120	61.16	1250
50	1	120	63.38	897	162	67.61	876	#120	64.79	635
100	1	*	*	*	120	60.56	887	*	*	*

* Initially, clear liquid drained through the bubbles, but after a while, particles also drained with the liquid through the bubbles. No clear separation was seen between clear liquid and bubbles.

6.3.2. Effect of different salts on microbubble stability when the particles are present

The two significant findings in the literature for microbubble stability are as follows: (a) the most stable microbubble is formed at the CMC (in the absence of salt or contaminants) (Moshkelani and Amiri, 2008), and (b) the stability decreases when surfactant concentration is more than its CMC (Yan et al., 2005). Figures 6.3 (a) and (b) show the stability behavior of SDS solution with the effect of salt and the co-effect of salt with the presence of particles. The absence of particles induces the half-lives of the ionic microbubbles to be higher in a broad range of 120–180 s at a high concentration of SDS, while in the presence of particles, similar observations are seen at the lower concentration of SDS 60–140 s. In the presence of particles, no variation in the clear liquid and microbubbles can be seen beyond 1.0 mol m^{-3} SDS concentration. The experimental results for the stability of particle-laden microbubbles in terms of half-life, holdup, and maximum dissolution time at different variables are given in Table

5.3. These results lead to the conclusion that particles have a synergistic effect on the surfactant solution with salt. On the basis of the adsorption of particles at the air-water interface, the synergistic behavior of these ionic microbubbles can be explained. Higher hydrophobicity (at low surfactant concentration with salt) enhances the affinity of particles for the solution/air interface and adsorption on the ionic microbubble surface.

The drainage curves at different concentrations of particles with various salt concentrations, from which the stability parameters were obtained, are shown in Figures 6.4 and 6.5.

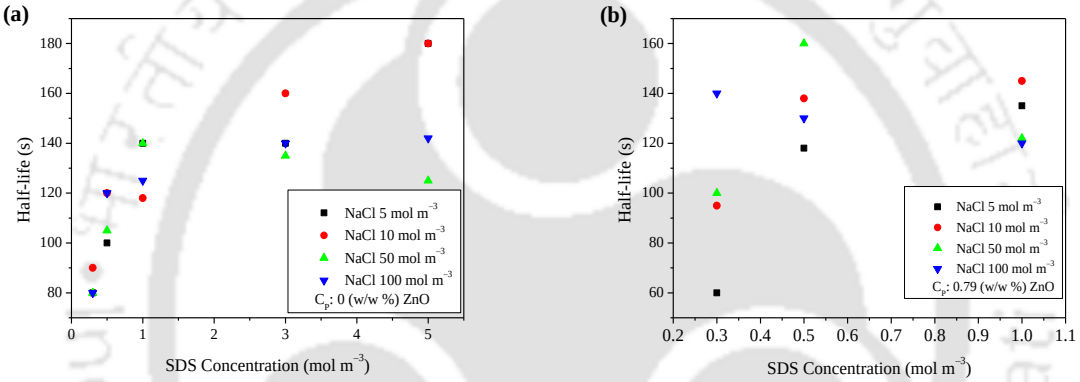

Figure 6.3. Effect of salt on the half-life of colloidal microbubbles in the presence of varying concentrations of SDS (a) microbubbles without particles and (b) microbubbles with ZnO particles at room temperature.

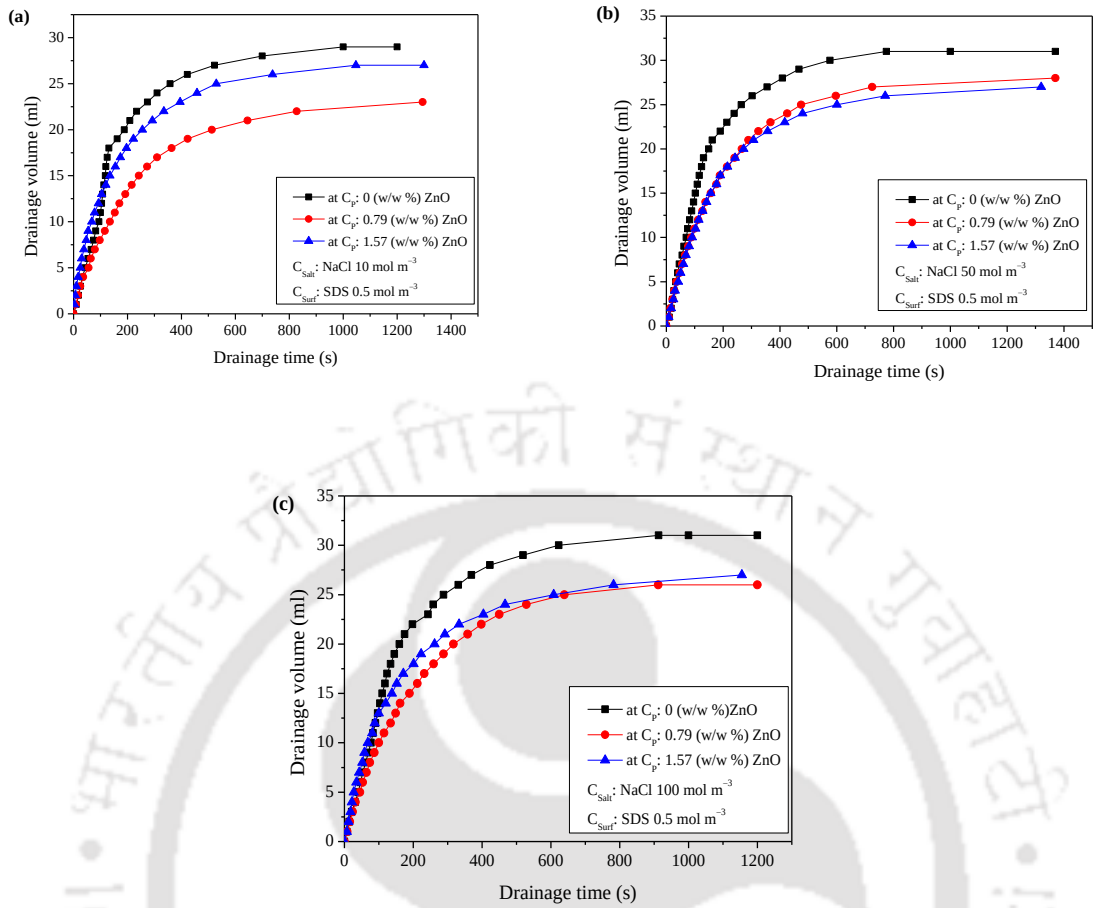

Figure 6.4. Effect of varying concentration of particles (ZnO) on the stability of charged microbubble prepared with anionic surfactant SDS of 0.5 mol m^{-3}, (a) in the presence of 10 mol m^{-3} NaCl, (b) in the presence of 50 mol m^{-3} NaCl, and (c) in the presence of 10 mol m^{-3} NaCl.

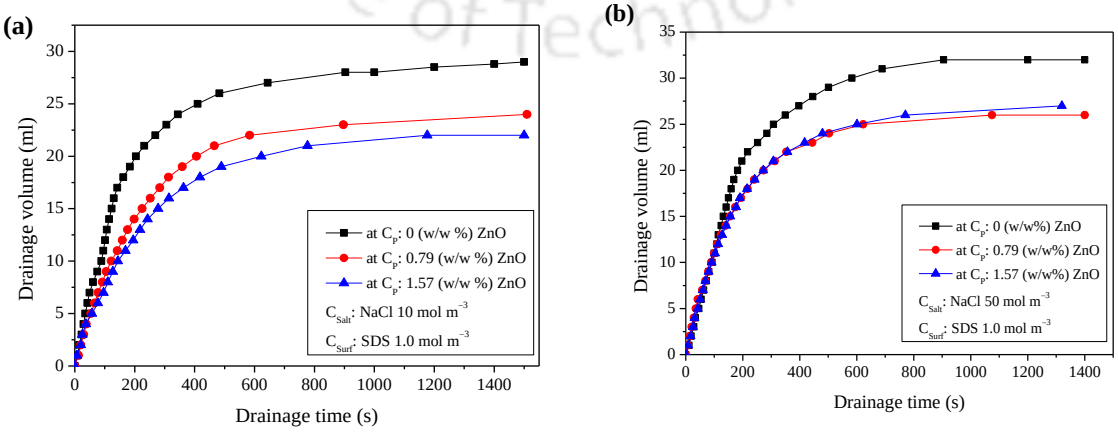

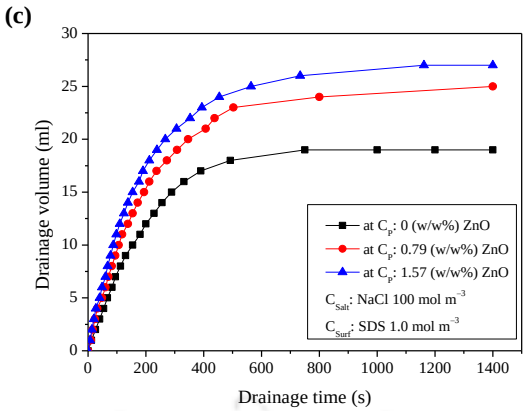

Figure 6.5. Effect of varying concentration of particles (ZnO) on the stability of charged microbubble prepared with anionic surfactant SDS of 1.0 mol m^{-3}, (a) in the presence of 10 mol m^{-3} NaCl, (b) in the presence of 50 mol m^{-3} NaCl, and (c) in the presence of 100 mol m^{-3} NaCl.

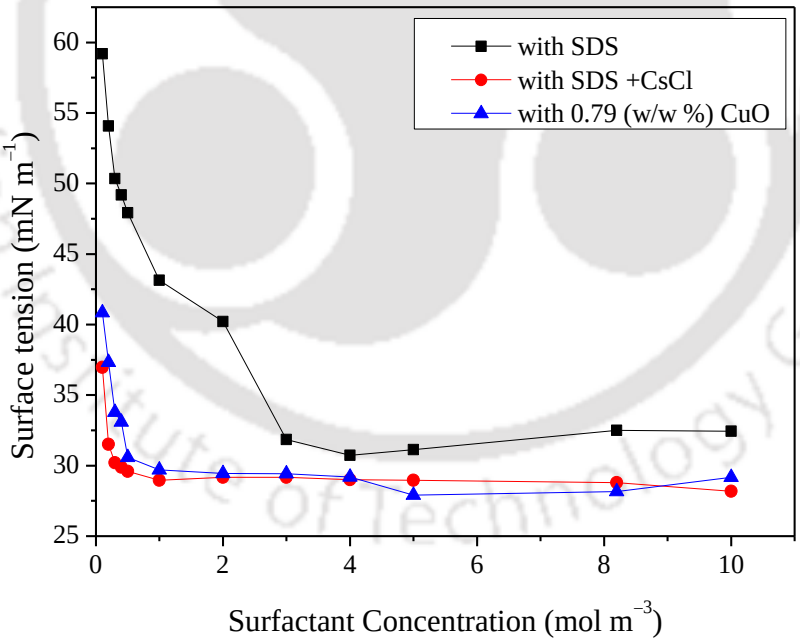

Figure 6.6. Effective surface tension as a function of SDS concentration. The SDS aqueous solutions with 0 mol m^{-3} salt (presented in squares), 50 mol m^{-3} CsCl salt (presented in circles), and 50 mol m^{-3} CsCl along with 0.79 w/w% (50 mol m^{-3}) CuO nanoparticles (presented in triangles).

The mechanism involved in the stability of microbubbles is investigated in the presence or absence of different salts with or without particles by measuring surface tension and the diameter of microbubbles. The change observed in the surface tension of the SDS solution with the addition of salt decreased significantly, and when the nanoparticles were added to the same solution, a little change can be seen, as shown in Figure 6.6.

The kinetics of microbubble stability in the presence of salts and micro-nano particles are analyzed based on the bubble size and the rate of liquid drainage of the microbubble solution. In the absence of nanoparticles, the microbubbles stabilized with SDS showed rapid liquid drainage from the lamellae of the microbubbles.

6.3.3. Effect of salt on drainage characteristic

The liquid drainage behavior of microbubbles can be empirically expressed by (Ruby and Majumder, 2018; Yan et al., 2005)

$$V_{d,t} = V_{d,\max} \frac{t_d^{n'}}{K^{n'} + t_d^{n'}} \tag{6.1}$$

where $V_{d,t}$ represents the drained liquid volume at time t_d, $V_{d,max}$ is the final volume of drained liquid, K is the half-life of the draining process of liquid, and n' represents the growth pattern of the drainage. These factors are considered to vary with surfactant concentration, type of surfactant, temperature, and pH of the solution. The rate of liquid drainage defines the stability of charged microbubble. The drainage rate of liquid (R_d) can be derived by differentiating Equation (6.1) with respect to time and expressed as:

$$R_d = \frac{dV_{d,t}}{dt_d} = \frac{n' V_{d,\max} K^{n'} t_d^{n'-1}}{(K^{n'} + t_d^{n'})^2} \tag{6.2}$$

After arranging Equation (6.2), the relation between t_d and $V_{d,t}$ can be expressed as

$$t_d = K\left(\frac{V_{d,t}}{V_{d,\max} - V_{d,t}}\right)^{1/n'} \tag{6.3}$$

Substitution of Equation (6.3) into Equation (6.2) yields the following kinetic equation

$$R_d = \frac{dV_{d,t}}{dt_d} = \frac{n'}{V_{d,\max}K} V_d^{(1-1/n')} (V_{d,\max} - V_{d,t})^{(1+1/n')} \tag{6.4}$$

where $\frac{n'}{V_{\max}K}$ represents the rate constant of drainage k_d, which signifies the stability of microbubbles. Salts addition adversely affected the stability of microbubbles, as shown in Figure 6.5. The k_d value varies from 4.75×10^{-4} to 4.02×10^{-4}, 3.65×10^{-4} to 4.86×10^{-4}, 3.89×10^{-4} to 3.98×10^{-4} with the addition of NaCl, LiCl, and CsCl, respectively on microbubble generated with anionic surfactant SDS at the concentration 0.5 mol m^{-3}. A similar trend of graphs is seen for different salts and their concentrations. The value of k_d decreases gradually with an increase in the concentration of salt, but when the particles are added at the same parameters, a significant decrease is seen in the value of k_d, as shown in Figures 6.7 (a) and (b). This observation is due to the fact that the anionic surfactant SDS includes chloride ions with the addition of salt, which improves repulsive electrostatic interaction to stabilize the microbubbles (Jarudilokkul et al., 2004).

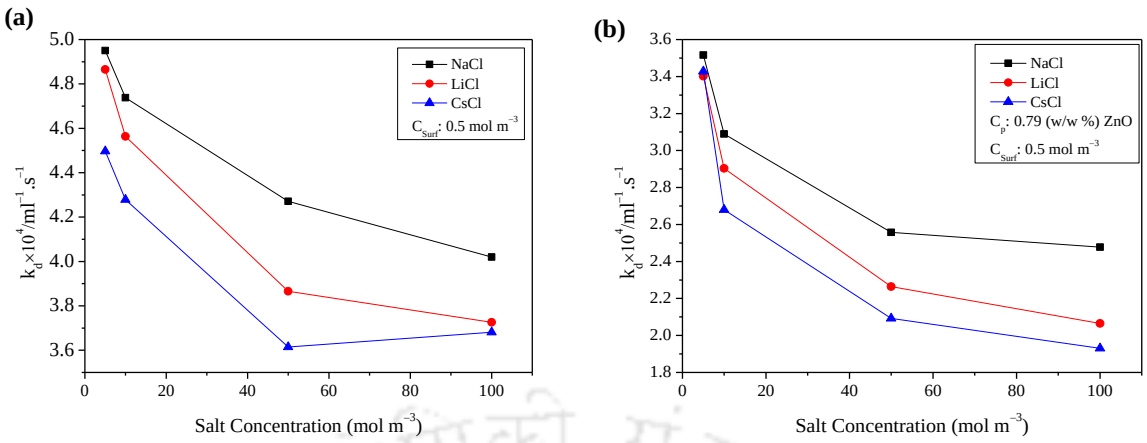

Figure 6.7. The rate constant k_d versus varying concentrations of salt (a) at the different types of salts without particles and (b) at the different types of salts with particles.

6.3.4. Effect of salt and particles on the stability and liquid drainage

The impact of particles on stability has been investigated with and without salt. Adsorption of SDS on the surface of the particles makes the particle more hydrophobic. The present characterization is concerned with the interfacial properties of the aqueous SDS solution in the presence of different salts and their concentrations. The bubble stability decreases with an increase in particle size and increases with an increase in particle concentration. As the particle size increases, the gravity drainage process controls the factor for stability, while in the case of smaller particle size, the diffusion process turns to the dominating factor. Kam and Rossen (1999) explained that when the particles are present, the stabilization of the bubble occurs against dissolving gas into the surrounding liquid, which causes the bubble to get collapsed. This is due to the fact that the stress between particles is large and can drive the sintering of the particles into a rigid framework. They explained that for a bubble coated by solids, solids could move freely to get placed or leave the bubble surface during bubble shrinking and expansion. In this regard, gas dissolution into the surrounding liquid will not make the bubble

stable. A rapid increment of stability with the addition of NaCl in the aqueous phase between 1.8 and 2 mol dm^{-3} is observed. The change in stability pattern with salt addition can be justified by the changes in the indices of particle contact angle. Furthermore, it needs to make the particles adequately hydrophobic for enhanced adsorption and to minimize the tendency of aggregation in a bulk aqueous phase.

A correlation between the rate of liquid drainage of the ionic microbubbles and time (Eq. 5.14) has been derived in the previous section. Figure 6.8 represents the graphical differentiation to obtain the drainage rates. As the drainage process starts, a rapid increase is seen in the drainage rate because the top-heavy liquid starts to redistribute. This is the first phase of the drainage, while in the second phase, there is a sharp decrease in the drainage rate with time, and in the final phase, the rate of drainage declines toward zero with increasing time. The primary region in the first phase was due to gravity drainage, and going through the next region, thinning of the films occurs because the rate of drainage is influenced by the initial distribution of the liquid between the film and plateau border. Thinning of the film continues to a large extent after the second phase as the drainage of liquid occurs from lamellae very slowly, influenced by plateau boarder suction. In a short time interval, the film drainage attains equilibrium in the third phase. The liquid films get ruptured, or the bubbles coalesce as they are affected by the London-van der Waals forces and the repulsive forces.

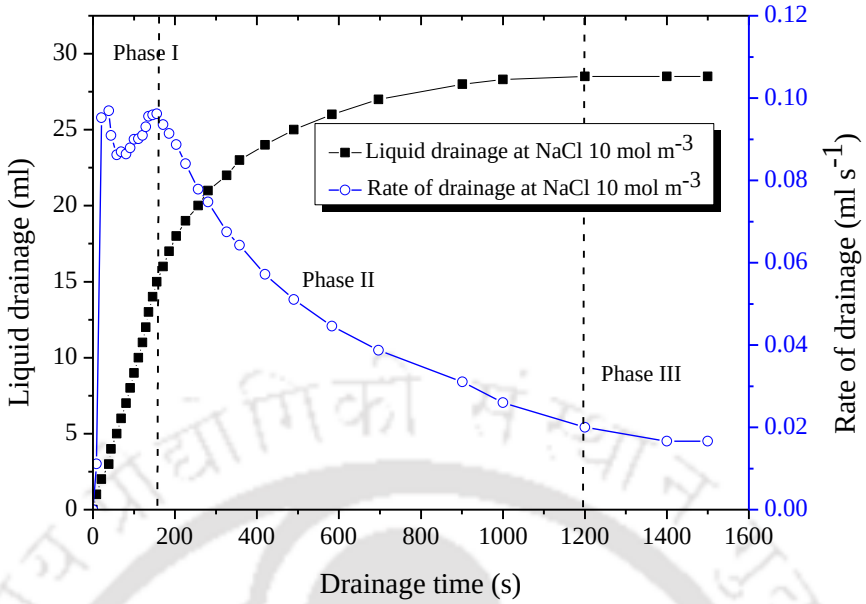

Figure 6.8. Drainage rate variation as a function of time through microbubbles in the presence of salt (NaCl) and particles CuO (0.79 w/w %) at 4 mol m^{-3} concentrations of SDS.

6.4. Conclusions

Increasing salt concentration decreased the stability of the ionic microbubbles. The half-life decreases with fixed 0.3 mol m^{-3} SDS concentration from 120s, 90s, and 80 s at 10, 50, and 100 mol m^{-3} NaCl, respectively, whereas with LiCl, it remained around 80 s. However, a mixed effect was seen with cesium chloride in the stability study. In the presence of particles, the effect of NaCl addition was inverse to that in the absence of particles, which increased from 95, 95, and 140 s at 10, 50, and 100 mol m^{-3} NaCl, respectively. The concentrations of different salts show a significant effect on the bubble stability, bubble gas holdup, bubble size, and adsorption of particles. The ion-specific behavior played a vital role in bubble holdup, bubble life span, and the rate of drainage, which can help in the control of bubble holdup and other characteristic properties of microbubbles.

Chapter 7

7. Overall Conclusion and Future Recommendation

This chapter provides the overall conclusions and future recommendations based on the present research in the three-phase micro-structured column.

7.1. Overall conclusions

- The effect of temperature, particle concentration, particle size, and surfactant concentration on the drainage of microbubbles are investigated.
- The microbubbles' size is determined by the drainage rate of ionic microbubbles. Increasing the surfactant concentration enhances ionic microbubble stability both in the presence and absence of particles in the solution. Increasing the surfactant concentration enhances ionic microbubble stability both in the presence and absence of particles in the solution. Stability increases with an increase in particle size. At a fixed concentration of surfactant (SDS 500 ppm), the half-life of colloidal microbubbles at a fixed particles concentration is 142 s for CuO (< 50 nm and 6.31 g/m^3), 150 s for ZnO (4.47µm and 5.61 g/cm^3), 155 s for Al_2O_3 (19.6 µm and 3.95 g/m^3).
- The most stable microbubbles are produced at the higher concentration of ZnO particles of 7.41 wt. %. The stability of ionic microbubbles increases with increasing ZnO particle concentration at a fixed concentration of surfactant. This shows the synergistic effect, which may be explained based on the adsorption of ZnO at the air-water interface.
- Higher hydrophobicity enhances the affinity of particles for the solution/air interface and adsorption on the ionic microbubbles. Whereas the increase in the concentration of Al_2O_3 particles shows the different effects on its stability at different concentrations.

- The half-life of microbubbles produced with Al_2O_3 particles is less at lower concentrations, i.e., at 0.79 wt. %, 1.57 wt. %, 2.34 wt. %, and 3.10 wt. %, while at a higher concentration of 3.85 wt. % and 7.41 wt. % the stability is higher. This shows the variation of stability with the type of particles.
- Microbubbles generated in the presence of particles behave similarly to those in the absence of particles with varying pH from 5 to 9 as per present work.
- A general correlation is developed based on the wide range of experimental conditions to predict the degree of stability of the ionic microbubble, which may be useful for the design of plant prototypes for microbubble-aided chemical and biochemical processes.
- As we know, the degree of micellar growth varies in the inverse order of the radius of the counter-ion. Here it was found that the caesium hydrated ions interact more strongly with the oppositely charged heads, as the hydrated Cs^+ has the smallest hydrated ionic size than other ions in the present study. Consequently, these strong interactions favor micelle formation and binding to the Cl^- at the surface. Present results show that with an increase in the size of the hydrated counter-ion, the CMC increases, whereas the degree of counter-ion binding decreases.
- It was also observed that salt addition affected the CMC of the surfactant up to the critical concentration of particular salt until which saturation was achieved. Increasing salt concentration decreased the stability of the ionic microbubbles. The half-life decreases with fixed 0.3 mol m^{-3} SDS from 120s, 90s, and 80s at 10, 50, and 100 mol m^{-3} NaCl, respectively, whereas with LiCl, it remained around 80s. While a mixed effect was seen with Cesium chloride in the stability study.
- Salts addition adversely affected the stability of microbubbles, and the *K* (rate constant of drainage) value varies from 4.75×10^{-4} to 4.02×10^{-4}, 3.65×10^{-4} to 4.86×10^{-4}, 3.89×10^{-4} to 3.98×10^{-4} with the addition of NaCl, LiCl, and CsCl, respectively on

microbubble generated with anionic surfactant SDS at the concentration 0.5 mol m^{-3}. The value of K decreases gradually with an increase in the concentration of salt, but when the particles are added at the same parameters, a significant decrease is seen in the value of k_d. This observation is due to the fact that the anionic surfactant SDS includes chloride ions with the addition of salt, which improves repulsive electrostatic interaction to stabilize the microbubbles

- In the presence of particles, the effect of NaCl addition was inverse to in the absence of particles, it increased from 95s, 95s, and 140s at 10, 50, and 100 mol m^{-3} NaCl, respectively.
- The concentrations of different salts show a significant effect on the bubble stability, bubble gas holdup, bubble size, and adsorption of particles. The ion-specific behavior played a vital role in bubble holdup, bubble life span, and the rate of drainage, which can help in the control of bubble holdup and other characteristic properties of microbubbles.
- The addition of nanoparticles decreases bubble size as it modifies the bubble surface.
- With the addition of salt, a holdup in anionic microbubbles decreases from 53.66% to 50.77% with an increase in salt concentration (NaCl) and at a fixed concentration of SDS surfactant.
- The surface tension decreases significantly with an increase in salt concentration, thus reducing the size of the ionic microbubble.
- From drainage rate analysis, it is clear that the rise velocity of microbubbles increases with an increase in temperature, thus decreasing its stability.
- The parameters V_{max}, $t_{1/2}$, and n were estimated using nonlinear least-squares regression. It is observed that value of n increase with increasing the concentration of surfactant,

temperature, and glycerol concentration. As *n* increases, the half-life of the bubble increases, thus corresponding to a more stable charge microbubble.

7.2. Future recommendation

This section discusses future recommendations based on the present research.

- The rising velocity of air bubbles can be investigated in different other aqueous solutions of hexadecyl amine (HDA) and methyl isobutyl carbinol (MIBC) as surface-active agents at varying concentrations at a constant gas flow rate.
- Bubble characteristics and wake structure of rising bubbles in water /medium depending on the volumetric gas flow rate can be studied by optical methods like Shadowgraphy and Particle Image Velocimetry (PIV).
- Shadowgraphy can be applied to determine main bubble characteristics, such as equivalent diameter, morphology, and rising velocity. From these characteristics, critical parameters like the concentration at the minimum bubble velocity can be derived. Simultaneous application of Particle Image Velocimetry (PIV) provided information about hydrodynamic parameters, e.g., the induced liquid velocities and vortex shedding.
- From surface tension measurements, the concentration of adsorbed species on the interface and packing densities of any surface-active agents on the bubble surface could be calculated. The ionic character of any surface-active agent can decide its adsorption capability and packing density which affects the bubble characteristics.
- HDA exhibited better adsorption and a higher packing density on the bubble surface compared to MIBC due to the ionic character and the straight hydrocarbon chain. The bubble characteristics were, therefore, more strongly affected by HAD than by MIBC.

- The synergistic effect of particle heterogeneity and size on the surface hydrophobicity characterization can be studied as they affect the particle's induction time and wettability.
- Column flotation technology is one of the most important developments in mineral processing, particularly for the separation of fine particles, where the internal flow field has an enormous influence on flotation performance. PIV (particle image velocimetry) and CFD (computational fluid dynamics) are the most effective methods to study flow fields that can be further studied.
- The complex interplay between the surface chemistry and system hydrodynamics can be studied experimentally and may commence the numerical modeling for the flotation column.
- The coupled CFD-DEM approach is the capability of modeling forces at the microscale, which is critical in modeling the particle attachment and detachment steps and, at the same time, predicting macroscale flow behavior. It is considered that future progresses in this area can only be achieved through multiscale modeling by incorporating CFD simulation of the hydrodynamics in the macro-scale and DEM simulation of discrete phase in the microscale simultaneously.

Nomenclature

Chapter 1

Notations

a	Specific interfacial area (m^2/kg)
D_B	Diameter of bubble (m^2)
d_b	Mean bubble diameter (m^2)
E	Strength of the applied electric field (V/m)
g	Acceleration due gravity (m/s^2)
R	Radii of curvature (m)
v_e	Electrophoretic velocity (m/s)
E	Collection efficiency (–)
E_a	Attachment efficiency (–)
E_c	Collision efficiency (–)
E_s	Stability efficiency (–)

Greek letters

μ_L	Liquid viscosity (Pa.s)
ϵ_g	Gas hold up (–)

ε_e	Dielectric permittivity of vacuum ($s^2.C^2/kg.m^3$)
ε_r	Relative dielectric permittivity of the liquid ($s^2.C^2/kg.m^3$)
ζ	Zeta potential (V)
ΔP	Pressure difference (N/m^2)
γ	Surface tension of liquid (mN/m)

Abbreviation

AOT	Sodium bis– (2–ethyl hexyl) sulfosuccinate
CTAB	Cetyltrimethylammonium bromide
DAF	Dissolved air flotation
DTAB	Dodecyltrimethyl ammonium bromide
DLVO	Derjaguin-Landau-Verwey-Overbeek
HCB	Hexachlorobenzene
HTAB	Hexadecyltrimethyammoniumbromide
MNB	Micro-Nano Bubble
SDBS	Sodium dodecylbenzenesulfonate
SDS	Sodium dodecyl sulfate
TTAB	Tetradecyltrimethylammonium bromide

Chapter 2

Greek letters

μ Viscosity (m^2/s)

μ_e Effective viscosity (Pas)

μ Dynamic viscosity (kg/ms)

τ^* Shear stress (N/m^2)

Dimensionless groups

*Ca** Capillary number ($\mu_f U_c/\sigma$) (–)

Re Reynold's number

Abbreviation

AFE	Air-filled emulsion
BSA	Bovine serum albumin
CCD	Closed Camera
CGA	Colloidal Gas Aphron
CMC	Critical micelle concentration
CLA	Colloidal Liquid Aphron
CTAB	Cetyltrimethylammonium bromide
DAF	Dissolved Air Flotation
DSC	Differential scanning calorimetry

EC	Electrical Conductivity
EWP	Egg white protein
HTAB	Hexadecyltrimethy ammonium bromide
IEP	Isoelectric Point
PAX	Potassium Amyl Xanthate
PEG	Polyethylene glycol
SDBS	Sodium dodecylbenzenesulfonate
SDS	Sodium dodecyl sulfate
TEM	Transmission electron microscopy
TTAB	Tetradecyltrimethyl ammonium bromide

Chapter 3

Notations

C_s	Concentration of surfactant (ppm)
C_p	Concentration of the particle (wt. %)
d_b	Diameter of the bubble (m^2)
d_{bi}	Diameter of i^{th} microbubble (m^2)
d_{mb}	Diameter of microbubble (m^2)
d_{bs}	Sauter mean diameter of microbubble (m^2)

g Acceleration due to gravity (m/s^2)

h_o Initial height of froth and solution (m)

h_t Total height of froth and solution (m)

$h_{d,o}$ Height of liquid drainage at time $t = 0$ (m)

$h_{d,t}$ Total height of microbubbles and liquid (m)

m Coefficient (–)

rpm Rotation per minute

t Time (s)

u_{mb} Rise velocity of microbubbles (m/s)

$V_{g,t}$ Volume of gas in microbubbles (ml)

V_t Volume of microbubbles and liquid (ml)

$V_{d,t}$ Volume of liquid drained (ml)

$V_{d,max}$ Maximum volume of liquid drained (ml)

Greek symbols

ρ Density (kg/m^3)

ρ_l Density of liquid (kg/m^3)

ρ_g Density of gas (kg/m^3)

μ Viscosity (m^2/s)

μ_l Viscosity of liquid (m^2/s)

ε_o Holdup of gas at time *t* equal to zero (–)

ε_g Holdup of gas (–)

α Coefficient (–)

τ Dummy variable in eq. 4.11

Subscripts

d drainage

mb microbubbles

min minimum

t at time *t* (s)

Abbreviation

ERT Electrical resistant tomography

BET Brunauer-Emmett-Teller

CCD Closed Camera

CMC Critical micelle concentration

CTAB Cetyltrimethylammonium bromide

DGD Dynamic gas disengagement

DSA	Dodecyl sulfonic acid
PDS	Potassium dodecyl sulfate
SDS	Sodium dodecyl sulfate
TEM	Transmission electron microscopy

Chapter 4

Notations

A_H	Hamaker constant (J)
c_o	Initial concentration of surfactant (mol m^{-3})
c	Concentration of surfactant (mol m^{-3})
c_s	Concentration of salt (mol m^{-3})
C_1, C_2	Constants in eq. 4.9 (N/m)
D	Diffusivity in the bulk solution
e	Electronic charge (C)
K_L	Adsorption equilibrium constant for the Langmuir isotherm
k	Boltzmann′s constant (m^2 kg/s^2 K)
n	Number of molecules (or ions) per unit volume (m^{-3})
N_A	Avogadro's number (mol^{-1})
R	Universal gas constant (J mol^{-1} K^{-1})

t Time (s)

T Temperature (K)

z Valence of ion (–)

Greek symbols

ε Dielectric constant for the solvent (-)

ψ Potential developed at the interface (V)

γ Interfacial tension (N/m)

γ_o Interfacial tension in the absence of surfactant (N/m)

Π_T Total disjoining pressure (N/m^2)

Π_{vdW} Disjoining pressure (van der Waals force of attraction) (N/m^2)

Π_{EDL} Disjoining pressure (Electrostatic double-layer force) (N/m^2)

Γ Surface excess concentration of the surfactant (mol/m^2)

Γ_∞ Adsorption capacity (mol/m^2)

κ^- Debye-Huckel parameter (m)

δ Separation between two surfaces (m)

Subscripts

mb microbubbles

vdW van der Waals force

EDL Electric double-layer

s Surfactant

Abbreviation

CMC Critical micelle concentration

DLVO Derjaguin-Landau-Verwey-Overbeek

EOS Equation of state

SDS Sodium dodecyl sulfate

Chapter 5

Notations

C_s Concentration of surfactant (ppm)

C_p Concentration of particle (wt. %)

d_b Dimeter of microbubble (m^2)

d_p Particle size (µm)

h_o Initial height of liquid solution (m)

h_t Total height of microbubbles and liquid (m)

pH_{exp} pH at experimental parameter

pH_w pH of water

R_d Drainage rate (m^3/s)

rpm Rotation per minute

t time (s)

t_d Drainage time (s)

$t_{1/2}$ half-life (s)

T_{exp} Experimental temperature (K)

T_{room} Room temperature (K)

V_t Volume of microbubbles and liquid (m^3)

$V_{d,t}$ Volume of drainage (m^3)

$V_{g,t}$ Volume of gas in microbubbles (m^3)

$V_{d,max}$ Maximum volume of liquid drained (m^3)

Greek symbols

ρ density (kg/m^3)

ρ_l Density of liquid (kg/m^3)

ρ_g Density of gas (kg/m^3)

ρ_{sl} Density of slurry (kg/m^3)

ρ_{sol} Density of solution (kg/m^3)

μ Viscosity ($N\text{-}s/m^2$)

μ_{sl} Viscosity of slurry (m^2/s)

μ_{sol} Viscosity of solution (m^2/s)

σ Surface tension (N/m)

σ_{exp} Experimental surface tension (N/m)

σ_w Surface tension of water (N/m)

μ_l Viscosity of liquid (m^2/s)

λ Correlation coefficient (-)

Subscripts

b microbubbles

d drainage

exp experimental

max maximum

p particle

sol solution

sl slurry

w water or aqueous phase

Abbreviation

CMC	Critical micelle concentration
CTAB	Cetyltrimethylammonium bromide
SDS	Sodium dodecyl sulfate

Chapter 6

Notations

C_{surf}	Concentration of surfactant (mol m^{-3})
C_p	Concentration of particle (w/w %)
c_s	Concentration of salt (mol m^{-3})
d_{mb}	Diameter of microbubble (m^2)
R_d	Drainage rate (m^3/s)
k_d	Rate constant of drainage (–)
t	Time (s)
t_d	Drainage time (s)
$t_{1/2}$	Half-life (s)
t_{max}	Maximum dissolution time (s)
$V_{d,t}$	Volume of liquid drained (ml)
$V_{d,max}$	Maximum volume of liquid drained (ml)

K Half-life of microbubbles (s)

Subscripts

d drainage

p particle

mb microbubbles

max maximum

s Surfactant

t at time *t* (s)

Abbreviation

BSA Bovine serum albumin

CMC Critical micelle concentration

SDS Sodium dodecyl sulfate

References

Abidi, A., Elamari, K., Bacaoui, A., Yacoubi, A., 2014. Entrainment and true flotation of a natural complex ore sulfide. Journal of Mining Science 50, 1061-1068.

Akdemir, Ü., Sönmez, İ., 2003. Investigation of coal and ash recovery and entrainment in flotation. Fuel Processing Technology 82, 1–9.

Agarwal, A., Ng, W.J., Liu, Y., 2011. Principle and applications of microbubble and nanobubble technology for water treatment. Chemosphere 84, 1175–1180.

Amiri, M., Sadeghialiabadi, H., 2014. Evaluating the stability of colloidal gas aphrons in the presence of montmorillonite nanoparticles. Colloid Surfaces A: Physicochemical and Engineering Aspects 457, 212-219.

Amiri, M., Valsaraj, K., 2004. Effect of gas transfer on separation of whey protein with aphron flotation. Separation and Purification Technology, 35, 161-167.

Amiri, M., Woodburn, E., 1990. A method for the characterisation of colloidal gas aphron dispersions. Chemical Engineering Research and Design 68, 154-160.

Bascur, O., Herbst, J., 1982. Dynamic modeling of a flotation cell with a view toward automatic control. Preprints XIV IMPC, Session III 17–23.

Basu, S., Malpani, P., 2001. Removal of methyl orange and methylene blue dye from water using colloidal gas aphron—Effect of processes parameters. Separation Science and Technology 36, 2997-3013.

Bergh, L., Yianatos, J., 1993. Control alternatives for flotation columns. Minerals Engineering 6, 631-642.

Bisshop, J.P., White, M.E., 1976. Study of particle entrainment in flotation froth. Transactions of the Institution of Mining and Metallurgy C85, C191–C194.

Boström, M., Kunz, W., Ninham, B.W., 2005. Hofmeister effects in surface tension of aqueous electrolyte solution. Langmuir 21, 2619-2623.

Bredwell, M., Telgenhoff, M., Worden, R., 1995. Formation and coalescence properties of microbubbles. Oak Ridge National Lab., TN (United States).

Caballero, M., Cela, R., Perez-Bustamente, J., 1989. Studies on the use of colloidal gas aphrons in coflotation and solvent sublation processes. A comparison with the conventional technique. Separation Science and Technology 24, 629-640.

Cascão Pereira, L.G., Theodoly, O., Blanch, H.W., Radke, C.J., 2003. Dilatational rheology of BSA conformers at the air/water interface. Langmuir 19, 2349-2356.

Chalkosh Amiri, M., 1990. Separation of ultra-fine sulphur particles from NTA dispersion by aphron flotation. International Journal of Engineering 3, 148-153.

Chang, C.-H., Franses, E.I., 1995. Adsorption dynamics of surfactants at the air/water interface: a critical review of mathematical models, data, and mechanisms. Colloids and Surfaces A: Physicochemical and Engineering Aspects 100, 1-45.

Chaphalkar, P., Valsaraj, K., Roy, D., 1993. A study of the size distribution and stability of colloidal gas aphrons using a particle size analyzer. Separation Science and Technology 28, 1287-1302.

Chaphalkar, P., Valsaraj, K., Roy, D., 1994. Flotation using microgas dispersions for the removal of pentachlorophenol from aqueous solutions. Separation Science and Technology 29, 907-921.

Cheng, H.C., Lemlich, R., 1983. Errors in the measurement of bubble size distribution in foam. Industrial and Engineering of Chemistry Fundamentals 22, 105-109.

Choi, Y.J., Kim, Y.-J., Nam, K., 2009. Enhancement of aerobic biodegradation in an oxygen-limiting environment using a saponin-based microbubble suspension. Environmental pollution 157, 2197-2202.

Cilek, E.C., 2009. The effect of hydrodynamic conditions on true flotation and entrainment in flotation of a complex sulphide ore. International Journal of Mineral Processing 90, 35–44.

Cilek E.C., Umucu Y., 2001. A statistical model for gangue entrainment into froths in flotation of sulphide ores, Minerals Engineering 14 (9), 1055–1066.

Ciriello, S., Barnett, S., Deluise, F., 1982. Removal of heavy metals from aqueous solutions using microgas dispersions. Seperation Science Technology 17, 521-534.

Cistola, D.P., Atkinson, D., Hamilton, J.A., Small, D.M., 1986. Phase behavior and bilayer properties of fatty acids: hydrated 1: 1 acid-soaps. Biochemistry 25, 2804-2812.

Cistola, D.P., Hamilton, J.A., Jackson, D., Small, D.M., 1988. Ionization and phase behavior of fatty acids in water: application of the Gibbs phase rule. Biochemistry 27, 1881-1888.

Cistola, D.P., Small, D.M., 1990. Micelle formation and phase separation. Journal of the American Chemical Society 112, 3214-3215.

Collins, G.L., Jameson, G.J., 1977. Double-layer effects in the flotation of fine particles. Chemical Engineering Science, 32, 239–246.

Conway, B., Ayranci, E., 1999. Effective ionic radii and hydration volumes for evaluation of solution properties and ionic adsorption. Journal of solution chemistry 28, 163–192.

Coutoa, H.J., Françaa, S.C., Biscaia Jr, E.C., Sant'Anna Jr, G.L., 2008. A study of the production and characterization of foams for subsequent aplication on separation process.

Couto, H.J.B., Nunes, D.G., Neumann, R., Franca, S.C. A., 2009. Microbubble size distribution measurement by laser diffraction technique. Minerals Engineering 22, 330-335.

Craig, V.S., Ninham, B.W., Pashley, R.M., 1993. The effect of electrolytes on bubble coalescence in water. The Journal of Physical Chemistry 97, 10192-10197.

Cutting, G. W., 1989. Effect of Froth Structure and Mobility on Plant Performance. Mineral Processing and Extractive Metallurgy Review 5, 169–201.

Dai, Y., & Deng, T., 2003. Stabilization and characterization of colloidal gas aphron dispersions. Journal of colloid and interface science, 261(2), 360–365.

Dahmounea, F., Madania, K., Jauregib, P., De Faveric, D.M., Spigno, G., 2013. Fractionation of a red grape marc extract by colloidal gas aphrons. Chemical Engineering 32, 1903–1908.

Daiguji H, Makuta T, Kinoshita H, Oyabu T, Takemura F., 2007. Fabrication of hollow melamine-formaldehyde microcapsules from microbubble templates, Journal of Physics and Chemistry B, 111, 8879-8884.

Den Engelsen, C., Isarin, J., Gooijer, H., Warmoeskerken, M., Wassink, J.G., 2002. Bubble size distribution of foam. Autex Research Journal, 12, 14-27.

Denkov, N.D., Marinova, K.G., 2006. Antifoam effects of solid particles, oil drops and oil-solid compounds in aqueous foams. Colloidal particles at liquid interfaces, 383-444.

Denkov, N.D., Tcholakova, S., Golemanov, K., Ananthpadmanabhan, K., Lips, A., 2009. The role of surfactant type and bubble surface mobility in foam rheology. Soft Matter 5, 3389-3408.

Derjaguin, B., Dukhin, S., 1993. Theory of flotation of small and medium-size particles. Progress in Surface Science 43, 241-266.

Derjaguin, B., Landau, L., 1993. Theory of the stability of strongly charged lyophobic sols and of the adhesion of strongly charged particles in solutions of electrolytes. Progress in Surface Science 43, 30-59.

Dermiki, M., Gordon, M.H., Jauregi, P., 2008. The use of colloidal gas aphrons as novel downstream processing for the recovery of astaxanthin from cells of Phaffia rhodozyma. Journal of Chemical Technology & Biotechnology: International Research in Process, Environmental & Clean Technology 83, 174-182.

Dermiki, M., Gordon, M.H., Jauregi, P., 2009. Recovery of astaxanthin using colloidal gas aphrons (CGA): A mechanistic study. Separation and purification technology 65, 54-64.

Dibbern, E.M., Toublan, F.J.-J., Suslick, K.S., 2006. Formation and Characterization of Polyglutamate Core− Shell Microspheres. Journal of the American Chemical Society 128, 6540-6541.

Dorman, D.C., Lemlich, R., 1965. Separation of liquid mixtures by non-foaming bubble fractionation. Nature 207, 145-146.

Engel, M., Middlebrook, P., Jameson, G., 1997. Advances in the study of high intensity conditioning as a means of improving mineral flotation performance. Minerals Engineering 10, 55-68.

Feng, W., Singhal, N., Swift, S., 2009. Drainage mechanism of microbubble dispersion and factors influencing its stability. Journal of Colloid and Interface Science 337, 548-554.

Flach, C.R., Gericke, A., Mendelsohn, R., 1997. Quantitative determination of molecular chain tilt angles in monolayer films at the air/water interface: infrared reflection/absorption spectroscopy of behenic acid methyl ester. The Journal of Physical Chemistry B 101, 58-65.

Fuda, E., Jauregi, P., Pyle, D., 2004. Recovery of lactoferrin and lactoperoxidase from sweet whey using colloidal gas aphrons (CGAs) generated from an anionic surfactant, AOT. Biotechnology progress 20, 514-525.

Fuerstenau, D., Jang, H., 1991. On the nature of alkylsulfonate adsorption at the rutile/water interface. Langmuir 7, 3138-3143.

Fujiwara A., 2006. Technique microbubble generation using a venturi tube, ECO Industries, 11, 27–30.

Fujiwara, A., Okamoto, K., Hashiguchi, K., Peixinho, J., Takagi, S., Matsumoto, Y., 2007. Bubble breakup phenomena in a venturi tube, Fluids Engineering Division Summer Meeting, 553-560.

Fujiwara, A., Takagi, S., Watanabe, K., Matsumoto, Y., 2003. Experimental study on the new micro-bubble generator and its application to water purification system, Fluids Engineering Division Summer Meeting, 469-473.

Gaudin, A.M., 1957. Flotation. McGraw-Hill, New York.

George, P., Nguyen, A.V., Jameson, G.J., 2004. Assessment of true flotation and entrainment in the flotation of submicron particles by fine bubbles. Minerals Engineering, 17, 847–853.

Ghosh, P., 2004. Coalescence of air bubbles at air–water interface. Chemical Engineering Research and Design 82, 849-854.

Ghosh, P., 2009. Colloid and interface science. PHI Learning Pvt. Ltd., Delhi.

Ghosh, P., Juvekar, V., 2002. Analysis of the drop rest phenomenon. Chemical Engineering Research and Design 80, 715-728.

Giribabu, K., Reddy, M.L.N., Ghosh, P., 2007. Coalescence of air bubbles in surfactant solutions: role of salts containing mono-, di-, and trivalent ions. Chemical Engineering Communications 195, 336-351.

Graham, D., 1976. Structure of adsorbed protein films and stability of foams and emulsions. Unilever Research Laboratory, CNAA.

Grossmann, I.E., 2004. Challenges in the new millennium: product discovery and design, enterprise and supply chain optimization, global life cycle assessment. Computers & Chemical Engineering 29, 29-39.

Haberman, W.L., Morton, R.K., 1953. An experimental investigation of the drag and shape of air bubbles rising in various liquids. Taylor Model Basin Report TMB, 802.

Han, M. and Dockko, S., 1998. Zeta potential measurement of bubbles in DAF process and its effect on the removal efficiency. KSCE Journal of Civil Engineering, 2(4), 461–466.

Han, M., Park, Y., Lee, J., Shim, J., 2002. Effect of pressure on bubble size in dissolve air flotation. Journal of Water and Science Technology 2, 41–46.

Hasegawa, H., Nagasaka, Y., Kataoka, H., 2008. Electrical potential of microbubble generated by shear flow in pipe with slits. Fluid Dynamics Research, 40, 554–564.

Hashim, M.A., Gupta, B.S., 1998. The application of colloidal gas aphrons in the recovery of fine cellulose fibres from paper mill wastewater. Bioresource technology 64, 199-204.

Hashim, M.A., Mukhopadhyay, S., Gupta, B.S., Sahu, J.N., 2012. Application of colloidal gas aphrons for pollution remediation. Journal of Chemical Technology & Biotechnology 87, 305-324.

Hemmings, C., 1981. On the significance of flotation froth liquid lamella thickness. Transactions of the Institution of Mining and Metallurgy 90, C96–C102.

Huang, C., Zhang, H., Bai, R., 2017. Advances in ultrasound-targeted microbubble-mediated gene therapy for liver fibrosis. Acta Pharmaceutica Sinica B 7, 447-452.

Hunter, R.J., 2001. Foundations of Colloid Science. Oxford University Press, New York 806.

Hunter, R.J., 2013. Zeta potential in colloid science: principles and applications. Academic press, London.

Hunter, T.N., Pugh, R.J., Franks, G.V., Jameson, G.J., 2008. The role of particles in stabilising foams and emulsions. Advances in colloid and interface science 137, 57-81.

Israelachvili, J., 1997. Intermolecular and Surface Forces Academic Press Limited. London, UK.

Jacobi, W., Woodcock, K., Grove, C., 1956. Theoretical investigation of foam drainage. Ind. Eng. Chem. 48, 2046-2051.

Jameson, G.J., 1984. Experimental techniques in flotation. In The Scientific Basis of Flotation (pp. 193-228). Springer, Dordrecht.

Jarudilokkul, S., Rungphetcharat, K., Boonamnuayvitaya, V., 2004. Protein separation by colloidal gas aphrons using nonionic surfactant. Separation and purification technology 35, 23-29.

Jarudilokkul, S., Sinthuphisut, N., Boonamnuayvitaya, V., 2008. Dust collection by using colloidal gas aphrons. Environmental engineering science 25, 1175-1180.

Jauregi, P., Gilmour, S., Varley, J., 1997. Characterisation of colloidal gas aphrons for subsequent use for protein recovery. The Chemical Engineering Journal and the Biochemical Engineering Journal, 65, 1–11.

Jauregi, P., Mitchell, G.R., Varley, J., 2000. Colloidal gas aphrons (CGA): dispersion and structural features. AIChE journal 46, 24-36.

Jeelani, S., Hartland, S., 1994. Effect of interfacial mobility on thin film drainage. Journal of Colloid and Interface Science 164, 296-308.

Jianhong, L., Jun, L., HUANG, P., HUANG, M., 2009. Kinetic rate constant of liquid drainage from colloidal gas aphrons. Chinese Journal of Chemical Engineering 17, 955-959.

Johnson, N. W., 1972. The flotation behaviour of some chalcopyrite ores, PhD thesis, The University of Queensland, Brisbane, Australia.

Johnson, N. W., 2005. A review of the entrainment mechanism and its modelling in industrial flotation processes. Centenary of Flotation Symposium. Brisbane, Australia.

Johnson, N. W., Mckee, D. J., Lynch, A. J., 1974. Flotation rates of nonsulfide minerals in chalcopyrite flotation processes. Transactions of the American Institute of Mining, Metallurgical and Petroleum Engineers 256, 204–209.

Josm, J., Parasu, U.V., Prasad, C.V., Phanikumar, D.V. , Deshphande, N.S., Thokre, S.S., Thorat, B.N., , 1998. Gas hold-up structure in bubble column reactors'. PINSA 64.

Jowett, A., 1966. Gangue mineral contamination of froth. British Chemical Engineering 11, 330–333.

Joye, J.L., Hirasaki, G.J., Miller, C.A., 1992. Dimple formation and behavior during axisymmetrical foam film drainage. Langmuir 8, 3083-3092.

Kam, S.I., Rossen, W.R., 1999. Anomalous capillary pressure, stress, and stability of solids-coated bubbles. Journal of Colloid and Interface Science 213, 329-339.

Kantarci, N., Borak, F., Ulgen, K.O., 2005. Bubble column reactors. Process Biochemistry 40, 2263-2283.

Karger, B.L., Devivo, D.G., 1968. General survey of adsorptive bubble separation processes. Separation Science and Technology 3, 393-424.

Kirjavainen, V. M., 1996. Review and analysis of factors controlling the mechanical flotation of gangue minerals. International Journal of Mineral Processing 46, 21–34.Kommalapati, R.R., Valsaraj, K.T., Constant, W.D., Roy, D., 1998. Soil flushing using colloidal gas aphron suspensions generated from a plant-based surfactant. Journal of Hazardous Materials 60, 73-87.

Koopal, L.K., Ralston, J., 1986. Chain length effects in the adsorption of surfactants at aqueous interfaces: Comparison of existing adsorption models with a new model. Journal of Colloid and Interface Science 112, 362-379.

Kubota, K., Hayashi, S. and Inaoka, M., 1983. A convenient experimental method for measurement of zeta-potentials generating on the bubble suspended in aqueous surfactant solutions. Journal of colloid and interface science, 95(2), 362−369.

Kulkarni, A.A., Joshi, J.B., 2005. Bubble formation and bubble rise velocity in gas liquid systems: a review. Industrial and Engineering Chemistry Research 44, 5873−5931.

Kurup, N., Naik, P., 2010. Microbubbles: a novel delivery system. Asian Journal of Pharmaceutical Research and Health Care 2, 228-234.

Larmignat, S., Vanderpool, D., Lai, H.K., Pilon, L., 2008. Rheology of colloidal gas aphrons (microfoams). Colloids and Surfaces A: Physicochemical and Engineering Aspects 322, 199-210.

Lessard, R.R., Zieminski, S.A., 1971. Bubble coalescence and gas transfer in aqueous electrolytic solutions. Industrial & Engineering Chemistry Fundamentals 10, 260-269.

Liang-Shih Fan and Katsumi Tsuchiya, 1990. Bubble Wake Dynamics in Liquids and Liquid-Solid Suspensions, Butterworth Heinemann Series in Chemical Engineering 1–13.Longe, T.A., 1989.

Colloidal gas aphrons: Generation, flow characterization and application in soil and groundwater decontamination. Virginia Polytechnic Institute and State University.

Lu, J., Purcell, I., Lee, E., Simister, E., Thomas, R., Rennie, A., Penfold, J., 1995. The composition and structure of sodium dodecyl sulfate-dodecanol mixtures adsorbed at the air-water interface: a neutron reflection study. J Colloid Interface Sci. 174, 441-455.

Lye, G., Stuckey, D., 1998. Structure and stability of colloidal liquid aphrons. Colloids and Surfaces A: Physicochemical and Engineering Aspects 131, 119-136.

Lye, G.J., Stuckey, D.C., 2000. Extraction of erythromycin-A using colloidal liquid aphrons: I. Equilibrium partitioning. Journal of Chemical Technology Biotechnology: International Research in Process, Environmental & Clean Technology 75, 339-347.

Lynch, A., Johnson, N., Manlapig, E., Thorne, C., 1981. Mineral and coal flotation circuits, Elsevier, Amsterdam.

Ma, H., Luo, M., Dai, L.L., 2008. Influences of surfactant and nanoparticle assembly on effective interfacial tensions. Physical Chemistry Chemical Physics 10, 2207-2213.

Maldonado, M., Quinn, J., Gomez, C., Finch, J., 2013. An experimental study examining the relationship between bubble shape and rise velocity. Chemical Engineering Science 98, 7-11.

Mansur, E., Wang, Y.-D., Dai, Y.-Y., 2004. Separation of fine particles by using colloidal gas aphrons. Chinese Journal of Chemical Engineering 12, 286-289.

Marcelja, S., 2006. Selective coalescence of bubbles in simple electrolytes. The Journal of Physical Chemistry B 110, 13062-13067.

Maske, S.K., Rai, D.S., Kale, V.S., Raut, B.D., Chintale, G.A., 2012. Microbubble and its applications. International Journal of Pharmacy and Life Science 3, 2228-2235.

Mathe Z.T., Harris M. C., O'Connor C. T., (2000). A review of methods to model the froth phase in non-steady state flotation systems, Minerals Engineering 13(2), 127-140.

Matis K. A., Gallios G. P. and Kydros K. A., 1993. Separation of fines by flotation techniques. Seperation Technology, 3, 76−90.

Matsushita, K., Mollah, A., Stuckey, D., Del Cerro, C., Bailey, A., 1992. Predispersed solvent extraction of dilute products using colloidal gas aphrons and colloidal liquid aphrons: aphron preparation, stability and size. Colloids Surfaces 69, 65-72.

McCaffrey, D.L., Nguyen, S.C., Cox, S.J., Weller, H., Alivisatos, A.P., Geissler, P.L., Saykally, R.J., 2017. Mechanism of ion adsorption to aqueous interfaces: Graphene/water vs. air/water. Processing and National Academy of Science 114, 13369-13373.

Miller, D.N., 1980. Gas holdup and pressure drop in bubble column reactors. Industrial & Engineering Chemistry Process Design and Development 19, 371-377.

Miyamoto, M., Ueyama, S., Matsui, H., Kuzumoto, M., 2008. Mitsuishi Electric Technical Report, 82 (8), 489.

Mohamedi, G., Azmin, M., Pastoriza-Santos, I., Huang, V., Pérez-Juste, J., Liz-Marzán, L.M., Edirisinghe, M., Stride, E., 2012. Effects of gold nanoparticles on the stability of microbubbles. Langmuir 28, 13808-13815.

Moshkelani, M., Amiri, M., 2008. Electrical conductivity as a novel technique for characterization of colloidal gas aphrons (CGA). Colloids and Surfaces A: Physicochemical and Engineering Aspects 317, 262-269.

Moshkelani, M. and Chalkesh, A.M., 2008. An Insight into Colloidal Gas Aphron Drainage Using Electrical Conductivity Measurement. Iranian Journal of Chemistry and Chemical Engineeing 27, 3, 63−68.

Moys, M.H, 1978. A study of a plug-flow model for flotation froth behaviour. International Journal of Mineral Processing 5, 21–38.

Mukerjee, P., Mysels, K., Kapauan, P., 1967. Counterion specificity in the formation of ionic micelles-size, hydration, and hydrophobic bonding effects. The Journal of Physical Chemistry 71, 4166-4175.

Mukherjee, S., Mukhopadhyay, S., Pariatamby, A., Hashim, M.A., Redzwan, G., Gupta, B.S., 2015. Optimization of pulp fibre removal by flotation using colloidal gas aphrons generated from a natural surfactant. Journal of The Taiwan Institute of Chemical Engineers 53, 15-21.

Mukhopadhyay, S., Mukherjee, S., Hashim, M.A., Gupta, B.S., 2015. Application of colloidal gas aphron suspensions produced from Sapindus mukorossi for arsenic removal from contaminated soil. Chemosphere 119, 355-362.

Mulligan, C.N., Wang, S., 2006. Remediation of a heavy metal-contaminated soil by a rhamnolipid foam. Engineering Geology 85, 75-81.

Nakatake, Y., Watanaba, K., Eguchi, T., 2007. Improved combustion in diesel engines with fuel containing ejector-generated microbubble. Nihon Kikai Gakki Ron-bunsho 73, 2368-2374.

Narsimhan, G., Ruckenstein E., 1986. Hydrodynamics, Enrichment, and Collapse in Foams. Langmuir, 2, 230−238.

Neethling, S.J., Cilliers, J.J., 2003. Modelling flotation froths. International Journal of Mineral Processing 72, 267–287.

Neethling, S. J., Cilliers, J. J., 2002. The entrainment of gangue into a flotation froth. International Journal of Mineral Processing 64, 123–134.

Neethling, S. J., Cilliers, J. J., 2009. The entrainment factor in froth flotation: Model for particle size and other operating parameter effects. International Journal of Mineral Processing 93, 141–148.

Nguyen Anh V., Jameson G. J., 2006. Demonstration of a minimum in the recovery of nanoparticles by flotation: Theory and experiment, Chemical Engineering Science 61, 2494–2509.

Nguyen A.V. and Schulze H.J., 2004. Colloidal science of flotation, Marcel Dekker, New York, 840.

Noskov, B., Mikhailovskaya, A., Lin, S.-Y., Loglio, G., Miller, R., 2010. Bovine serum albumin unfolding at the air/water interface as studied by dilational surface rheology. Langmuir 26, 17225-17231.

Ohnari, H., 2006. All about microbubbles. Nippon Jitsugyo Shuppan Co., Japan (in Japanese).

Paluch, M., 2000. Electrical properties of free surface of water and aqueous solutions. Advances in colloid and interface science 84, 27-45.

Oliveira, C., Rubio, J., 2011. Zeta potential of single and polymer-coated microbubbles using an adapted microelectrophoresis technique. International Journal of Mineral Processing, 98, 118−123.

Ozcan Y. Gulsoy, 2005. A simple model for the calculation of entrainment in flotation, Korean Journal of Chemical Engineering 22(4), 628−634.

Pandey, S., Bagwe, R.P., Shah, D.O., 2003. Effect of counterions on surface and foaming properties of dodecyl sulfate. Journal of Colloid and Interface Science 267, 160-166.

Paluch, M., 2000. Electrical properties of free surface of water and aqueous solutions. Advances in Colloid and Interface Science, 84, 27–45.

Parhizkar, M., Stridea, E., Edirisinghe, M., 2014. Preparation of monodisperse microbubbles using an integrated embedded capillary T-junction with electrohydrodynamic focusing. RSC Adv. 2437–2446.

Parmar, R., Majumder, S.K., 2013. Microbubble generation and microbubble-aided transport process intensification—A state-of-the-art report. Chemical Engineering Processes.: Process Intensification 64, 79-97.

Parmar, R., Majumder, S.K., 2014. Hydrodynamics of microbubble suspension flow in pipes. Industrial & Engineering Chemistry Research 53, 3689-3701.

Parmar, R., Majumder, S.K., 2015. Terminal rise velocity, size distribution and stability of microbubble suspension. Asia-Pacific Journal of Chemical Engineering 10, 450−465.

Pérez-Garibay, R., Bueno-Tokunaga, A., Estrada-Ruiz, R.H., Camacho-Ortegón, L.F., 2018. Effect of surface electrical charge on microbubbles' terminal velocity and gas holdup. Minerals Engineering 119, 166-172.

Poskanzer, A.M., Goodrich, F.C., 1975. Surface viscosity of sodium dodecyl sulfate solutions with and without added dodecanol. Journal of Physical Chemistry 79, 2122–2126.

Prince, M.J., Blanch, H.W., 1990. Transition electrolyte concentrations for bubble coalescence. AIChE Journal 36, 1425-1429.

Qu F., Morais P. C., 1999. Energy levels in metal oxide semiconductor quantum dots in water-based colloids. The Journal of chemical physics, 111(18), 8588−8594.

Ripley, M.B., Harrison, A.B., Betts, W.B., Dart, R.K., Wilson, A.J., 2000. Enhanced degradation of a model oil compound in soil using a liquid foam-microbe formulation. Environmental science & technology 34, 489-496.

Rodrigues, R. T., Rubio J., 2003. New basis for measuring the size distribution of bubbles. Minerals Engineering, 16, 8, 757−765.

Ronteltap, A., Prins, A., 1989. Contribution of drainage, coalescence and disproportionation to the stability of aerated foodstuffs and the consequences for the bubble size distribution as measured by a newly developed optical glass-fibre technique. Food colloids 75, 39.

Rovers, T.A., Sala, G., van der Linden, E., Meinders, M.B., 2016. Temperature is key to yield and stability of BSA stabilized microbubbles. Food Hydrocolloids 52, 106-115.

Roy, D., Valsaraj, K., Constant, W., Darji, M., 1994. Removal of hazardous oily waste from a soil matrix using surfactants and colloidal gas aphron suspensions under different flow conditions. Journal of Hazardous Materials 38, 127-144.

Roy, D., Valsaraj, K., Kottai, S., 1992. Separation of organic dyes from wastewater by using colloidal gas aphrons. Seperation Science and Technology 27, 573-588.

Ross V. E., 1989. Flotation and entrainment of particles during batch flotation tests. Minerals Engineering, 3, 245−256.

Ross, V.E., 1989. Determination of the contributions by true flotation and entrainment during the flotation process. International Colloquium: Developments in Froth Flotation. Southern African Institute of Mining and Metallurgy, Gordon's Bay, South Africa.

Ross, V.E., Van Deventer, J.S.J., 1988. In: Sastry, K. (Ed.), Column Flotation'88 - Proceedings of an International Symposium. SME Inc., Littleton, 383–386.

Ruby, K., Majumder, S.K., 2018. Studies on stability and properties of micro and nano-particle-laden ionic microbubbles. Powder Technol. 335, 77-90.

Sadatomi, M., Kawahara, A., 2012. Fluids mixer and fluids mixing method. Japanese Patent.

Savassi O. N., Alexander D. J., Manlapig E. V., 1998. An empirical model for entrainment in industrial flotation plants, Minerals Engineering 11(3), 243−256.

Save, S.V., Pangarkar, V.G., 1994. Characterisation of colloidal gas aphrons. Chemical Engineering Communications 127, 35-54.

Save, S.V., Pangarkar, V.G., Kumar, S.V., 1993. Intensification of mass transfer in aqueous two-phase systems. Biotechnology and bioengineering 41, 72-78.

Sebba, F., 1962. Ion flotation. Elsevier Publishing Company.

Sebba, F., 1987. Foams and Biliquid Foams-Aphrons. John Wiley & Sons, New York.

Sebba, F., 1971. Microfoams—an unexploited colloid system. J. Colloid Interface Sci. 35, 643-646.

Shams, M.M., Dong, M., Mahinpey, N., 2014. Viscosity and rheological behavior of microbubbles in capillary tubes. AIChE Journal 60, 2660-2669.

Sharma, M., Shah, D., Brigham, W., 1985. The influence of temperature on surface and microscopic properties of surfactant solutions in relation to fluid displacement efficiency in porous media. AIChE Journal 31, 222-228.

Shen, Y., Longo, M. L., Powell, R. L., 2008. Stability and rheological behavior of concentrated monodisperse food emulsifier coated microbubble suspensions. Journal of Colloid and Interface Science, 327, 204–210.

Sivamohan, R., 1990. The problem of recovering very fine particles in mineral processing−a review. International Journal of Mineral Processing, 28(3-4), 247−288.

Smith, C. A., 1984. Dynamic simulation of sulphide flotation circuits, PhD thesis. The University of Queensland, Brisbane, Australia.

Smith, P. G., Warren, L. J., 1989. Entrainment of Particles into Flotation Froths. Mineral Processing and Extractive Metallurgy Review 5, 123–145.

Somasundaran, P., Grieves, R.B., 1975. Advances in interfacial phenomena of particulate/solution/gas systems; applications to flotation research, Aiche Symposium Series, 71, 150, 1975-191.

Subrahmanyam, T.V., Forssberg, E., 1988. Froth characteristics and grade−recovery relationships in the flotation of lead−zinc and copper ores. Minerals Engineering 1, 41–52.

Subramaniam, M.B., Blakebrough, N., Hashim, M.A., 1990. Clarification of suspensions by colloidal gas aphrons. J. Chem. Technol. Biotechnol. 48, 41-60.

Svitova, T., Wetherbee, M., Radke, C., 2003. Dynamics of surfactant sorption at the air/water interface: continuous-flow tensiometry. Journal of Colloid and Interface Science 261, 170-179.

Szatkowski, M., 1987. Factors influencing behaviour of flotation froth. Institution of Mining and Metallurgy Transactions (Section C. Mineral Processing and Extractive Metallurgy) 96 115–122.

Tajima, K., Muramatsu, M., Sasaki, T., 1970. Radiotracer studies on adsorption of surface active substance at aqueous surface. I. Accurate measurement of adsorption of tritiated sodium dodecylsulfate. Bulletin of the Chemical Society of Japan 43, 1991-1998.

Takahashi, M., 2005. ζ potential of microbubbles in aqueous solutions: electrical properties of the gas− water interface. The Journal of Physical Chemistry B 109, 21858-21864.

Takahashi, M., Chiba, K., Li, P., 2007. Free-radical generation from collapsing microbubbles in the absence of a dynamic stimulus. The Journal of Physical Chemistry B 111, 1343-1347.

Takahashi, M., Kawamura, T., Yamamoto, Y., Ohnari, H., Himuro, S., Shakutsui, H., 2003. Effect of shrinking microbubble on gas hydrate formation. The Journal of Physical Chemistry B 107, 2171-2173.

Taki G. and Unal A., 2012. Statistical evaluation of flotation and entrainment behavior of an artificial ore. Transactions of Nonferrous Metals Society of China, 22; 199−205.

Tao D., Luttrell G. H., Yoon R. H., 2000. A parametric study of froth stability and its effect on column flotation of fine particles, International Journal of Mineral Processing 59, 25-43.

Tchuenbou-Magaia, F.L., Norton, I.T., Cox, P.W., 2009. Microbubbles with protein coats for healthy food: Air filled emulsions, Gums and Stabilisers for the Food Industry 15, pp. 113-125.

Tchuenbou-Magaia, F.L., Cox, P.W., 2011. Tribological study of suspensions of cysteine-rich protein stabilized microbubbles and subsequent triphasic A/O/W emulsions. Journal of Texture Studies 42, 185-196.

Temesgen, T., Bui, T.T., Han, M., Kim, T.-i., Park, H., 2017. Micro and nanobubble technologies as a new horizon for water-treatment techniques: A review Advance Colloid Interface Science 246, 40-51.

Terasaka, K., Hirabayashi, A., Nishino, T., Fujioka, S., Kobayashi, D., 2011. Development of microbubble aerator for waste water treatment using aerobic activated sludge. Chemical Engineering Science 66, 3172-3179.

Tsuge, H., 2010. Fundamentals of microbubbles and nanobubbles. Bulletin of the Society of Sea Water Science, Japan 64, 4-10.

Tsuge, H., 2014. Characteristics of microbubbles. Micro-and nanobubbles fundamentals and applications 2, 978-981.

Trahar W. J., 1981. A rational interpretation of the role of particle size in flotation. International Journal of Mineral Processing, 8, 289–327.

Trahar, W.J., Warren, L.J., 1976. The floatability of very fine particles–a review. International Journal of Mineral Processing 3, 103–131.

Tuteja, R., Spottiswood, D., Misra, V., 1995. Column parameters: Their effect on entrainment in froth. Minerals Engineering 8, 1359-1368.

Topallar, H., Karadag, B., 1998. Mechanism of micelle formation in sodium dodecyl sulfate and cetyltrimethylammonium bromide. Journal of Surfactant and Detergent 1, 49–51.

Usui, S., Sasaki, H. and Matsukawa, H., 1981. The dependence of zeta potential on bubble size as determined by the dorn effect. Journal of Colloid and Interface Science, 81(1), 80-84.

Verma, A., Chauhan, G., Ojha, K., 2018. Characterization of α-olefin sulfonate foam in presence of cosurfactants: Stability, foamability and drainage kinetic study. Journal Molecular Liquids 264, 458-469.

Vignes-Adler, M., Weaire, D., 2008. New foams: Fresh challenges and opportunities. Current Opinion in Colloid Interface Science 13, 141-149.

Ventura-Medina, E., Cilliers, J.J., 2002. A model to describe flotation performance based on physics of foams and froth image analysis. International Journal of Mineral Processing 67, 79–99.

Wang L., Peng Y., Runge K. and Bradshaw D., 2015. A review of entrainment: Mechanisms, contributing factors and modelling in flotation. Mineral Engineering 70, 77–91.

Wang, Y., Weinstock, I.A., 2012. Polyoxometalate-decorated nanoparticles. Chemical Society Reviews 41, 7479–7496.

Wang, T.-Y., E Wilson, K., Machtaler, S., K Willmann, J., 2013. Ultrasound and microbubble guided drug delivery: mechanistic understanding and clinical implications. Current pharmaceutical biotechnology 14, 743-752.

Warren, L.J., 1985. Determination of the contributions of true flotation and entrainment in batch flotation tests. International Journal of Mineral Processing, 14, 33–44.

Waters, K., Hadler, K., Cilliers, J., 2008. The flotation of fine particles using charged microbubbles. Minerals Engineering 21, 918-923.

Weissenborn, P.K., Pugh, R.J., 1996. Surface tension of aqueous solutions of electrolytes: relationship with ion hydration, oxygen solubility, and bubble coalescence. Journal of Colloid and Interface Science 184, 550-563.

Wills, B.A., 2006. Will's Mineral Processing Technology, 12. Oxford, UK.

Wills, B., Napier-Munn, T., 2005. Froth flotation: Mineral Processing Technology. Oxford, Butterworth-Heinemann, 284-316.

Xu, Q., Nakajima, M., Ichikawa, S., Nakamura, N., Roy, P., Okadome, H., Shiina, T., 2009. Effects of surfactant and electrolyte concentrations on bubble formation and stabilization. Journal of Colloid and Interface Science 332, 208-214.

Xu, Q., Nakajima, M., Ichikawa, S., Nakamura, N., Shiina, T., 2008. A comparative study of microbubble generation by mechanical agitation and sonication. Innovative Food Sci. Emerging Technol. 9, 489-494.

Yalcin, T., Byers, A., 2006. Dissolved gas flotation in mineral processing. Mineral Processing and Extractive Metallurgy Review 27, 87-97.

Yan, Y.-l., Qu, C.-t., Zhang, N.-s., Yang, Z.-g., Liu, L., 2005. A study on the kinetics of liquid drainage from colloidal gas aphrons (CGAs). Colloids and Surfaces A: Physicochemical and Engineering Aspects 259, 167-172.

Yang, C., Dabros, T., Li, D., Czarnecki, J. and Masliyah, J.H., 2001. Measurement of the zeta potential of gas bubbles in aqueous solutions by microelectrophoresis method. Journal of Colloid and Interface Science, 243(1), 128–135.

Yasuda, T., Takahashi, N., Baba, M., TEI, K. and Yamaguchi, S., 2008. An experimental study on micro-bubble generation by laser–induced breakdown in water. The Review of Laser Engineering, 36(APLS), 1273–1275.

Yianatos, J., Contreras, F., Díaz, F., Villanueva, A., 2009. Direct measurement of entrainment in large flotation cells. Powder Technology 189, 42–47.

Yoon, R. H., 1993. Microbubble flotation. Mineral Engineering Vol. 6, 6, 619–630.

Yoon, R.-H., Yordan, J.L., 1986. Zeta-potential measurements on microbubbles generated using various surfactants. Journal of Colloid and Interface Science 113, 430-438.

Zhang, Y., Chang, Z., Luo, W., Gu, S., Li, W., An, J., 2015. Effect of starch particles on foam stability and dilational viscoelasticity of aqueous-foam. Chinese Journal of Chemical Engineers 23, 276–280.

Zheng X., Franzidis J. P., Johson N., 2006a. An evaluation of different models of water recovery in flotation. Minerals Engineering 19, 871–882.

Zheng X., Johnson N. W., Franzidis J. P., 2006b. Modeling of entrainment in industrial flotation cells: Water recovery and degree of entrainment. Minerals Engineering 19, 1191–1203.

Ziaee, H., Arabloo, M., Ghazanfari, M.H., Rashtchian, D., 2015. Herschel–Bulkley rheological parameters of lightweight colloidal gas aphron (CGA) based fluids. Chemical Engineering Research and Design 93, 21-29.